This is to certify that the

dissertation entitled

Spectroscopic Studies
of Mass-Selected,
Matrix-Isolated Cations

presented by

Jerry T. Godbout

has been accepted towards fulfillment
of the requirements for

Ph.D. degree in Chemistry

Major professor

Date June 26, 1996

SPECTROSCOPIC STUDIES OF MASS-SELECTED, MATRIX ISOLATED CATIONS

By

Jerry T. Godbout

A DISSERTATION

Submitted to
Michigan State University
in partial fulfillment of the requirements
for the degree of

DOCTOR OF PHILOSOPHY

Department of Chemistry

1996

ABSTRACT

SPECTROSCOPIC STUDIES OF MASS-SELECTED, MATRIX ISOLATED CATIONS

By

Jerry T. Godbout

The elucidation of the structures of polyatomic ions has been a daunting task over the years. Attempts at structure determination have generally employed one of two experimental methodologies: molecular spectroscopy or mass spectrometry. While molecular spectroscopy yields structural information directly, the high reactivity of ionic species can make direct spectroscopic measurements exceedingly difficult. Whereas the sensitivity of mass spectrometric methods facilitates the detection of ions, structural information is indirectly and incompletely obtained at best.

We have merged mass spectrometric techniques with matrix isolation spectroscopy to allow the vibrational spectra of polyatomic ions trapped in rare gas matrices to be observed. In this method, ions are made in a conventional electron impact ionization source and mass selected using a quadrupole mass filter. The mass-selected ion beam is then guided to a 4 K cryogenic window where it is co-condensed with excess neon. The trapped ions are then analyzed using conventional Fourier Transform Infrared (FTIR) spectroscopy.

Initial feasibility studies were performed using small cations with known IR spectra. The cations were observed without the concurrent deposition of anions, although negative charge carriers were indirectly detected. Further experiments with trapped beams

of CO_2^+ generated from CO_2 have allowed the issue of charge neutrality to be addressed. The addition of CO_2 to the system results in the production of CO_2^- and $(CO_2)_2^-$. The addition of CO_2 also seems to enhance the concentration of cations stabilized in the matrix by a factor of ~5. The origin of these anions was found to be neutral CO_2 molecules adsorbed onto various cold copper surfaces surrounding the matrix window. Issues such as fragmentation of the mass-selected cations the use of visible emission as an alternate detection method are also discussed.

Dedicated to Mom, Dad, and Joe

and in loving memory of

Grandma St. Pierre

ACKNOWLEDGEMENTS

Although this dissertation bears the name of only one author, the work described in it was made possible by the combined efforts of many people. First and foremost, I would like to thank Professors George Leroi and John Allison for their never-ending support, always-accessible guidance and countless suggestions when things weren't working. I should also thank them for their patience when I didn't follow those suggestions, especially when they were right after all. Working for two advisors can be a mixed blessing, but I think that the benefits outweigh the disadvantage of having to appease two people. Besides the obvious advantage of being able to draw from two fairly distinct scientific backgrounds, their also distinct views on life in general gave me a hopefully more balanced perspective. Interaction with and support from the other members of the Leroi and Allison groups was also invaluable.

I once heard someone (J. P. Maier I believe) describing experiments similar to ours as "conceptually simple, but a technical nightmare". On that note the people who kept us up and running need to be thanked. The machine shop staff (Russ Geyer, Dick Menke, and Sam Jackson) always amazed me with their ability to translate what I asked for into what I actually needed, and their handling of my jobs that always seemed to be dire emergencies (well, they were to me). The electronics support from Ron Haas and Scott Sanderson constantly kept the electrocution hazard we called and instrument from going up in flames, or at least diagnosed the cause and replaced the damaged components when

it did. I am sorry to say that I also need to thank the staff of the glass shop (Scott Bancroff, Manfred Langer, and Keki Mistry). I make this acknowledgment with reservation not because of the quality of their work (which was superb and should be considered art) but because needing their help usually meant that I had just broken something.

Finally, as far as science goes, I need one more. This work would not have been possible without the dedicated efforts of my labmate, Elvis Presley (currently assuming the identity of Tom Halasinski). Along with his many scientific contributions (such as the ion source) his unique presence made all those 30 hour experiments almost tolerable, and always interesting.

Science isn't everything though, and on that note:

- Dan: We never seemed to reduce Michigan's fish and pheasant population as much as we wanted to, but oh well.
- Paul and Deena: Now whose going to feed me?
- Matt: For putting up with me (I guess it's not my lab anymore), helping with flood prevention/recovery and most notably for your assistance in our brief stint in aerodynamic engineering.
- Phil: If all Republicans were like you, maybe, just maybe.
- Wanda: Sometimes I still wish things had been different (one way or the other), but I'm glad we're still friends and I wish you the best.
- Jeff and Claudia: Support, advice, and friendship early on, even during Jeff's "plenty friendly" period.

- Michelle, Don, and Donny: Home life worth leaving the lab for.
- Kerry and Rob: Legendary Christmas parties.

Overall, I'd have to say that grad school was OK, but it was stressful at times. For helping relieve that stress, I'd like to thank (in no particular order):

- Any of the "Happy Hour" regulars not already mentioned (Michelle, Chris, Sara, Nocera, Gerry).
- The programmers at id Software and Netscape Communications Corp., without whom I would have graduated months earlier.
- The gang at Dagwood's (Brenda, Tee, and Randy) especially for their assistance during the actual writing of this dissertation.
- The Michigan DNR, the game they manage, and the Remington Arms Company.

TABLE OF CONTENTS

LIST OF FIGURES

Chapter 1

Introduction

Polyatomic ions have long been of interest to chemists. They are thought to be quite common in interstellar space[1] and are also thought to play an important role in many atmospheric processes.[2] The most common technique used for the terrestrial study of polyatomic ions is mass spectrometry. Mass spectrometric studies can provide a wealth of kinetic and thermodynamic data, but generally provide structural information only indirectly. A classic example is the question of the structure of the ions with the formula $C_2H_3O^+$ (m/z = 43) formed from many organic molecules. The two most stable predicted geometries for these ions are the following:

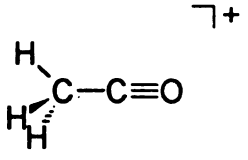

a

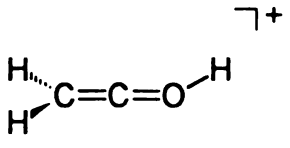

b

Structure **a** is thought to be the more stable,[3] and is generally referred to as the acetyl cation. Structure **b**, referred to as oxygen-protonated ketene, is thought to be less stable by ~42 kcal/mole.[4] To determine if different precursors would generate $C_2H_3O^+$ ions having different structures, Weber and Levsen[5] performed a series of tandem mass spectrometric experiments on a wide variety of compounds that produce a fragment ion with m/z 43. They determined that the m/z 43 fragment ion generated from electron impact of glycerol had a chemistry different than that of the m/z 43 ion generated from

other carbonyl-containing compounds such as acetone. This difference in chemical behavior implied that the ions had two different structures, but it did not, however, determine their geometries. From mechanisms based on condensed phase organic chemistry, Weber and Levson postulated that the ion made from acetone was the acetyl cation, while the m/z 43 ion from glycerol was probably oxygen protonated ketene. This postulation is still, however, not without it's critics.[6]

I. The Spectroscopy of Polyatomic Ions

Differentiating and assigning structures **a** and **b** would be trivial if the vibrational spectrum of each were available. The IR spectrum of structure **a** should exhibit a prominent absorption in a wavenumber region indicative of a carbonyl group, while the spectrum of structure **b** would have a distinct absorption in a wavenumber region associated with the stretching of its hydroxyl group. Molecular spectroscopy, however, has not been routinely applied to polyatomic ions for a number of reasons. The foremost difficulty arises from the reactivity of these ionic species. Their high reactivity does not allow them to be stable in typical confining media such as solutions. Even in the exceptional cases where these ions can be stabilized, the confining medium typically causes severe perturbations of the guest species. The problem of reactivity is generally circumvented by doing studies in the gas phase. In the case of charged species, however, some other problems arise. .Due to Coulombic repulsion, the theoretical "space charge limit" of ions in the gas phase is about 10^6 ions/cm^3, which corresponds to femtomolar concentrations[7], far below the detection limits of routine vibrational spectroscopic methods such as Fourier Transform Infrared (FTIR) or Raman spectroscopy. Despite

these experimental challenges, polyatomic ions have not completely eluded spectroscopists.

A. Early Spectroscopic Studies of Polyatomic Ions

Beginning in the late 1960s and early 1970s, the electronic absorption and emission spectra of several small polyatomic ions in electrical discharges were observed.[8] Ion concentrations higher than the space charge limit can be achieved in discharges due to the presence of both positively and negatively charged species. Unfortunately, these experiments had some serious limitations. First, the discharge ionization is non-selective, and can produce several ionic and neutral species. As a result, the identity of the absorbing and/or emitting species is not always clear. Second, the ions are formed in highly excited states, which can make their spectra quite complicated and difficult to assign.[8] Third, the harsh conditions of the discharge allow only relatively small species to be observed.

B. Laser-Based Gas-Phase Techniques

Spectroscopic observation of polyatomic ions can be facilitated by addressing one of two major problems: namely increasing the sensitivity of the experiment, or finding a way to achieve ion concentrations high enough for standard spectroscopic techniques. The development of lasers in the 1970s and 1980s made polyatomic ion spectroscopy more feasible by means of the first method. In 1976, Wing et al. reported the first infrared absorption of a gas-phase, polyatomic, ionic species.[9] In these experiments, the rotational-vibrational transitions of HD^{+}, formed in a discharge, were driven by a CO laser, and absorption was indirectly detected by monitoring a change in charge exchange cross-section with a neutral target gas. Because of it's high sensitivity, indirect detection

became the basis of several other successful spectroscopic techniques such as photofragmentation[10] and photo-detachment[11] spectroscopy.

In 1979, Saykally et al. obtained the first direct infrared absorption spectrum of HBr^+ in a plasma, using newly developed laser magnetic resonance (LMR) spectroscopy.[12] In 1980, Oka and co-workers developed the highly successful method of IR difference frequency spectroscopy and reported the IR spectrum of H_3^+.[13] While these techniques were sufficiently sensitive to be applied to ions, they still suffered from the lack of ion-selective detection. As a result, ion signals were often obscured by absorptions from the much larger number of neutral species present in the discharge. Perhaps the most notable breakthrough in gas phase ion spectroscopy came in 1983 when Saykally and co-workers developed velocity modulation spectroscopy.[14] In this experiment, a single wavelength IR laser is passed coaxially through a mass-selected ion beam. By changing the velocity of the beam, different ro-vibrational transitions can be tuned into resonance with the laser by the Doppler shift. This provides a means of selectively exciting and detecting ions, even though a large number of neutrals may be present. Other high-sensitivity, high-resolution laser techniques which are variants of velocity modulation were soon developed.[15,16] These methods have two distinct advantages over the original discharge experiments. First, most are inherently mass selective, so the identity, or at least the mass to charge ratio, of the ion being studied is known. Second, the high resolution of these techniques allows rotational transitions to be observed, which can provide very accurate structural information about the species being studied.

Nonetheless, these techniques still have some shortcomings. One drawback is that even with the combinations of several velocities and lasers, not all spectral regions can be

covered, although this limitation is being rapidly overcome by advances in laser technology. Generally, only small portions of the IR spectrum (~0.25 cm^{-1}) can be scanned at a time, making coverage of the entire IR spectrum a very tedious and time consuming task. This problem is further exacerbated because the positions of the vibrational transitions are often unknown, so that a great deal of experimental time is spent scanning spectral regions where there are none. These studies are also limited to smaller ions for two reasons. First, these experiments are also dependent on discharge sources for ion production.[17] Second, most of the structural information is extracted from rotational analysis, which becomes more difficult as the size of the species increases.

C. Matrix Isolation Studies

In the early 1970s, however, some researchers were successful in obtaining vibrational spectra of polyatomic ions by addressing the second problem associated with ion spectroscopy, namely by devising a way to accumulate sufficient concentrations of ions for observation by more routine spectroscopic techniques such as FTIR and Raman spectroscopy. The solution to this problem involved finding a medium sufficiently inert to constrain these ions without interacting, or reacting with them. Matrix isolation provided this medium. This technique, developed initially in 1954 by Pimentel and co-workers, involves stabilizing the reactive species by trapping them in a rigid, inert matrix, usually argon or neon.[18] Figure 1.1 shows generic matrix isolation methodology. Matrix isolation was first shown to be quite useful in the study of highly reactive neutral species;[19] it has since been proven to be equally applicable to ionic species. The first report of a matrix isolated ion was by Kasai and in 1970.[20] He generated Na^+ in an Ar matrix from the photochemical reaction:

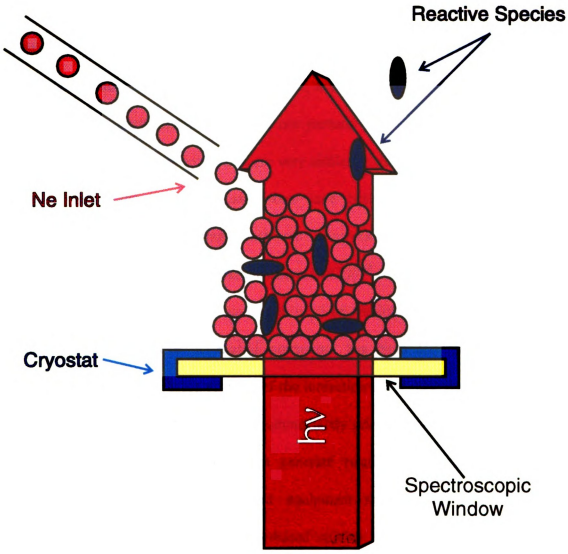

Figure 1.1: A generic matrix-isolation spectroscopy experiment

$$Na + HI + h\nu \rightarrow Na^{+} + I^{-} + H$$

In this system, an electron from the Na atom is photodetached and scavenged by the HI molecule. Because both positive and negative ions are present in the matrix, they are theoretically able to exist in concentrations higher than the space charge limit to allow spectroscopic observation. These ions, however, are assumed to be physically trapped in individual matrix "sites" and therefore do not perturb one another to any appreciable extent. As a result, the spectra obtained are very similar to those of the isolated gas-phase species.[21] Since then matrix isolated ions have been studied with a variety of spectroscopic methods, including electronic absorption,[22] fluorescence,[23] FTIR,[24] Raman,[25] ESR,[26] and magnetic circular dichroism (MCD).[27]

A wide variety of methods have been used to generate ions for matrix isolation studies, although photolysis of neutral precursors has been the most popular and successful. The common factor of most of the ionization techniques used to date is that the ionization takes place either *in situ* or immediately prior to co-condensation with the matrix gas.[28] Since these methods can generate relatively large numbers of ions, traditional spectroscopic techniques and equipment may be used, making these experiments much simpler than the laser-based studies. Being able to use common spectroscopic techniques has made matrix isolation a very useful method of determining the structures of polyatomic ions.

Most of the matrix isolation studies to date, unfortunately, are not without their drawbacks. The most serious problem generally involves the ionization process. In general, ionization techniques such as UV photolysis are non-selective, and give rise to many ionic and neutral products. As a result, the identity of the species being studied is

not always known,[28] resulting in the same problems that hindered the early discharge experiments.

The goal of the work described in this dissertation was to develop a methodology for structural analysis of polyatomic species. The approach used to achieve this goal involves coupling mass spectrometric technology with matrix isolation spectroscopy. This experiment and its principal instrumental components is depicted schematically in Figure 1.2. In such an experiment, ions would be generated in a remote source, mass selected using a quadrupole mass filter, and directed towards a growing matrix. It is believed that this methodology will combine the advantages of mass spectrometric selection with current spectroscopic technologies (matrix and gas phase), while also eliminating their drawbacks. First and foremost, direct structural analysis is possible with the application of molecular spectroscopy, particularly FTIR spectroscopy. Through the use of as mass filter, the identity (more specifically, the m/z value) of the ion being studied would now be known, making the task of spectral assignment much easier. This technique can be thought of as having ion-selective detection, provided that conformation is obtained by the proper control experiments This method was first developed by J. P. Maier and his group in 1989, who used it to measure the absorption spectra a wide variety of cations.[29] The technique was further extended to laser induced fluorescence (LIF) by Sabo et al, who reported the emission spectrum of mass-selected, matrix-isolated $CS_2^{\bullet+}$.[30]

II. Matrix Isolation Spectroscopy of Polyatomic Ions

It has been said that the microscopic "molecular" properties of a species can only be deduced from gas phase studies, since perturbations due to intermolecular forces can be very significant in the liquid and solid phases.[31] The more reactive a species becomes, the

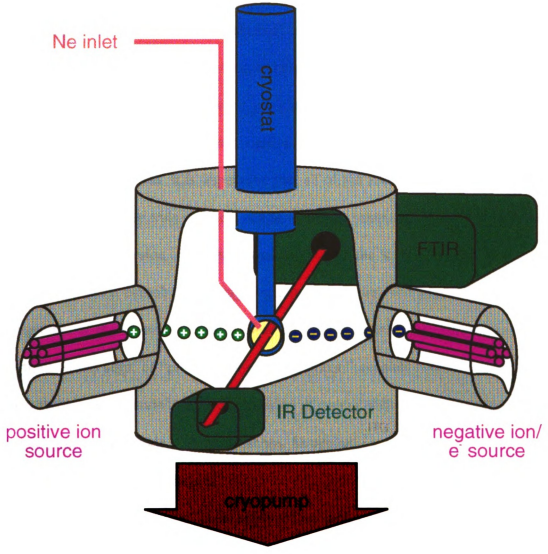

Figure 1.2: Schematic representation of a mass-selection matrix-isolation experiment.

more problematic these intermolecular (or interionic) forces become. With very reactive species, it is usually necessary to work at very low pressures (concentrations) and high effective temperatures. Even if these "isolated" conditions can be achieved, many reactive species still have very short lifetimes, thus making spectroscopic observations challenging. Matrix isolation provides an alternative to gas-phase studies. Matrix isolation is defined as the trapping of a reactive species in a rigid cage of a chemically inert substance (the matrix) at low temperatures. It is imperative that all of the above criteria are met for the species under study to be truly isolated. Cage rigidity is necessary to prevent the loss of reactive species by diffusion. Matrix inertness prevents the loss of sample by reaction. The low temperature contributes to cage rigidity and reduces the probability of internal rearrangement of the reactive species. These conditions, required to successfully reduce interactions to the point of "pseudo gas phase behavior," severely restrict the choices of matrix materials, and requires that a combination of several different technologies such as cryogenics, vacuum methods, and spectroscopy, be applied.

A. Ion Generation Techniques

Several techniques have been employed to generate ions in matrices. Matrix isolated ions can be of two kinds. The first kind is referred to as "chemically bound" ion pairs, such as $Li^+O_2^-$,[32] where, the cation and anion are in the same matrix cage, and can be thought of as a "chemically bound" pair. Their close proximity allows considerable overlap of the electron density of the ions, so the species may not resemble their isolated counterparts. The second kind of ion encountered in matrix isolation is an isolated ion, that is a part of what is called a Coulomb ion pair. In this case, the cation and anion are in separate matrix cages, and are therefore physically isolated from each other; however, they

are still stabilized by their coulombic force fields. The following is a brief review of some of the more successful ion generation and trapping schemes.

1. VUV Photolysis

This was the earliest technique, and is still the most widely used. As noted earlier, in 1970 Kasai and co-workers[20] produced Na^+ ions in an argon matrix by the photochemical reaction:

$$Na + HI + h\nu \rightarrow Na^{\cdot} + I^{-} + H$$

Electrons and H atoms can freely migrate in an argon matrix and can cause neutralization of cationic species. In this system, HI is used as a trap for the electrons removed from the Na atoms. HI undergoes dissociative electron capture and forms H and $I^{\cdot}$, which immobilizes the electrons and prevents the neutralization of $Na^{\cdot}$. An interesting aspect of this method is that light lower in energy than the ionization energy of the neutral precursor will induce photoionization. This can be understood in terms of the Coulomb-pair ions. The stabilization energy, E is calculated to be:

$$E = I.E. - E.A. - \frac{e^2}{4\pi\varepsilon r}$$

Where $I.E.$ is the ionization energy of the electron donor, $E.A.$ is the electron affinity of the acceptor, ε is the permittivity of the matrix, and r is the distance between the two ions. This is an example of ions being far enough away from each other to be chemically isolated, yet their coulomb fields still interact to stabilize the ion pair.[33] UV photolysis is usually performed *in situ,* although the matrix gases can be irradiated during deposition, also. This technique has the advantage of being relatively simple to implement, but suffers

from one major drawback. It is non-selective and usually results in the generation of several neutral and ionic products from the neutral precursor.[34]

2. Windowless Discharge

After photolysis, this is the second most popular form of ion generation. In this technique, the matrix gas is passed through a microwave discharge before condensation. Some of the atoms exit in a metastable state after passing through the discharge. There are two possible channels for ionization. The first is energy transfer upon a collision with a metastable atom. The second route is photoionization from the radiation released by the relaxing metastable atom.[35] This technique has been used to study ions such as $N_2O_2^{\bullet+}$,[36] $CO_2^{\bullet+}$,[37] $N_4^{\bullet+}$,[38] $O_4^{\bullet+}$,[39] and many others. With this method, secondary photophysical process are not as prevalent as in VUV photoionization, and it also seems to have greater ion yields than VUV photoionization. While this technique is somewhat more selective than VUV photolysis, there still can be several ionic products from a given precursor.

3. Ion Molecule Reactions

One of the more novel methods of ion generation involves the reactions of ions and neutral molecules. This technique was first reported by Knight, et al., in 1984.[40] Some of the systems studied were:

$$CO + CO^{\bullet+} \rightarrow C_2O_2^{\bullet+}$$

$$N_2^{\bullet+} + CO \rightarrow N_2CO^{\bullet+}$$

$$N_2^{\bullet+} + N_2 \rightarrow N_4^{\bullet+}$$

In these systems, the mechanism of ion formation is most likely co-condensation of the ion and neutral in the same matrix cage. The cage effect increases the collision frequency and

leads to formation of the ion-molecule pair. These experiments are very interesting in that along with spectroscopic information, the reaction chemistry can provide some insight into the dynamics of matrix isolated systems.

4. Chemical Ionization

In 1989 Hacaloglu and Andrews reported the use of a modified Finnigan 3200 chemical ionization source for generating ions for subsequent matrix isolation.[41] Argon and naphthalene vapor were passed through the source and focused onto the matrix window by a negatively biased (relative to the ion source) ring electrode placed near the substrate. They reported the appearance of $C_{10}H_8^{\bullet+}$ in the infrared spectrum, but it was not determined whether the ions were formed in the source, by collision with accelerated argon ions or by the discharge conditions existing in the vicinity of the ring electrode. This source was also used to study negative ions. A mixture of argon and Cl_2 was passed through the source and the ring electrode was biased to accelerate negative ions to the window. They reported the appearance of $Cl_2^{\bullet-}$ and Cl_3^- at higher source pressures.

5. Pulsed Glow Discharge

There has been debate about whether or not a sufficient number of ions can be externally generated and deposited onto a rare gas matrix for FTIR observation. A report by Vala and co-workers have shown that this is indeed possible.[42] In their experiment, ions are formed in a plasma generated between a stainless steel tube held at ground potential and a wire connected to a hemispherical grid held at +3 kV. The grid accelerates positive ions to the cryostat window, with focusing provided by a cylindrical lens. In preliminary experiments, a mixture of argon and p-dimethoxybenzene (PDMOB) was passed through the pulsed discharge. Many new bands appeared in the infrared spectrum

compared to observations in the absence of discharge. To test whether these were bands due to the PDMOB cation, photobleaching experiments were performed. During photobleaching, the intensity of a known electronic absorption of $PDMOB^+$ was monitored. Four of the new IR bands had photolytic decay characteristics which matched that of the electronic absorption, and were assigned to $PDMOB^+$. It is important to note, however, that the pulsed glow discharge is still a very non-selective technique, and that this experimental configuration provides only charge-selection, rather than mass-selection during deposition. Of the many new bands present under discharge conditions, only four were assignable to $PDMOB^+$.

6. Electron Bombardment

This technique was pioneered by Knight in 1983.[43] Electrons boiled off of a heated filament were focused onto and accelerated toward the matrix substrate. Knight found it necessary to float the matrix substrate at a positive potential to overcome the charge accumulation that developed. He used this method to study small ions such as $H_2O^{\bullet+}$, $CO^{\bullet+}$, $NH_3^{\bullet+}$, and $N_2^{\bullet+}$. Electron bombardment proved to produce greater ion signals than conventional ionization techniques such as windowless discharge. This method has the advantage of variability of the electron beam intensity and energy, but it is still not very selective. The experiments are also difficult to set up; Knight went to great lengths to electrically isolate the matrix target. Andrews has also reported use of this technique.[44] The Andrews group developed a thermionic emitter source capable of delivering 10-200 mA of electrons to a ring electrode placed near the matrix. Continuous bombardment of a 1000:1 argon:H_2O matrix resulted in spectroscopically observable amounts of OH^- and Ar_nH^+ ions, as well as OH radicals.

In recent years, this technique has perhaps been most successfully used in the Vala laboratory. By subjecting a gaseous mixture of argon, CCl_4, and precursor vapor to electron bombardment prior to condensation, they have been able to acquire the visible as well as FTIR spectra of the radical cations of several polycyclic aromatic hydrocarbons (PAHs) such as napthalene,[45] anthracene,[46] pyrene,[47] pentacene,[48] and tetracene.[49] In these experiments, CCl_4 is used as an electron scavenger to prevent neutralization of the cations. Although this technique does generate large amounts of cations, it still may not be a generally applicable technique. While electron bombardment resulted in the production of the molecular ions of the compounds studied, less stable precursors may undergo extensive fragmentation. Also, as in their pulsed glow discharge experiments, assignment of vibrational transitions depends on a correlation with a known electronic transition of the cation. Electronic transitions of the PAH radical cations are known, but this is not generally the case for polyatomic ions.

7. Mass Selected Deposition

The one feature common to all of the techniques mentioned previously is that the ionization is non-selective, albeit in varying degrees. Interpretation of the ensuing spectra would be much simpler if only one ionic species were present in the matrix, and its identity were known. In 1989, Maier and co-workers reported the development of the first successful mass-selective ion deposition source.[29] In their experiments, ions are formed in a remote source, mass filtered by a quadrupole mass spectrometer, and directed to the matrix substrate. As stated earlier in this chapter, the electronic absorption spectra of several cations were measured in the 220–1200-nm region by the waveguide technique. In 1991, Sabo et al. also reported the use of mass selected deposition to obtain the laser

induced fluorescence (LIF) spectrum of mass-selected $CS_2^{\bullet-}$ in argon.[30] The project described in this dissertation involves the application of mass-selected deposition to FTIR spectroscopy and gaining a more thorough understanding of this rather unique deposition process, particularly the maintenance of charge neutrality even though only positive ions are being presented to the matrix.

B. Criteria for Matrix Isolation

1. Inertness

This is perhaps the most obvious and important criterion for a matrix material. The matrix must be sufficiently inert so it will not chemically or physically perturb the guest species. The noble gases and molecular nitrogen are generally the only substances inert enough to trap highly reactive species, and therefore cryogenic temperatures must be employed to obtain rigid matrices. In the case of polyatomic ions, their high electron affinities leads to significant charge exchange interactions with xenon, krypton, and argon, necessitating the use of neon as the matrix host material. In some cases where the ion has an unusually low electron affinity (< 11 eV) argon may be used.

2. Rigidity

For the guest to be trapped and kept from reacting with other species in the matrix, the matrix must be rigid. Most matrices are considered rigid at 0.3 T_m, where T_m is the melting point of the host material. $0.3T_m$ corresponds to 7.3 K and 25 K for neon and argon, respectively. Being far below the boiling point of nitrogen (77 K), attaining these temperatures requires the use of special cryogenic techniques. Liquid hydrogen (20 K) and liquid helium (4.2 K) were the first refrigerants used. As liquid helium became more readily available the use of liquid hydrogen was disfavored because of its explosive

potential. In the early 1970s mechanical refrigerators capable of maintaining 12 K were developed and greatly expanded the field. Mechanical refrigerators capable of cooling to 3.6 K are now available, allowing neon matrices to be employed without the use of costly liquid helium. Maintenance of low temperatures also requires high vacuum conditions, since these cryogenic temperatures cannot be maintained at high pressures due to the increased heat load; moreover, the cooled substrates act as cryopumps, and would trap undesirable background gases in the matrix.

At temperatures above $0.5T_m$ matrix is considered non-rigid, and diffusion of trapped species occurs. In this case, reactive species will be lost due to reactions with other guests. Between $0.3T_m$ and $0.5T_m$ a process known as annealing occurs. Annealing is described as a rearrangement of the matrix at an atomic level to the most stable crystal structure. During this process, large trapped species can cause local rearrangement to give the best, or least perturbing cage. Annealing is often used to detect and minimize peaks caused by trapping of a guest species in multiple matrix sites. While this technique is commonly used with argon matrices, the relatively narrow annealing temperature range and volatility of neon makes the annealing of its matrices quite challenging.

3. Purity

Matrix impurities may cause perturbation of the guest species, should they become close enough to interact. Since it is essential that the guest be trapped in a uniform, inert matrix, the matrix material must therefore be very pure. This necessitates the use of high purity matrix material and high vacuum techniques to prevent contamination during deposition of the host and guest species on the cooled optical substrate.

4. Transparency

The matrix material must be transparent to the radiation being used for spectroscopic observation. Noble gas solids are exceptionally suitable in this respect. Being atomic solids, they exhibit no rotational or vibrational transitions. Argon and neon provide a spectroscopic window from the vacuum ultraviolet to approximately 100 cm^{-1}, where lattice vibrations become excited. The noble gases are also diamagnetic, which makes them transparent to ESR spectroscopy, although the magnetically active nuclei of krypton and xenon can affect the hyperfine splittings of trapped species.[31]

5. Thermal Properties

During condensation, the latent heat of fusion (L_f) of the matrix material is released. This heat must be conducted away from the surface through the matrix by the cryostat. The matrix must have a high thermal conductivity so that this heat conduction does not cause any local warming. Matrices experiencing local warming due to low thermal conductivity are often opaque and highly scattering, and can possibly lose reactive species through diffusion.

6. Volatility

In order to prevent loss of matrix material and the species trapped within due to evaporation, the matrix material must not be volatile at the temperatures being used.

C. Trapping Ions in Matrices

The trapping of ions in matrices is at times more an art form than a scientific process. Along with the proper choice of matrix material, the proper deposition conditions must also be maintained to ensure successful trapping. Optimization of such parameters as deposition rate and matrix to guest (M/G) ratio are critical. Also, since it

seems that the matrix must be approximately electrically neutral, counter ions must also be present to maintain charge neutrality.

1. Deposition Rate

As described previously, the temperature of the matrix must be kept below during deposition $0.3T_m$ to prevent annealing or diffusion. The matrix gas must also condense as fast as possible to ensure efficient trapping; i.e. the latent heat of fusion of the matrix gas must be conducted away by the cryostat as quickly as possible. This requires not only the use of a sufficiently powerful cryostat, but a slow enough deposition rate so that the latent heat of fusion released does not cause an appreciable warming of the matrix. The power liberated by the latent heat of fusion is given by the equation:

$$L_f n = \left\{ \frac{\lambda A (T - T_0)}{w} \right\}$$

where

L_f = latent heat of fusion ($^{cal}/_{mol}$)

n = deposition rate ($^{mol}/_{s}$)

λ = thermal conductivity ($\frac{cal}{cm \cdot s \cdot K}$)

T, T_o = surface and matrix temperature (K), respectively

w = matrix thickness

A= matrix surface area

The thickness of the matrix is given by:

$$w = \frac{nt}{\rho A}$$

where t is the deposition time and ρ is the molar density of the matrix material. The surface temperature of the matrix can now be described by the equation:

$$T = T_0 + \left\{ \frac{L_f n^2 t}{\lambda \rho A^2} \right\}$$

Substitution of typical parameter values indicate that deposition rates of 1-18 mmol/hr will result in a temperature increase of approximately one degree after several hours of continuous deposition. The deposition time will affect the maximum usable flow rate. When long depositions are expected, the matrix gas must be deposited very slowly to avoid excessive heating.[50]

2. Matrix-to-Guest (M:G) Ratio

To ensure complete isolation, the M:G ratio must be high enough that very few guests will have another guest as a nearest neighbor. For example, in the body centered cubic structure of solid neon, a substitutional site (created by the removal of one neon atom) has twelve nearest neighbors. A guest occupying that site may be considered to be isolated if all of its nearest neighbors are neon atoms. The probability that this guest is not isolated can be expressed as:[31]

$$P = (1 - r)^{12}$$

where r is the ratio of guest to matrix atoms. With a M:G ratio of 100:1 11.4% of the guests will have another guest as a nearest neighbor, leaving only 88.6% of the guest molecules completely isolated. A M:G ratio of 1000:1 will provide 98.8% isolation, and a ratio of 10 000:1 will provide 99.9 percent. Due to their size, most polyatomic species

will occupy multiple substitutional sites (site created by the removal of more than one neon atom). As an example, a species three times the size of a matrix atom will most likely occupy a site created by the loss of one atom, and its 12 nearest neighbors. Such a site creates a cage with 122 nearest neighbors. The probability of isolation in this cage is given by:

$$P = (1-r)^{122}$$

requiring ratios of 10 000:1 or greater to achieve 99% isolation.[31]

3. Counterions

It is usually assumed that an ion-containing matrix maintains at least approximate electrical neutrality. This neutrality is made possible by the existence of counter ions in the matrix, i.e. ions of opposite charge to the ions being studied. Since most matrix studies involve cations, the counter ions are usually negatively charged. Many researchers report the presence of both positively and negatively charged species in matrices but usually no correlation can be made between the relative intensities of the two types of ionic species.[34,51] To date, the most popular explanation for the formation of these anions is that they are formed by electron attachment to electronegative matrix impurities such as O_2, CO_2, and OH (from H_2O).[52] Although this concept seems quite intuitive, definitive experimental evidence is still lacking.

While counter ions are usually assumed to exist and not considered explicitly, some experiments have been performed that address the issue in some way. In one set of experiments, Knight purposely doped his matrix with an electrophile, F_2, in hopes of increasing the number of cations stabilized in the matrix.[53] Although an electron capture product was found after photolysis ($F_2^{\bullet-}$), the yield of the cation was not affected

appreciably by the intentional addition of the counterion. This contrasts with reports from the Vala laboratory that the addition of CCl_4 as an electron scavenger dramatically improves the yield of stabilized cations.[45]

While many of the ionization techniques, such as photolysis and discharge ionization, are capable of producing both positively and negatively charges species, this raises a special concern in the case of mass-selected deposition. In this case, ions of one type of charge only are intentionally introduced into matrix. Is there some mechanism by which anions can be generated, or will a separate source of negative ions be necessary to achieve the necessary approximate electrical neutrality of the matrix?

D. Matrix Effects on Ionic Spectra

Although matrices are ideally a non-perturbing medium, the interactions between the guest and host are sufficient to cause some spectral changes relative to the gas phase spectrum. Matrix vibrational spectra are characterized by narrow bands relative to the gas phase. Electronic transitions, however, are generally much broader in matrices than in the gas phase. In general, matrices have been seen to affect the position, appearance, and number of peaks. A brief discussion of these effects follows.

1. Number of Peaks

Since the matrix is never a perfectly ordered solid, all of the possible trapping sites are not identical. As a result, the interaction forces felt by the guest ions are not uniform. The differences in the interaction may be enough to produce distinct vibrational motions. Such multiple site features can usually be detected by annealing. During the annealing process, the matrix becomes more uniform, as do the trapping sites. If a certain multiplet is due only to inequivalent matrix sites, the multiplet will become a singlet. The multiplet

may remain, however, if the inequivalent site is due to an interaction with an impurity in the matrix.

2. Frequency Shift

There is in generally a shift between a matrix absorption frequency and the gas phase absorption frequency. These shifts can be explained by the types of interactions which also describe shifts between gas and solution phase frequencies. Solution interactions are generally described in terms of a combination of dipole-dipole, dipole-induced dipole, ion-ion, ion-dipole, and London dispersion forces. The strength of these interactions depends to a large extent on the polarizability of the molecule, and of the host. In a matrix, as in solution, the general trend is towards a lowering in energy (redshifting) of molecular transitions.

One fundamental difference between matrices and solutions is that the solvent cage is much more rigid in matrices. This gives rise to an interaction generally not encountered in solution, repulsive forces. The neglect of these forces is a serious shortcoming in the prediction of matrix spectral shifts, as these forces may become strong enough to overpower the attractive forces. This especially true of low energy vibrations, where the matrix cage can severely distort the vibrational motion. The total matrix frequency shift can be summed up by the expression:[54]

$$\Delta\nu = \nu_{matrix} - \nu_{gas} = \Delta\nu_{elec} + \Delta\nu_{ind} + \Delta\nu_{disp} + \Delta\nu_{rep}$$

where ν_{matrix} refers to the matrix-isolated frequency, ν_{gas} refers to the gas-phase frequency, $\Delta\nu_{elec}$ refers to the shifts due to the permanent dipole distribution, $\Delta\nu_{ind}$ refers

shifts due to induced dipole/induced dipole interactions, $\Delta\nu_{disp}$ refers the shifts due to dispersion forces and $\Delta\nu_{rep}$ refers to the shifts due to repulsive interactions.

As the host polarizability increases, interactions with guest species increase, and there is a trend towards redshifted frequencies. The shift usually becomes less negative as the frequency decreases. As the frequency of the vibration becomes even lower, the shift may become positive.[31] This is because vibrations characterized by a small force constant are easily distorted by the matrix cage. A recent review by Jacox[55] reports vibrational matrix shifts for diatomic species to be less than 1% for neon, and less than 2% in argon, with red shifts being more common than blue shifts. Larger than normal shifts are found in systems which exhibit 1) hydrogen bonding within the matrix, 2) cage stabilization of weakly bound species, 3) species with a large dipole moment, where it is assumed that both the gas phase and matrix transitions are correctly assigned. Neutral molecules are generally less affected than ions by this effect since they less strongly polarize the host atoms.

3. Spectral Distortion

In general, distortion of the guest spectra by the host is negligible for neutral species, but can be very significant for ionic species. Argon is fairly polarizable, and can interact with trapped ions by ion induced-dipole interactions. These interactions do not severely distort vibrational transitions, but they can markedly affect electronic spectra.[56] The electronic transitions are usually red shifted and broadened. As a result, ions with an electron affinity greater than about 10 eV experience electronic spectral distortion in argon. Neon is much less polarizable than argon, and is therefore the matrix of choice for ionic studies.

4. Vibrational Relaxation

In addition to the effects resulting from the perturbations of the electronic structure of the trapped ions, fluorescence experiments are affected in another way by the matrix. When an ion is excited to a vibrational level within an excited electronic state, two relaxation pathways are possible. The ion can fluoresce directly from the excited vibrational state to the ground electronic state, or it can relax to the ground vibrational level of the excited electronic state and then fluoresce to the ground electronic state. In the gas phase, the first pathway is commonly observed. Only large molecules having a high density of vibrational states exhibit vibrational relaxation in the excited electronic state. In matrices, vibrational relaxation is invariably observed, even for small molecules. This is because the phonon modes of the matrix are an efficient channel for the dissipation of vibrational energy.[57] This simplifies the spectra, but also limits the vibrational information obtainable from matrix fluorescence experiments to the ground electronic state of the guest.

List of References

(1) Szczepanski, J.; Vala, M. *Nature*, **1993,** *363*, 699.

(2) McEwan, M. J.; Phillips, L. F. *Chemistry of the Atmosphere;* Halsted: New York, 1975; Chapter 6.

(3) Bouchoux, G.; Hoppilliard Y. *J. Mol. Struct.* **1983,** *104*, 365.

(4) Based on HF calculation using 6-31g** basis set.

(5) Weber, R.; Levsen, K. *Org. Mass Spectrom.* **1980,** *15*, 138

(6) Terlouw, J. K.; Heerma, W.; Dijkstra, G. *Org. Mass. Spectrom.* **1980,** *15*, 660.

(7) Stepnowski, R.; Allison, J. *Anal. Chem.* **1987,** *59*, 1072A.

(8) Herzberg, G. In *Molecular Ions: Spectroscopy, Structure, and Chemistry;* Miller, T. A., Bondybey, V. E., Eds.; North Holland: New York, 1983; pp 1-9.

(9) Wing, W. H.; Ruff, G. A.; Lamb, W. E.; Speezeski, J. J. *Phys. Rev. Lett.* **1976,** *36*, 1488.

(10) Carrington, A.; Sarre, P. J. *Mol. Phys.* **1977.** *33*, 1488.

(11) Cosby, P. C.; Ozenne, J. B., Moseley, J. T.; Albrittion, D. L. *J. Mol. Spectrosc.* **1980,** *79*, 203.

(12) Saykally, R. J.; Evenson, K. M. *Phys. Rev. Lett.* **1979,** *43*, 515.

(13) Oka, T. *Phys. Rev. Lett.* **1980,** *45*, 531.

(14) Gudeman, C. S.; Begemann, M. H.; Pfaff, J.; Saykally, R. J. *Phys. Rev. Lett.* **1983,** *50*, 727.

(15) Foster, S. C.; McKellar, A. R. W.; Sears, T. J. *J. Chem. Phys.* **1984,** *81*, 578.

(16) Kawaguchi, K.; Hirota, E. *Ann. Rev. Phys. Chem.* **1985,** *36*, 53.

(17) Coe, J. V.; Saykally, R. J. "Infrared Laser Spectroscopy of Molecular Ions," in *Ion and Cluster Ion Spectroscopy and Structure;* J. P. Maier, Ed. Elsevier Science Publishers B. V., Amsterdam, 1989 Chap. 5

(18) Whittle, E.; Dows, D. A.; Pimentel, G. C. *J. Chem. Phys.* **1954,** *22*, 1943.

(19) Perutz, R. N. *Ann. Rep. Prog. Chem.* **1985,** *82*, 157.

(20) Kasai, P. H. *Acc. Chem. Res.* **1971,** *4,* 329.

(21) Jacox, M. E. *Chem. Phys.* **1994,** *189,* 149.

(22) Andrews, L.; Keelan, B. W. *J. Am. Chem. Soc.* **1981,** *103,* 99.

(23) Bondebey, V. E.; Miller, T. A. *J. Chem. Phys.* **1980,** *73,* 3053.

(24) Jacox, M. E.; Thompson, W. E. *J. Chem. Phys.* **1989,** *91,* 1410.

(25) Szczepanski, J.; Personette, W.; Pellow, R.; Chandrosekhar, T. M.; Roser, D.; Cory, M.; Zerner, M. Vala, M. *J. Chem. Phys.* **1992,** *96,* 35.

(26) Knight, L. B.; Steadman, J. *J. Chem. Phys.* **1982,** *77,* 1750.

(27) Rivoal, J. C.; Emampour, J. S.; Zeringue, K. J.; Vala, M. *Chem. Phys. Lett.* **1992,** *92,* 313.

(28) Bondybey, V. E. "Time-Resolved Laser-Induced Fluorescence Studies of Spectroscopy and Dynamics of Matrix-Isolated Molecules," in *Chemistry and Physics of Matrix-Isolated Species;* Andrews, L.; Moskovits, M. Eds.; Elsevier Science Publishers B. V.: Amsterdam, **1989,** Chapter 5, p 129.

(29) Forney, D.; Jakobi, M.; Maier, J. P. *J. Chem. Phys.* **1989,** *90,* 600.

(30) Sabo, M. S.; Allison, J.; Gilbert, J. R.; Leroi. G. E. *Appl. Spectrosc.* **1991,** *45,* 535.

(31) Cradock, S.; Hinchcliffe, A. J. *Matrix Isolation;* Cambridge University: Cambridge, 1975; Chapter 2.

(32) Knight, L. B., Jr, *J. Chem. Phys.* **1983,** *78,* 6715.

(33) Peruz, R. N. *Chem. Rev.* **1985,** *85,* 97.

(34) Prochaska, F. T.; Andrews, L. *J. Am. Chem. Soc.* **1978,** *100,* 2102.

(35) Jacox, M. E.; Thompson, W. E. *Res. Chem. Int.* **1989,** *12,* 33.

(36) Jacox, M. E.; Thompson, W. E. *J. Chem. Phys.* **1990,** *93,* 7603.

(37) Thompson, W. E.; Jacox, M.E. *J. Chem. Phys.* **1989,** *91,* 1410.

(38) Thompson, W. E.; Jacox, M. E. *J. Chem. Phys.* **1989,** *91,* 3856.

(39) Thompson, W. E.; Jacox, M. E. *J. Chem. Phys.* **1989,** *91,* 3826.

(40) Knight, L. B. Jr.; Steadman, J.; Miller, P. K.; Bowman, D. E.; *J. Chem. Phys.* **1984,** *80,* 4593.

(41) Hacaloglu, J.; Andrews, L. *Chem. Phys. Lett.* **1989,** *160,* 274.

(42) Szczepanski, J.; Personette, W.; Vala, M. *Chem. Phys. Lett.* **1991,** *185,* 324.

(43) Knight, L. B. Jr. *J. Chem. Phys.* **1983,** *78,* 6715.

(44) Suzer, S.; Andrews, L. *J. Chem. Phys.* **1988,** *88,* 916.

(45) Szczepanski, J.; Roser, D.; Personette, W.; Eyring, M.; Pellow, R.; Vala, M. *J. Phys. Chem.* **1992,** *96,* 7876.

(46) Szczepanski, J.; Vala, M; Talbi, D.; Parisel, O.; Ellinger, Y. *J. Chem. Phys.* **1993,** *98,* 4494.

(47) Vala, M; Szczepanski, J.; Pauzat, F.; Parisel, O.; Talbi, D.; Ellinger, Y. *J. Phys. Chem.* **1994,** *98,* 9187.

(48) Szczepanski, J.; Wehlburg, C.; Vala, M. *Chem. Phys. Lett.* **1995,** *232,* 221.

(49) Szczepanski, J.; Drawdy, J.; Wehlburg, C.; Vala, M. *Chem. Phys. Lett.* **1995,** *245,* 539.

(50) Moskovits, M; Ozin, A. In *Cryochemistry*; Moskovits, M.; Ozin, A. Eds.; John Wiley and Sons, New York, **1983,** Chapter 4.

(51) Suzer, S.; Andrews, L. *J Chem. Phys.* **1988,** *88,* 916.

(52) Andrews, L. *Ann. Rev. Phys. Chem.* **1979.** *30,* 79.

(53) Knight, L. B. Jr.; Earl, L.; Ligon, P. R.; Cobranchi, D. P. *J. Phys. Chem.* **1986,** *85,* 1228.

(54) Downs, A. J.; Peuke, J. C. *Molecular Spectroscopy: A Specialist Periodical Report;* Burlington House: London, **1973,** *1,* Chapter 9.

(55) Jacox, M. E.; *J. Mol. Spectrosc.* **1985,** *113,* 777.

(56) Bondybey, V. E.; English, J. H. *J. Chem. Phys.* **1979,** *71,* 777.

(57) Bondybey, V. E.; Miller, T. E. in *Molecular Ions: Spectroscopy, Structure, and Chemistry;* Bondybey, V. E.; Miller, T. E., Eds; North Holland: New York, NY, **1983;** Chap. 4.

Chapter 2

Instrumental

In order to better understand of the structure and chemistry of polyatomic species, instrumentation has been developed to isolate and spectroscopically observe mass-selected, matrix-isolated ions. In these experiments, cations are generated by electron impact ionization, mass selected by a quadrupole mass filter, and directed to a low-temperature window and condensed with an excess of neon. The trapped ions can then be studied by a variety of spectroscopic techniques, with FTIR absorption and visible emission being the focus of the work described in this dissertation. The instrumentation necessary for spectroscopic observation of mass-selected, matrix isolated ions relies on the implementation and coordination of several different technologies. Among these are mass spectrometry, ion optics, vacuum generation, cryogenics, spectroscopy, data acquisition, and signal processing. Instrumentation to apply the mass-selection technique to laser induced fluorescence (LIF) has been previously developed in this laboratory[1] and is described in detail elsewhere.[2] The instrumentation used in this research is based on that LIF system; however, many modifications and improvements have been implemented.

I. Ion Source, Mass Filter, and Ion Optics

In any study of polyatomic ionic species, the first, and usually most critical, step is to generate the ions of interest. The ion source in these experiments is a modified Finnigan 3200 quadrupole mass spectrometer. Cations are generated in the original electron impact ionization source. The quadrupole mass filter is then used to produce a beam of mass-selected ions. The emerging beam is then focused and directed to the

cryogenic window by a series of ion optics and steering plates. This system is capable of generating mass-selected ion currents of 20–80 nA for periods of up to 30 hours.

This ion source represents a great improvement over the previous ion sources.[3] The Finnigan source produces ion beams nearly two orders of magnitude greater than the original ion sources. The ion source and quadrupole are also differentially pumped, which has reduced the influx of neutral species into the UHV chamber by two orders of magnitude. The 1–700 Dalton mass range of the Finnigan source is also an improvement over the 1–200 and 1–60 Dalton ranges of the RGA ion sources.[3] A schematic of this ion source is shown in Figure 2.1. A complete description of the modification of the mass spectrometer and construction of the ion optical system can be found elsewhere.[4]

II. Vacuum System

The primary need for high vacuum conditions in matrix isolation experiments arises from the need to thermally isolate the cryogenic substrate. Without this insulation, the low temperatures necessary could not be achieved due to the excessive heat load from the surrounding atmosphere. While pressures of 1×10^{-5} Torr are sufficient for thermal insulation, certain aspects of our experiments required ultra-high vacuum (UHV) conditions ($< 1 \times 10^{-8}$ Torr). The main reason was to minimize the amount of residual gases in the system, in order to reduce the possibility that the small absorption of a mass-selected ion would be hidden by a large absorption due to residual gases. Another reason was to ensure matrix purity. As a rare gas matrix grows, the heat of fusion of the most recently condensed layer must be transported through the previously condensed layers to the cryostat. As the matrix thickens, this heat transport becomes less efficient. It is possible that the matrix will become thick enough that any additional gas cannot be cooled

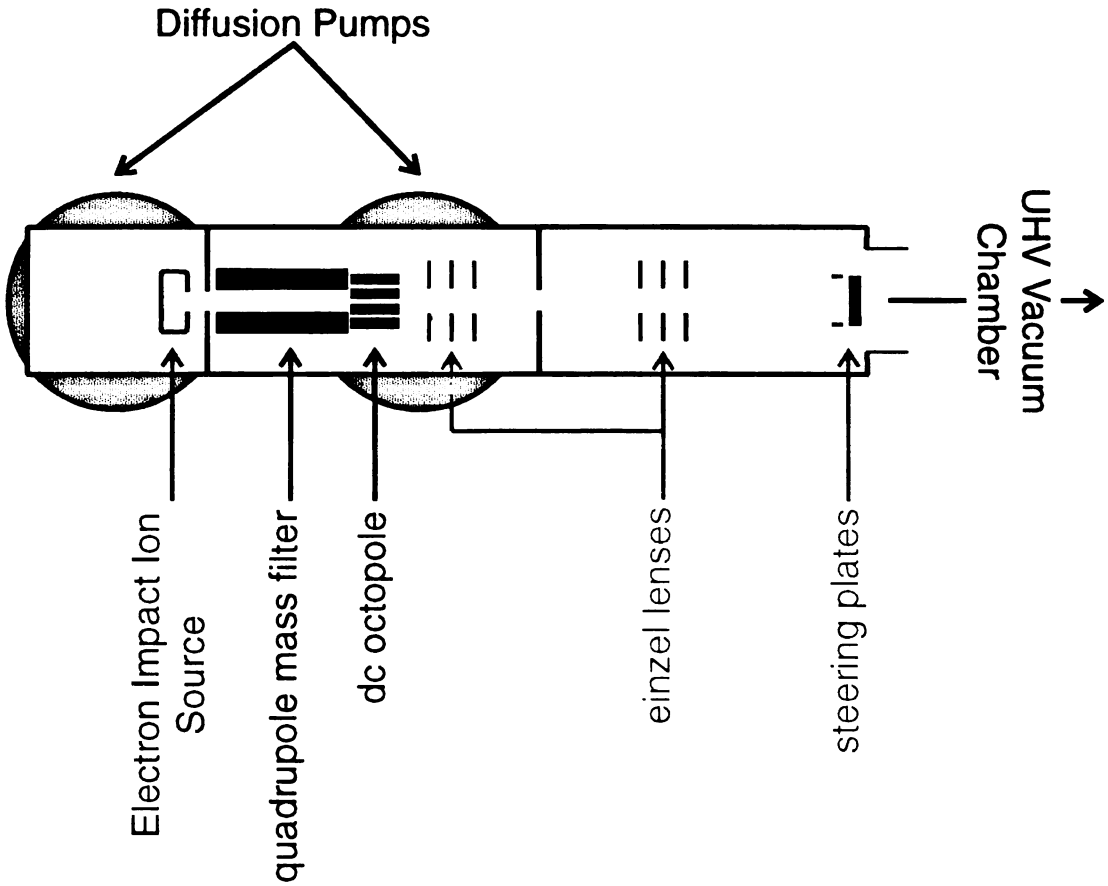

Figure 2.1: Schematic top view of mass-selected cation source based on modified Finnigan 3200 quadrupole mass spectrometer.

rapidly enough, and matrix growth will cease. Since long (25–30 h) deposition times were expected, very slow deposition rates were necessary to ensure adequate cooling of the matrix. With a small flux of matrix material on the substrate, the residual gases become a greater fraction of the material condensing on the cryogenic substrate. If residual gases make up 1% or more of the frozen material, at least 12 % of the ions will have a residual gas molecule as a nearest neighbor, and hence will not be truly isolated. The need for a such a pure matrix has dictated the design of the of the matrix isolation chamber and its vacuum system. The maintenance of pressures $< 1 \times 10^{-8}$ Torr is not a trivial task, and requires great care in choice of materials and construction methods.

A. Vacuum Chamber

The UHV chamber is constructed from a 8" O.D. stainless steel cylinder. To minimize the system's leak and outgassing rate, all permanent joints and seals are either welded or silver soldered, and all non-permanent seals are made with all-metal Conflat[®] flanges. The top and bottom of the tube is fitted with 10 in. Conflat® flanges. The top flange supports the cryostat, roughing line, and the residual gas analyzer (RGA). The bottom flange is connected to a 10" electropneumatic gate valve which acts as a support for the chamber and separates the chamber from the cryopump. The chamber is also fitted with various ports to allow connection of various components such as the ion source, optical windows, current measurement, N_2 purge, etc. The ion source is connected via a 6" Conflat® flange and is separated by a manual 4" gate valve (MDC #GV-400M). Optical access to the matrix window is provided by windows mounted on 2¾" conflat flanges. Depending on the spectroscopic application, either KBr, CaF_2, or sapphire windows were used.

B. Pumping System

To keep the UHV chamber as clean as possible, a cryopump is used to evacuate it. These pumps have the advantages of very high pumping speeds (~1500-2000 l/s), and low base pressures, and provide an oil free environment. The chamber was originally evacuated with a Leybold-Heraeus 8'' cryopump (RPK 1500) driven by a RW3 compressor. This unit sustained irreparable failure and has been replaced with an APD Cryogenics 8'' cryopump (APD-8) driven by a HC-2 compressor. When the chamber is at atmospheric pressure, it is first roughly evacuated with a direct drive mechanical pump (Leybold–Heraeus Trivac D16A). To minimize the amount of backstreaming from the rough pump, a molecular sieve trap (L–H 85415, 10 Å sieves) is used. The mechanical pump is separated from the chamber by a manual bellows valve (Hughes Aircraft #HVV-150-2). The main chamber is isolated from the cryopump by a 10" electropneumatic gate valve (VAT 10146-UE40). The foreline valve of the cryopump is sealed with a electropneumatic valve (L-H. 289-22-B1). Pressure in the chamber is measured with a residual gas analyzer (RGA, Dycor M100). This device is essentially a small quadrupole mass spectrometer with a high efficiency ion source. It has the advantage of not only measuring the total pressure in the chamber, but also makes it possible to identify the individual species present in the UHV chamber, as well as their relative amounts. The base pressure of the experimental as measured by the RGA is ~5 × 10^{-9} Torr. During matrix deposition, the pressure rises to ~ 7.5 × 10^{-7} Torr. A schematic of the UHV system is shown Figure 2.2.

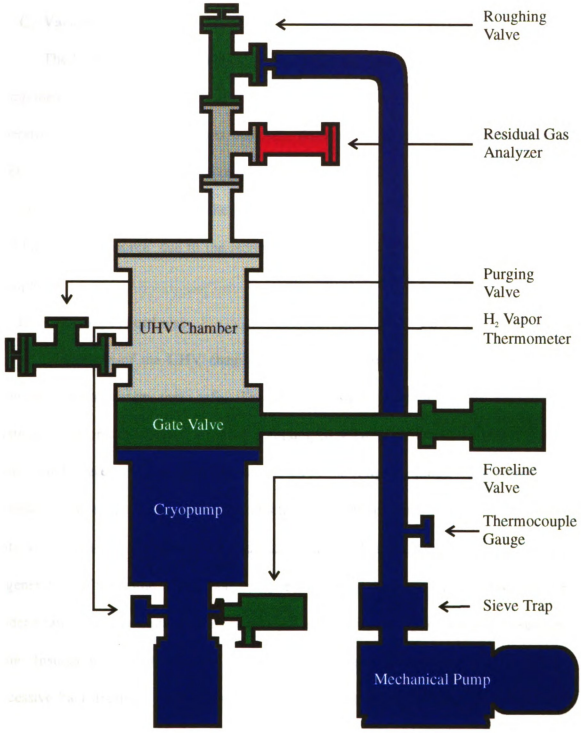

Figure 2.2: UHV pumping system.

C. Vacuum Interlock

The UHV system was designed with an interlock system to protect various system components in case of vacuum and/or power failure, and also to protect the system from operator error. The interlock was originally designed to control and supply power to every component of the mass-selected deposition system. While the protection scheme of this system remains unchanged,[2] the interlock is no longer be used to power the cryostat and Finnigan ion source, due to the increased electrical power requirements of the newer equipment.

D. Pumping Procedures

Evacuation of the UHV chamber is a relatively simple procedure, and with the interlock control system, quite safe. The vacuum system is similar to most cryopumped systems, with one exception. In most cryopumped vacuum systems, the pump and the main chamber are usually individually connected to the roughing pump. The cryopump is generally evacuated through its foreline and the chamber through a different valve, while a gate valve separates the cryopump and the chamber. This is usually done to facilitate regeneration of the pump. This was not a great concern, since our UHV system operates under a fairly low gas load, and the cryopump does not require regeneration for weeks at a time. Instead, we roughly evacuate the cryopump through the main chamber. To prevent excessive backstreaming of the mechanical pump oil, the chamber then is purged with nitrogen while the pump cools to its ultimate temperature of ~14 K, and to pump it down to no less than 50 mTorr before the gate valve is opened The standard pumpdown procedure for the ultra high vacuum chamber, if the cryopump is at room temperature is as follows:

1. shut off nitrogen purge
2. close cryopump foreline valve
3. open gate valve (should already be opened)
4. open roughing valve and evacuate chamber and cryopump to ~ 15 mTorr with mechanical pump
5. close gate valve
6. turn on cryopump
7. close roughing valve
8. purge chamber with house nitrogen until cryopump is cool
9. once cryopump cools (~ 90 min), shut of nitrogen purge
10. open roughing valve and evacuate chamber to ~ 50 mTorr
11. close roughing valve
12. open gate valve
13. turn on RGA
14. engage interlock

If the cryopump is already cooled, the following procedure should be used:

1. shut off nitrogen purge
2. open roughing valve and evacuate chamber to ~ 50 mTorr
3. close roughing valve
4. open gate valve
5. turn on RGA
6. engage interlock

E. Faraday Plate Modifications

The UHV chamber was originally designed with a Faraday plate to measure the ion current impringing on the matrix window and to allow re-optimization of the ion beam during deposition. The Faraday plate is mounted on a linear motion feedthrough (MDC LM-133-2) to allow it to be moved in and out of the ion beam. The replacement of the Displex® cryostat with the three-stage Heliplex® required some modifications to the Faraday plate, which is now used to measure the ion current emanating **from** the matrix upon warming as well. First, to account for the smaller window size, the plate was reduced to ¾" diameter. The Displex® also did not require a radiation shield, whereas the use of one is critical for the Heliplex®. To provide appropriate clearance of the radiation shield, ~ ¾" was cut off of the end of the feedthrough. A thin strip of stainless steel was attached to the end of the feedthrough. This strip was bent forward to allow the Faraday plate to clear the radiation shield. The Faraday plate is secured to the stainless steel strip by a small nut and bolt, and electrically isolated by the use of ceramic washers. The Faraday plate is electrically connected to an ammeter via a Teflon coated copper wire and a BNC feedthrough mounted on a 1 ⅓" Conflat® flange. This assembly is shown in Figure 2.3.

III. Cryostat

It has been the goal of this project to build an instrument which permits trapping and spectroscopic observation of a variety of polyatomic ions of interest to chemists. Since many of these ions have electron affinities close to the ionization potential of argon, neon matrices must be used. Initial experiments in this project were performed using an Air Products Displex® 202 cryostat driven by an air-cooled 1R02A

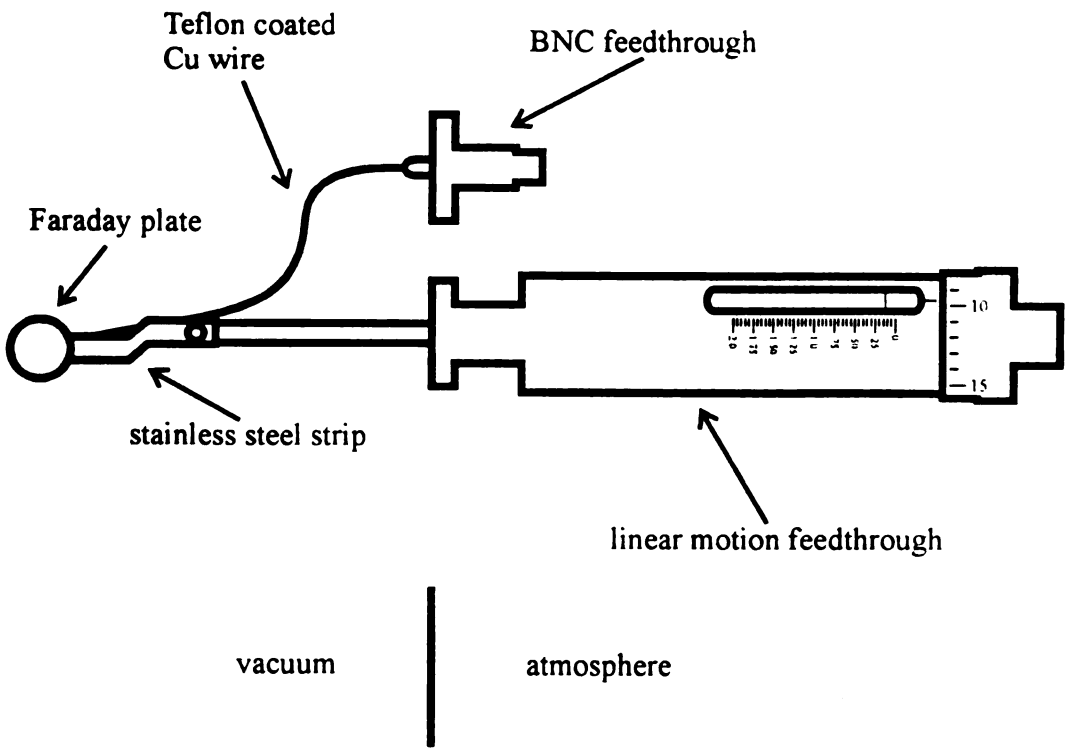

Figure 2.3: Faraday plate assembly

compressor. A description of this system and its adaptation to the UHV chamber can be found elsewhere.[2] This two-stage closed cycle unit was capable of reaching temperatures as low as 16 K. This restricted studies to argon matrices, which severely limited the number of ions that could be studied.

Even when they run at peak performance, the lowest temperature than can be attained with such two-cycle Gifford-McMahon refrigerators is ~10 K. Since neon matrices require a temperature of 7.2 K or less, a more efficient cooling system is required. The two preferred methods are the use of liquid helium, or the use of a three-stage closed cycle refrigerator. Since the high cost of liquid helium makes very long (24 hour) experiments prohibitively expensive, the Displex® was replaced with an APD Cryogenics HS-4B Heliplex® closed cycle cryostat.

A. Refrigerator

The Heliplex® cryostat achieves temperatures below the 10 K limitation of two-stage Gifford-McMahon refrigerators by implementing a third cooling stage based on the Joule–Thompson (J–T) effect. This cooling stage is based on the principle that a gas will cool when undergoing free expansion. Each gas, however, has a characteristic temperature (the J–T inversion temperature) above which the effect is inverted and the gas will actually warm upon expansion. The J–T inversion temperature of helium is 100 K, and the gas must be significantly below this temperature for cooling to be efficient. In the Heliplex® refrigeration cycle, the helium refrigerant is split into two streams. One stream undergoes the two-stage Gifford–McMahon cycle and is successively cooled to approximately 50 K and 10 K. The other stream of helium is then cooled by these two cold stations. This helium is now well below it's J–T inversion temperature, and

undergoes significant cooling upon free expansion. The expansion is controlled by changing the diameter of the orifice through which the helium expands. This is accomplished via a rotary motion feedthrough on the cryostat's refrigeration shroud. The Heliplex® refrigeration cycle is shown in Figure 2.4. This three stage cryostat has a cooling capacity of 1 Watt at 4.2 K, with a ultimate temperature of 3.6 K or lower. Figure 2.5 shows a typical cooldown to 4 K, which generally takes ~3 hours.

The HS-4B cryostat is factory modified for ultra-high vacuum service. These modifications include:

- 6" o-ring flange replaced with a 8" rotatable Conflat® flange
- o-ring sealed instrumentation feedthroughs replaced with equivalent conflat hardware
- standard HMX series vacuum shroud deleted
- standard evacuation port and valve deleted
- the third stage was lengthened so that the sample window would be centered in the UHV chamber windows
- the rotary motion feedthrough controlling the Joule–Thompson expansion valve was replaced with a comparable UHV compatible feedthrough

The replacement of the rotary motion feedthrough with a similar UHV feedthrough changed the operating procedures of the cryostat. The numbering convention of the UHV feedthrough is reversed from that of the standard feedthrough. On HS-4B, the J–T valve is fully open when the micrometer reads 0.000 and is fully closed when the micrometer reads 0.170. The micrometer should never be adjusted below 0.000 or above 0.170, or permanent damage to the J–T expansion circuit my result.

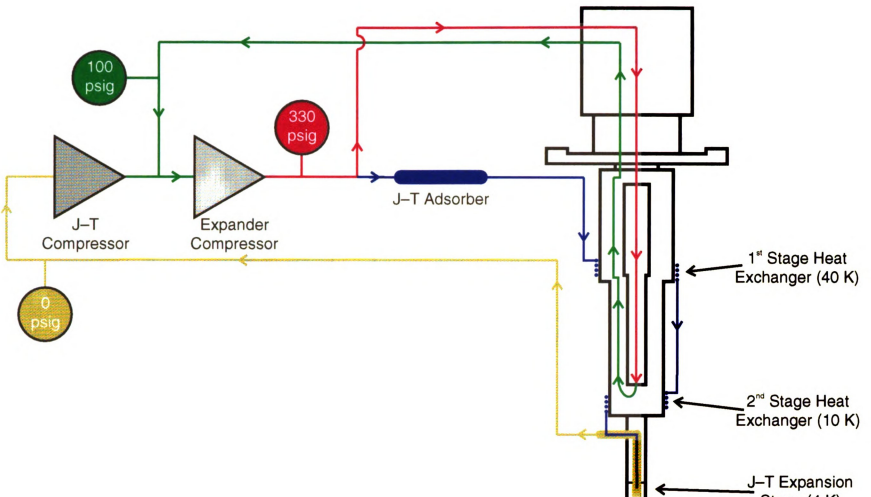

Figure 2.4: Heliplex piping schematic diagram. Pressures and temperatures shown are with the system operating at minimum temperature.

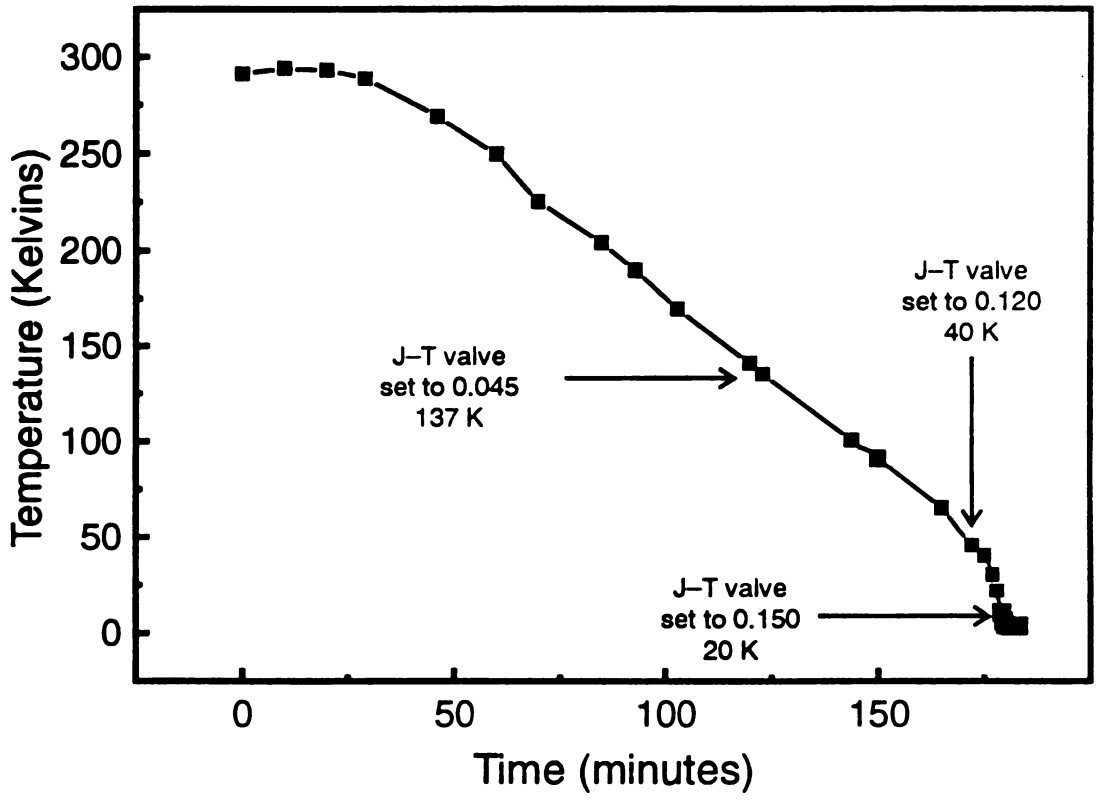

Figure 2.5: Typical Heliplex cooldown. Temperature is measured at the fixed third-stage sensor.

The addition of a J–T expansion circuit allows liquid helium temperatures to be reached, but also introduces some complications into the maintenance of the system. First, the helium gas is expanded through a very small orifice, which can be easily clogged by the condensation of impurities such as air and water in the gas. This results in the refrigerator being extremely sensitive to helium contamination. Second, the efficiency of the J–T expansion cycle is also dependent on the initial temperature of the helium gas. If the supply pressure of helium is too low, the temperature of the two Gifford–McMahon stages will be somewhat high, which in turn raises the temperature of the helium stream undergoing J–T expansion, resulting in less efficient cooling and a decreased refrigeration capacity. Finally, the return pressure of the J–T circuit is dependent of the J–T valve setting. At temperatures below 4.4 K, the return pressure is below atmospheric pressure. Under these conditions, any leaks in this circuit will result in air leaking into the system, and will severely degrade its performance. A more complete description of the system maintenance can be found in the Heliplex® Refrigeration System Technical Manual.[5]

A new top flange for the vacuum chamber was designed to accommodate the larger size of the three stage cryostat. The cryostat mates to the top flange through a 4'' OD tube which is welded to an 8'' Conflat® flange. This flange then connects with an 8'' conflat at the bottom of the 5'' shroud of the Heliplex®. The upper end of this shroud is connected to a 8'' Conflat® on the instrumentation skirt of the refrigerator. This assembly is shown in Figure 2.6.

B. Temperature Control

Temperature control of the cryostat is maintained by two Si diode sensors (Lake Shore Cryotronics DT-470), and a 36 Ω foil heater, controlled by a Lake Shore 330

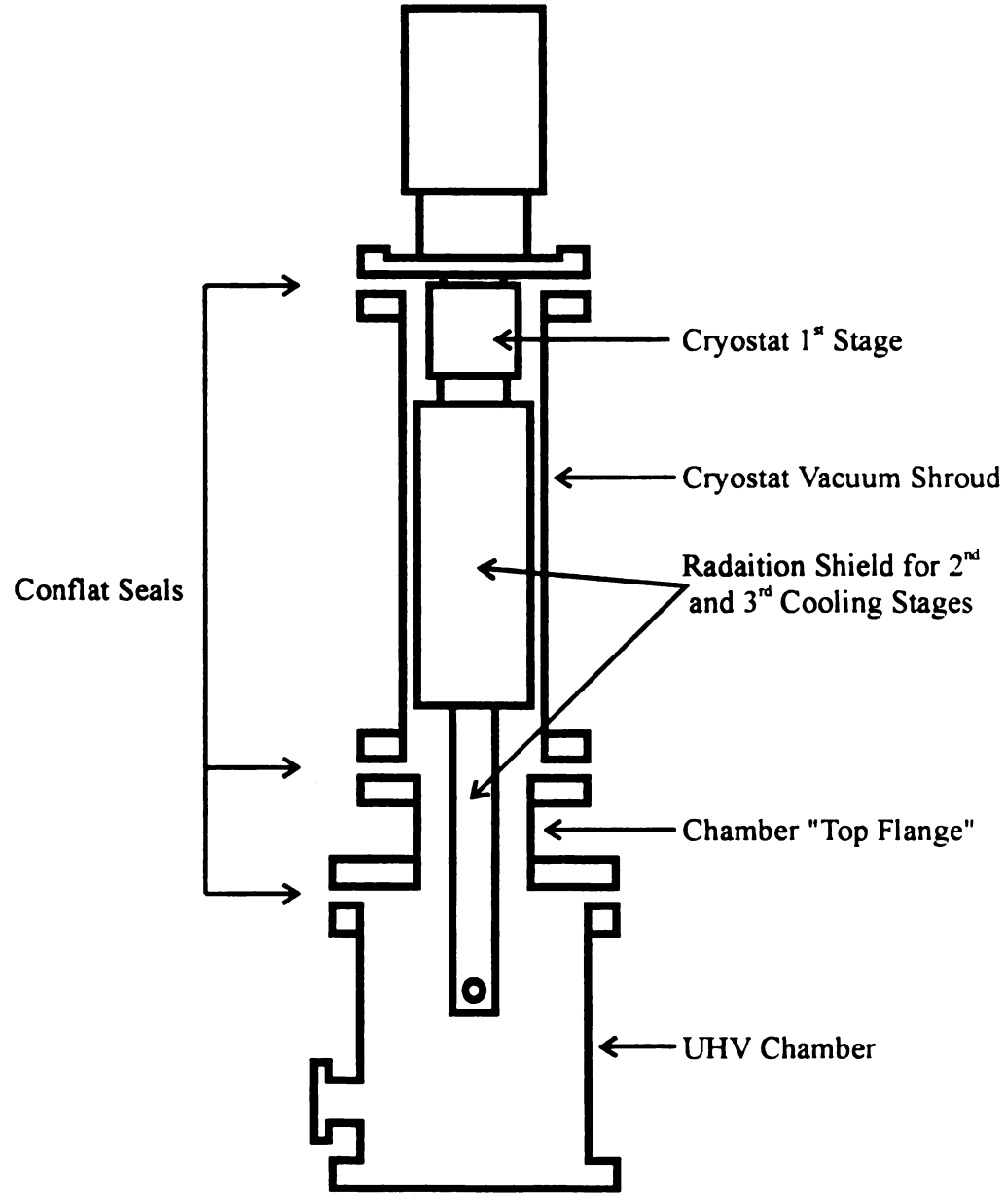

Figure 2.6: Adaptation of the Heliplex cryostat to the UHV chamber.

autotuning temperature controller. One diode is affixed to the third stage of the cryostat with Stycast epoxy. This places the sensor in close proximity to the cold head and the heater, which results in more accurate temperature control. The calibrated diode is attached to the outer side of the sample window holder, giving an accurate measurement of the cryostat window temperature. The diode is fastened using bare copper wire strung through three holes drilled into the widow holder. These wires are threaded through the non-removable piece of the sample holder, which allows the sample window to be removed and cleaned without removal of the diode. A thin layer of Apiezon N vacuum grease is applied between the window holder and the Si diode to maximize thermal contact between the two. This assembly is shown in Figure 2.7.

C. Radiation Shield Modifications

Modifications to the radiation shield were necessary to improve the ion collection efficiency of the experiment. The original HMX series radiation shield, in the region of the window was a 1.5''. diameter tube of nickel-plated copper. Optical access to the sample holder was via two ⅝'' holes drilled in the tube. Since these apertures were smaller that the exposed window diameter of ¾'', a significant portion of the mass-selected ion beam was being clipped. While an ion current of 25 nA was measured at the Faraday plate directly in front of the radiation shield, only 8 nA was measured at the sample window.

To make more efficient use of the ion beam, the apertures were enlarged to ⅞" diameter. This, unfortunately had the adverse effect of increasing the amount of radiative heat reaching the window to a level greater that it could dissipate. As a result, the window could not be cooled below approximately 10 K. As noted above, the

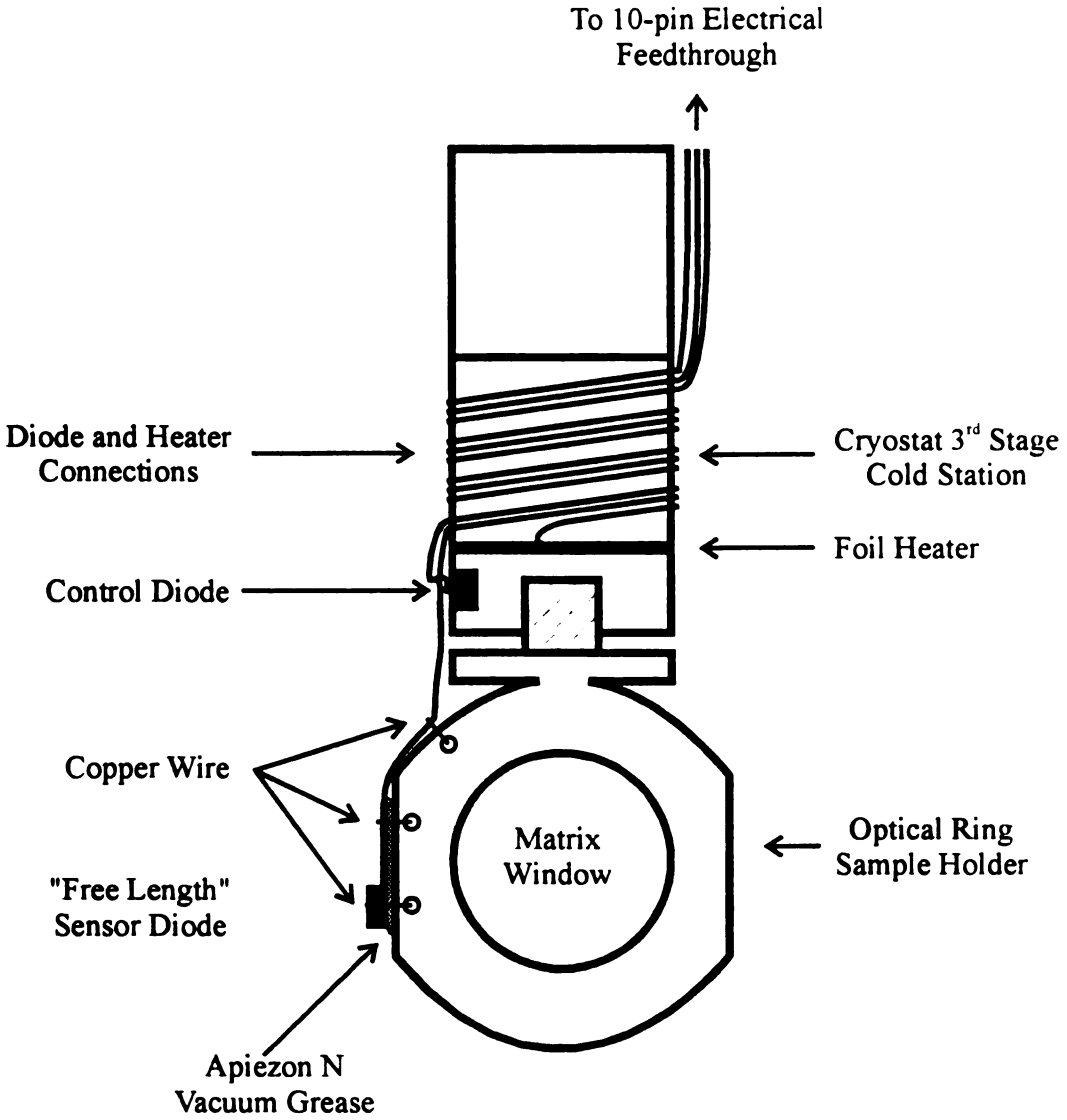

Figure 2.7: Attachment of temerature control diodes to cryostat and optical ring sample holder.

original radiation shield was blocking too much of the ion beam to be used in its manufactured form. The low throughput was caused from the openings in the cylindrical radiation shield being ~0.70". from the surface of the cryogenic window. If this distance could be shortened, an aperture smaller than ⅞" could be used, with less of a shadowing effect. The solution was to replace the bottom portion of the radiation shield with a new end piece, which also had a rectangular cross-section like the window holder, and could be attached to the remaining cylindrical radiation shield. The original and modified radiation shields are shown in Figure 2.8. The first modified end piece was constructed from a solid copper block and was fastened to the radiation shield with a two set screws. The temperature of the window holder was now measured to be about 6.5 K. The ion current measured at the window was now on the order of 60% of the incoming beam, instead of 30%..

While a temperature of 6.5 K is sufficient for Ne matrices, the difference from the expected temperature was still concerning. The warming was originally attributed to poor thermal contact between the end cap and the radiation shield. To improve the contact, the new end piece was silver-soldered to the radiation shield. After this modification, the temperature of the cryostat window actually rose to 10 K, which is unusable for neon. Similar results were obtained with a end cap made from copper foil and attached with bare copper wire. The cause of this warming was eventually found to be stray radiation leaking into the radiation shield, being reflected off of the inside copper surface, and eventually warming the sample window. This is a very common problem in cryogenic systems. The most common solution to this problem is to blacken the reflective surface, but most paints outgas significantly and are not UHV compatible. The inside of the shield cap was made

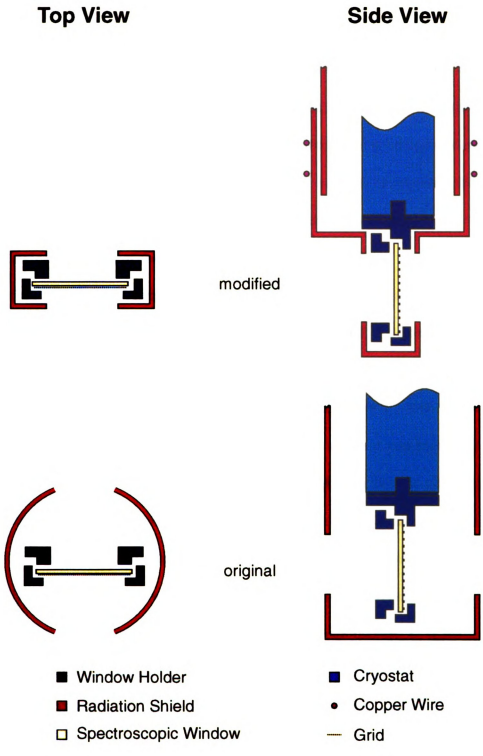

Figure 2.8: Modified and original radiation shield assemblies. Grid shown on spectroscopic window was not present for all experiments.

non-reflective by painting it with Stycast epoxy, which is UHV compatible. Once the shield cap was painted with the epoxy, the window temperature was ~ 4.5 K, which was actually an improvement over the original radiation shield. The epoxy also showed no outgassing detectable by the Dycor RGA. Because removal of the solid cap soldered onto the radiation shield also proved to be cumbersome and wasteful of relatively expensive indium, the copper foil shield cap was used in all subsequent experiments.

D. Electrical Isolation of the Sample Window Holder

In the course of investigating the method by which counter-ions were being formed in the matrix as mass-selected cations are being deposited, it became necessary to electrically isolate the cryostat window holder from earth ground. This would prove to be challenging, as the cryostat and the UHV chamber are both metallic, and connected to earth ground by various electrical components such as the cryostat and cryopump valve motors, and the electropneumatic valves. Our approach was to replace the screw and base of the window holder with an electrically insulating material. The challenge was in finding a material that is an electrical insulator, machinable, has a high thermal conductivity, and is mechanically robust enough to withstand repeated cycling from room temperature to 4 K.

The requirement of machinability severely limited our choices of materials with which we could fabricate the screw. Vespel™, a machinable polyamide polymer was used for this purpose. The original copper screw was removed from the window holder and the Vespel™ screw was put in it's place. The Vespel™ screw is fastened to the window holder by a small brass screw placed inside of the Vespel™ screw. To further strengthen this attachment, the two pieces were also glued together using Stycast epoxy. A sapphire window (Edmund Scientific A43, 368) was modified by the MSU Scientific Glassblowing

Laboratory and used as a washer between the base of the window holder and the cryostat cold head. Some of the original base material was removed to compensate for the thickness of the sapphire window. This design is shown in Figure 2.9. The combination of the Vespel™ screw and sapphire washer was successful in electrically isolating the window holder, and had sufficient thermal conductivity to maintain the window at approximately the same temperature as the original window holder. An electrical connection to the window holder is made with 28 gauge magnet wire. This wire was wrapped around the cryostat third stage for heat-sinking purposes and is connected to a BNC feedthrough on the instrumentation skirt on the Heliplex®.

E. Sample Windows

The sample window is the standard HMX series optical sample holder (APD 78332A2). This ring holder accepts 25 × 1 mm windows. CsI windows (APD 254138132) were used for IR studies, and a 25 × 1 sapphire window (Royln Optics 55.6025) was used for the dispersed emission experiments. The CsI windows, unfortunately, have a relatively short lifetime. The cryostat windows require frequent cleaning. CsI is very soft, and as such the polishing process invariably removes some material from the window. After 5–8 polishings, the windows become too thin to use and must be replaced.

IV. Matrix Gas Line

The vacuum manifold used to prepare matrix gas and introduce the gas into the UHV chamber is shown in Figure 2.10. This system consists of a glass manifold pumped by a water-cooled 2'' oil diffusion pump (Varian HS-2) backed by a direct drive mechanical pump (Edwards 8). Low pressures are read with a standard Bayard-Alpert ion

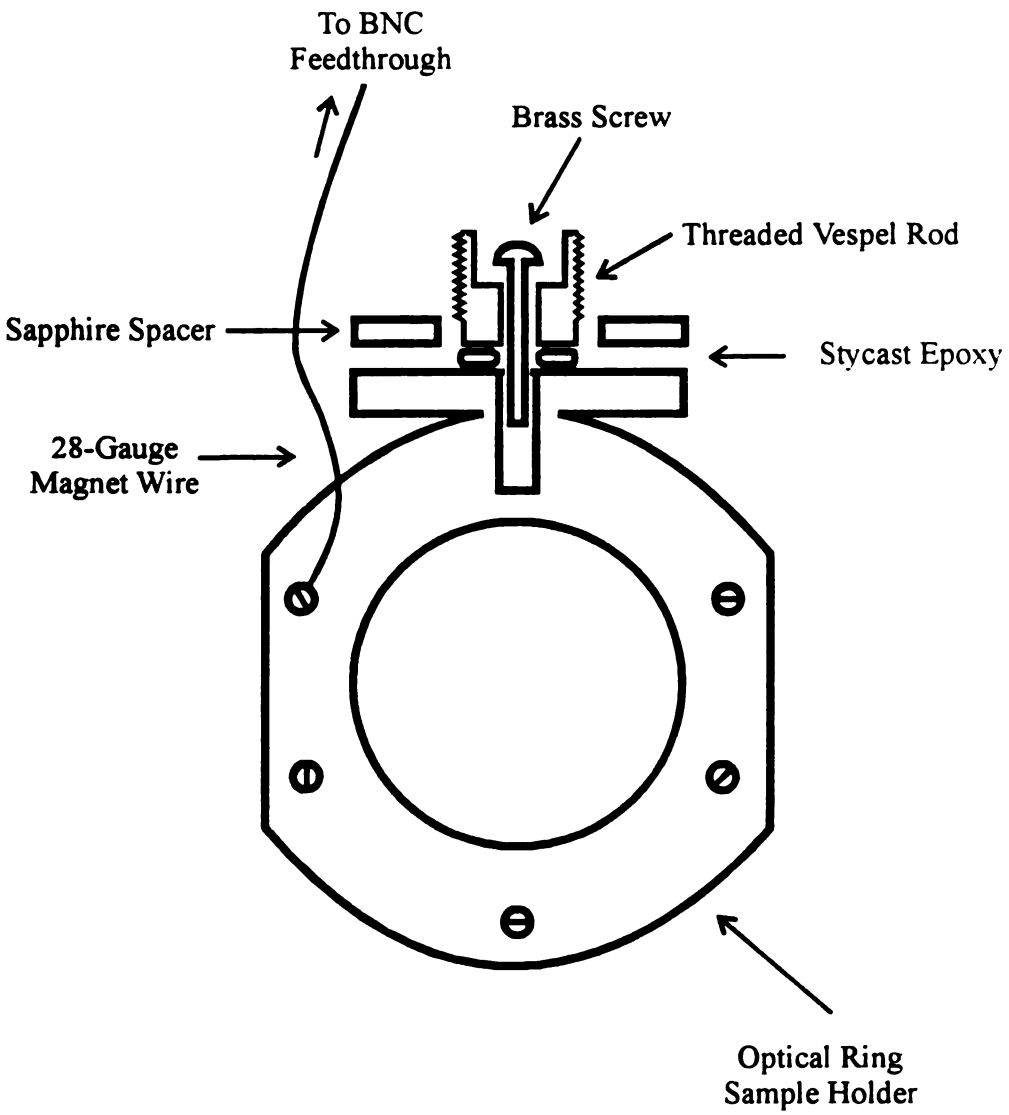

Figure 2.9: Cross-sectional view of spectroscopic window holder modified for electrical isolation.

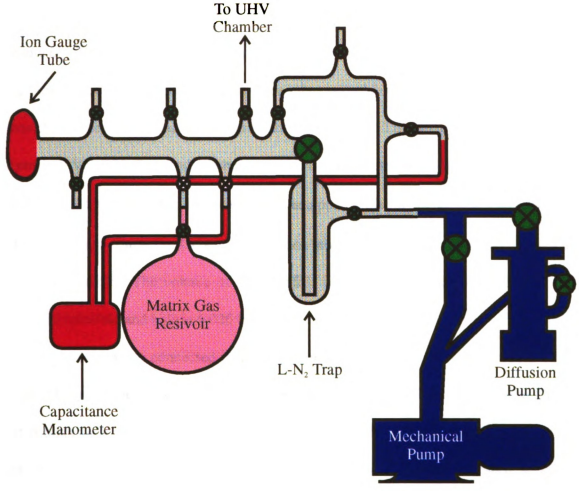

Figure 2.10: Vacuum manifold used for matrix gas preparation and its introduction into the UHV chamber.

gauge (thoriated iridium filament) controlled by a Veeco RG-830 ion gauge controller. A DV-6M thermocouple is also placed after the diffusion pump to monitor the forepressure, as well as the manifold's pressure during rough evacuation. High (> 1 mTorr) pressures are read with a Celesco DM2 digital capacitance manometer equipped with a DP-30 transducer. The original display of the manometer consisted of 4 nixie tubes, all of which have burned out. Since replacement of these tubes is prohibitively expensive, the pressure is now read from the output terminals of the manometer. The response function of this output is 1 Volt/100 Torr and can be read with any voltmeter. The base pressure of this system is ~ 7.5×10^{-7} Torr. The manifold is equipped with several ground glass and ¼'' OD tubular glass connections sealed with Teflon stopcocks. A 5.225 liter bulb is used as the main reservoir. The volume of the manifold is 0.801 liters, and the volume of the connected manifold and bulb is 6.026 liters.

The manifold is connected to the UHV chamber by ¼'' OD copper tubing. The coupling between the glass and copper tubing consists of two stainless steel Cajon Ultra-Torr fittings with a ¼'' diameter flexible stainless steel bellows tubing in between. This type of coupling should always be used when connecting rigid tubing to glass to avoid breaking the glass tubulation. The matrix gas transfer line is connected to the UHV chamber by a Cajon Ultra-Torr fitting on the inlet of a Vacuum Generators MD7 high-precision leak valve.

High purity Ne (AGA) and Ar (Matheson), both 99.9995%, were used as received as matrix gases. In some experiments, CO_2 (Aldrich, 99.8+%) was added to the matrix gas. Matrix gas mixtures were made according to standard manometric techniques.

V FTIR System

A. FTIR Spectrometer

The spectrometer originally used for these experiments was a Bomem DA3 FTIR spectrometer. This high resolution, high sensitivity, research grade spectrometer was ideally suited for this research in terms of sensitivity and flexibility. Its interfacing to the UHV chamber is described in detail elsewhere.[2] It did however, have one serious design flaw, which resulted in the great Christmas Eve flood of 1991. The source cooling shroud began to leak, introducing approximately 100 gallons of H_2O into the spectrometer, promptly dissolving roughly 25% of the KBr beamsplitter. Contact with the ensuing KBr solution also destroyed virtually all of the optics and electronics in the spectrometer bench. The bench was a total wash (pun very much intended).

The Bomem spectrometer was replaced with a Nicolet 520P FTIR spectrometer. This is a dedicated mid-IR instrument. The instrument's source is a closed-cycle, water-cooled SiC Globar™ which is useful over the range of 250–10,000 cm^{-1}. The heart of the optical system is an air bearing Michelson interferometer equipped with a Ge/KBr beamsplitter. The specified spectral range of this beamsplitter is 7400–350 cm^{-1}. A HeNe laser is used for position referencing of the moving mirror. The 520P bench has two optical paths. The standard path focuses the IR beam in the bench's sample compartment and into the internal detector compartment. The spectrometer can alternatively be configured to direct a collimated beam through a port on the side of the bench to a remote location. A computer controlled mirror inside the bench is used to select the optical path. For the experiments reported here, the external beam is focused through the UHV chamber by a series transfer optics originally used in the Bomem spectrometer (the only

ones that survived). This series of optics consists of two mirrors, M1 (90° off-axis paraboloid, 6'' effective focal length, 3'' aperture) and M2 (90° off-axis ellipsoid, 2" and 22" focal lengths, 1.25" aperture). After the IR beam passes through the UHV chamber it is focused onto a remote detector. Two detectors were used in these experiments. For high sensitivity, a narrow-band mercury-cadmium-telluride (MCTA) detector (Nicolet 840-111900) was used. Unfortunately, this detector's increased sensitivity comes at a cost of spectral range and is useful only between 4800 and 720 cm^{-1}. Spectral data below 720 cm^{-1} were obtained with a wide-band mercury-cadmium-telluride (MCTB) detector (Nicolet #840-11200) was employed. As received from Nicolet, the range of this detector is 6,000500 cm^{-1}. The original MCT crystal was damaged, and replaced with a different crystal (Belov Technologies). This MCT crystal is somewhat more sensitive that the original and its peak sensitivity is near 500 cm^{-1} which better complements the MCTA detector. The detectors are placed in an aluminum housing mounted on a table equipped with roller bearings for height and side adjustment of the detector. All aspects of spectrometer bench control, data acquisition, and data processing are controlled by an IBM compatible microcomputer, using Nicolet's PC/IR software (version 3.2).

B. Interfacing of the Spectrometer to the UHV Chamber:

The Nicolet FTIR spectrometer is placed on a table constructed so that the external IR beam is at the same height as the spectroscopic windows on the UHV chamber. Since the IR beam is difficult to visualize, alignment of the various components of the system was performed using the HeNe beam, which follows the same optical path of the interferometer, whenever possible. When necessary, the IR beam was visualized with an IR viewer borrowed from the MSU LASER Laboratory. The transfer optics

salvaged from the Bomem system are attached on a shelf which is screwed into the baseplate of the spectrometer bench. After the mirrors are properly aligned, the bench and mirrors are placed close (~ 3–5 mm) to the window on the UHV chamber, and aligned so that the HeNe beam passes through the center of the two windows and the intervening matrix substrate of the chamber. The detector housing is then place relatively close to the window on the opposite (exit) side of the UHV chamber. Fine alignment is accomplished with the help of the ALIGN function of the PC/IR software. This function triggers data collection and displays the interferogram as well as its peak intensity as it is being collected. The height and position of the detector are adjusted until this signal is at a maximum. When the system is correctly aligned, the throughput should be 20 000 counts with the small aperture, MCTA, gain of 2, and the CsI window in the cryostat. The external optical system is quite efficient, achieving 50% of the throughput achieved in the bench. Figure 2.11 illustrates this optical system, as well as the UHV chamber and mass-selective ion source.

The windows originally used on the UHV chamber were made of CaF_2 mounted on 2¾" Conflat® flanges (Harshaw 8960-1-CaF_2). These windows were chosen due to the favorable vacuum properties of CaF_2, namely high rigidity and low permeation rate, and because its optical properties are suitable for both IR and LIF spectroscopy. Unfortunately, the CaF_2 do not transmit light below 900 cm^{-1}. To extend the spectral range of the system, these windows were later replaced with KBr windows (Harshaw 8960-1-HBr), also mounted on 2¾" Conflat® flanges. Although the KBr windows have a slightly higher leak rate, the UHV system is quite capable of compensating for the increased load, and no difference in seen in the matrix background spectra. To remove

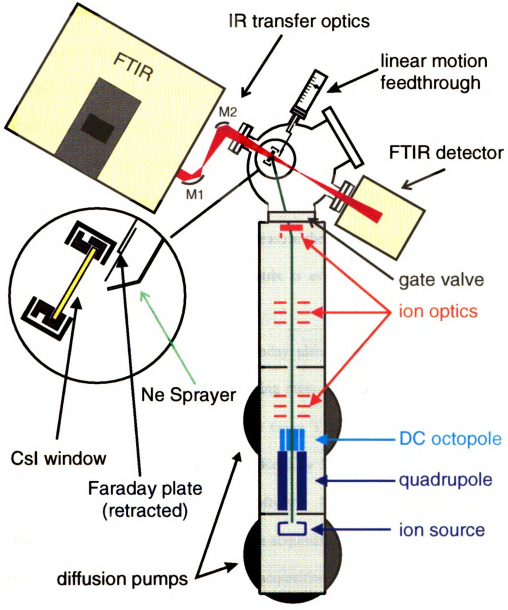

Figure 2.11: Instrument for FTIR spectroscopy of mass-selected, matrix isolated cations showing UHV chamber, ion source, and FTIR spectrometer.

atmospheric gases from the optical path, and to protect the KBr windows, the spaces between the spectrometer, the UHV chamber, and detector housing are sealed with polyethylene and purged with dry nitrogen supplied by bleed-off from the MSU Chemistry Department liquid nitrogen tank.

VI. "Allions" Measurements

While initial FTIR experiments showed that mass-selected cations could be trapped in sufficient quantities for FTIR detection, in some cases the identity of the anionic species that must be present to maintain charge neutrality was still unknown. The "allions" experiments were attempts to at least indirectly detect the presence of anionic species. The idea behind these experiments was to measure the transient current produced by ions striking the Faraday plate as the neon matrix is evaporated. A typical experimental configuration is shown in Figure 2.12.

The ion detector used was the Faraday plate, which had been installed in the chamber to measure and monitor the incoming mass-selected ion beam. Allions current was measured and converted to a voltage using a Keithley 480 picoammeter. The transient signal was then recorded with a Keithley DAS-8 data acquisition board and processed using Keithley Easyest LX 1.0 software. Data were typically collected in the strip chart mode at 50 Hz. The Keithley data acquisition system was later replaced with a National Instruments AT-MIO-16X data acquisition board, controlled with National Instruments LabVIEW 3.1 for Windows. In the LabVIEW environment, the programs developed for instrumental control are referred to as Virtual Instruments (VIs). Data were usually collected using the allions11.vi VI. This is a modification of a basic signal acquisition VI supplied with the LabVIEW software package. The "wiring diagram" for

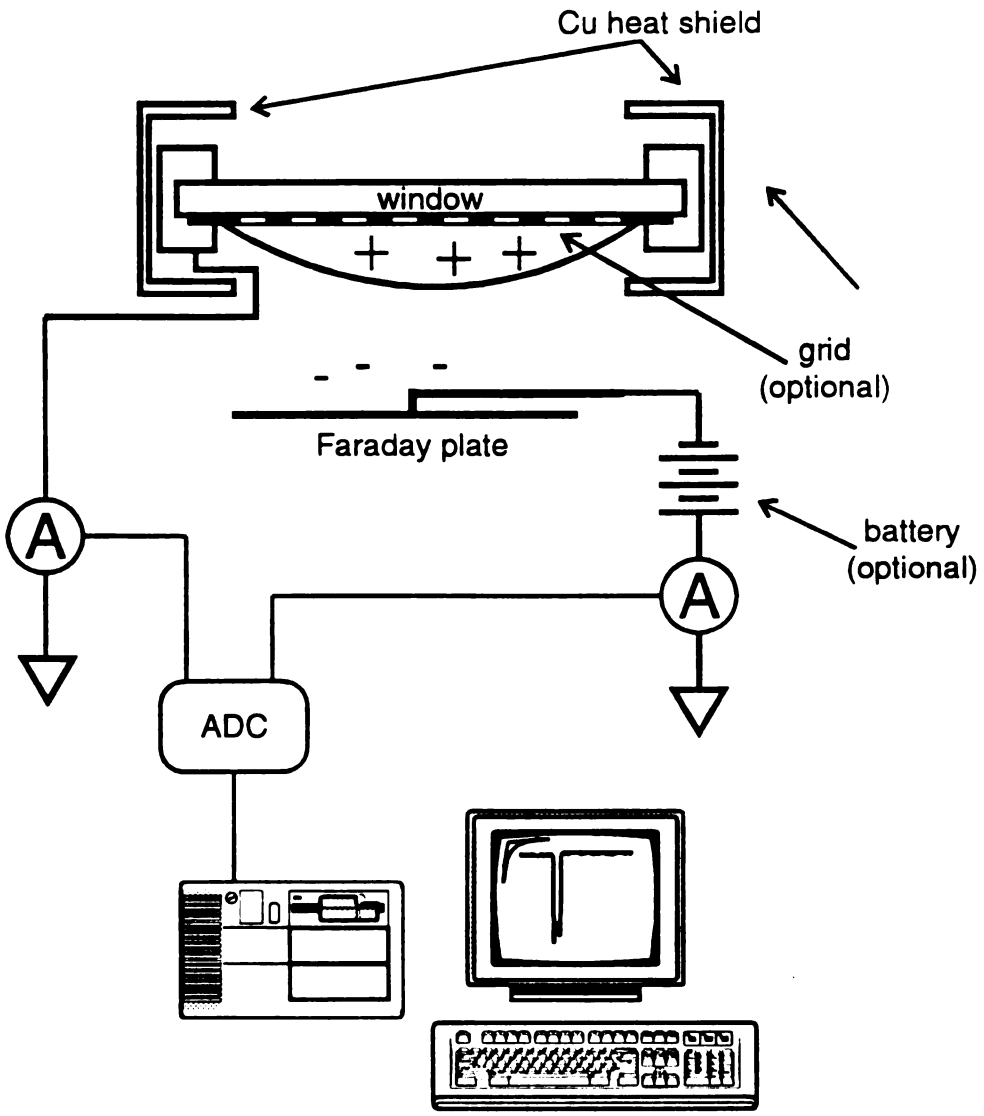

Figure 2.12: Schematic description of "Allions" experiments. Components marked optional were not used in all experiments.

the allions VI can be found in the file allion11.vi. The ADC was typically set to a ±10 Volt input range and sampled at 10 Hz.

In the original allions experiments, all components were held at ground potential. Positive and negative ions alike can strike the Faraday plate, allowing all ions to be sampled (hence the name). Since the ions were not influenced by any directing fields, however, cation/anion recombination was the dominant process, and currents representing only a small fraction of the deposited ions were observed. To improve collection efficiency, either the window/window holder or the Faraday plate was held at some potential other than ground. Attempts to float these components with a power supply were unsuccessful owing to fluctuations in the power supply that caused erratic currents larger than those due to the ion signal. To alleviate these problems, the Faraday plate or window holder was floated by placing a battery (either 70 or 300 Volts) in-line between the picoammeter and the component to be floated. Use of the battery introduced an offset due to leakage current in the BNC cables; however, it was constant and did not interfere with the ion current measurements.

VII. Counter Ion Generation Measurements

Once the identity of the counter ions was determined (see Chapter 4), experiments were undertaken to determine their origin. The goal of these experiments was to measure an anion current as a function of the incoming cation beam. The ion current was measured simultaneously at the Faraday plate in its retracted position and at a copper plate substituted for the CsI window. The ion currents were measured and voltage converted by two Keithley 480 picoammeters. The voltage signals were then filtered with 10-Hz low-pass RC filters, digitized by a National Instruments AT-MIO-16X data acquisition

board and processed using LabVIEW software. In some cases it was necessary to float the copper plate that replaced the CsI window at 300 V in order to deflect the incoming cation beam. This was done by placing a 300 V battery (Eveready 493) between the copper plate and the picoammeter. This experimental configuration is shown in Figure 2.13.

VIII. Matrix Emission Studies.

It is believed that most ions undergo charge recombination neutralization once the matrix is warmed beyond annealing temperatures. Since this recombination most likely results in highly excited neutral species, emission is expected; detection of emission and has been suggested as a test for ion-containing matrices.[6] This emission was first visually detected in a CH_3^+/CO_2^- containing matrix. This matrix exhibited an eerie blue-white glow for several minutes after the cryostat had been turned off.

The total emission accompanying the warming of several ion-containing neon matrices was measured using a photomultiplier tube (Hamamatsu R928) placed in front of a window on the UHV chamber. These signals were generally quite intense, and focusing was not required The experimental configuration is shown in Figure 2.14. Anode potentials of 800-1000V were applied to the PMT using a HP 6110A DC power supply. The signal current was measured as a voltage across a 1 MΩ resistor with a National Instruments AT-MIO-16X data acquisition board and manipulated with LabVIEW 3.1 software. Data were acquired using the matrix emission VI (emis10.vi)

Wheras these experiments demonstrated that ion-containing matrices do emit upon warming, they did little to identify the species responsible for the emission. The next step was to disperse the emission from the warming matrix. This was accomplished using a

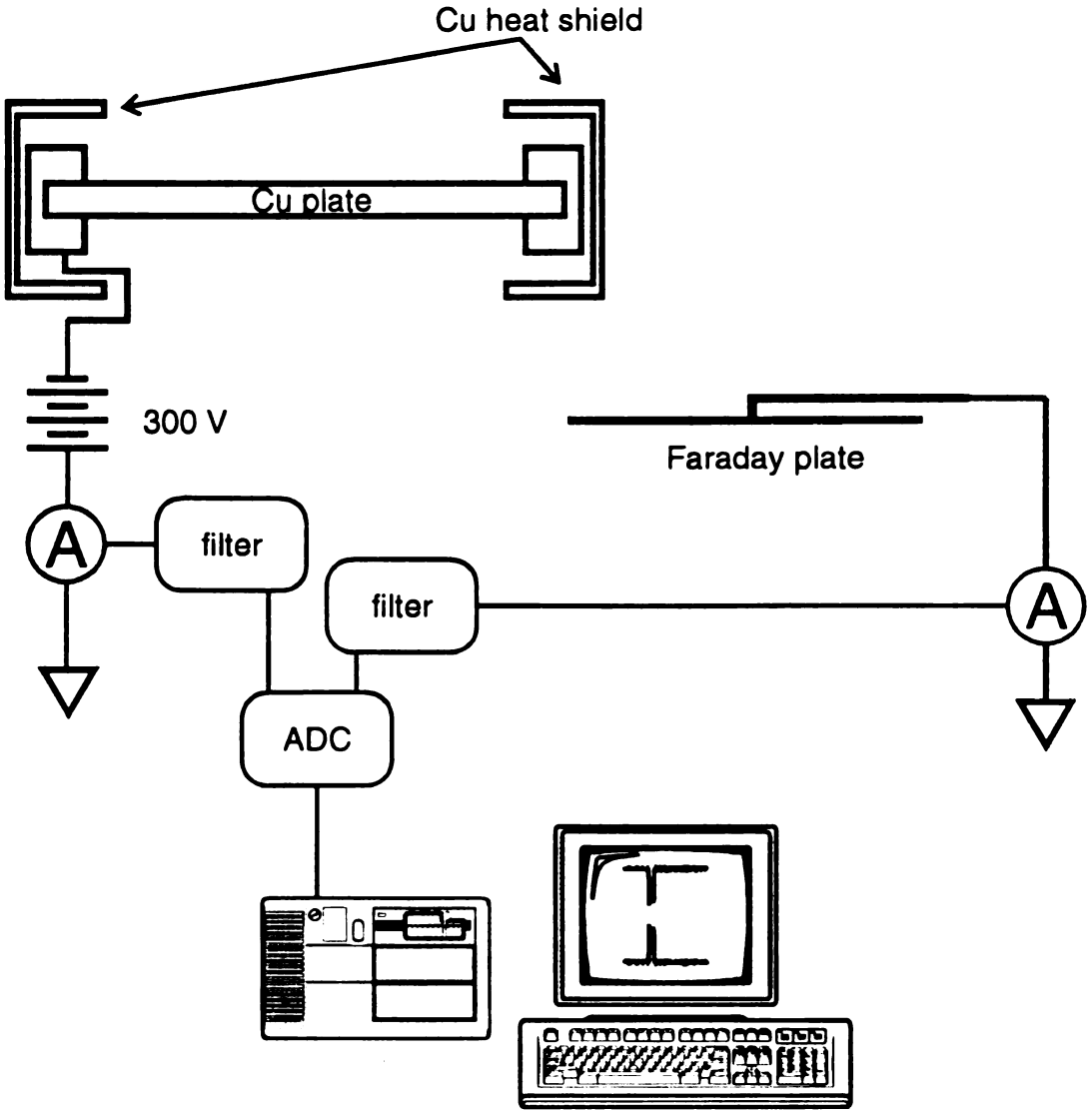

Figure 2.13: Schematic illustration of anion measurement experiments.

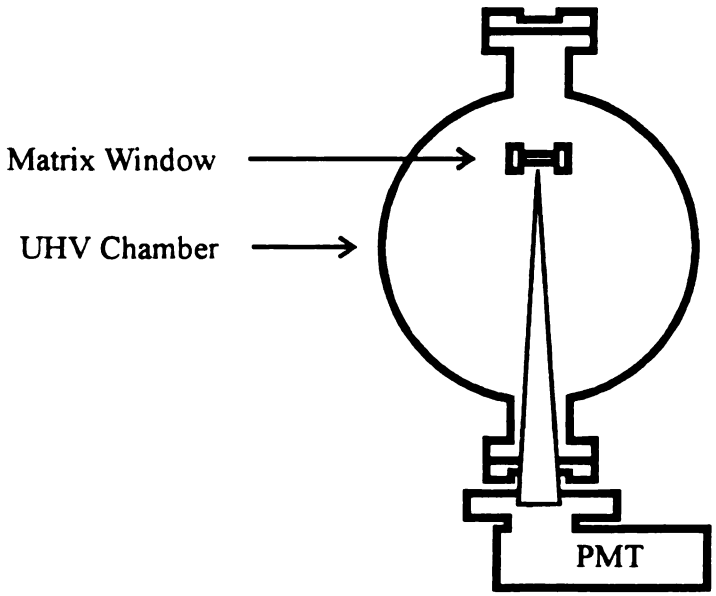

Figure 2.14: Schematic diagram of instrumentation used to collect total emission from a warming matrix

UV/VIS spectrometer system borrowed from the MSU LASER Laboratory. The system consists of a 0.22 meter monochromator (SPEX 1681) with a 300 grove/mm grating blazed at 4^{th} order. The detector is a 1024 element intensified photodiode (Princeton Instruments TRY-1024 N/RB). Data collection and processing is controlled with a IBM compatible microcomputer using Princeton Instruments' NSMA software.

During the dispersed emission experiments, some problems were encountered with undispersed light. Initially, the optical setup shown in Figure 2.15 was used. This configuration was chosen because it involved removing only the FTIR detector, and not the FTIR bench, making it more compatible with other experiments. However, it had some serious problems. The distance between the cryostat window and the vacuum chamber is ~ 8''. The first focusing optic can be at best placed just outside this vacuum chamber window, resulting in a low collection efficiency. Also, due to the reflective nature of the chamber interior, a great deal of scattered light was also collected. While this scattered light was emission from the matrix, it had a wide angular distribution, and could not be focused to a point. As a result, a large amount of undispersed light reached the detector, resulting in intense, but unfortunately useless signals.

Several measures were taken to remove the undispersed light. First, the collection optics were moved closer to the matrix window by collecting from the FTIR side of the UHV chamber. Second, an aluminum "light pipe" was added. This pipe extends from the cryostat radiation shield to the UHV chamber window and blocks out any light that has been reflected from the chamber walls. In the new configuration, the light must pass through the cryostat window. The CsI window was replaced with a sapphire window, owing to its more favorable UV/Visible transmission properties. The emission was now

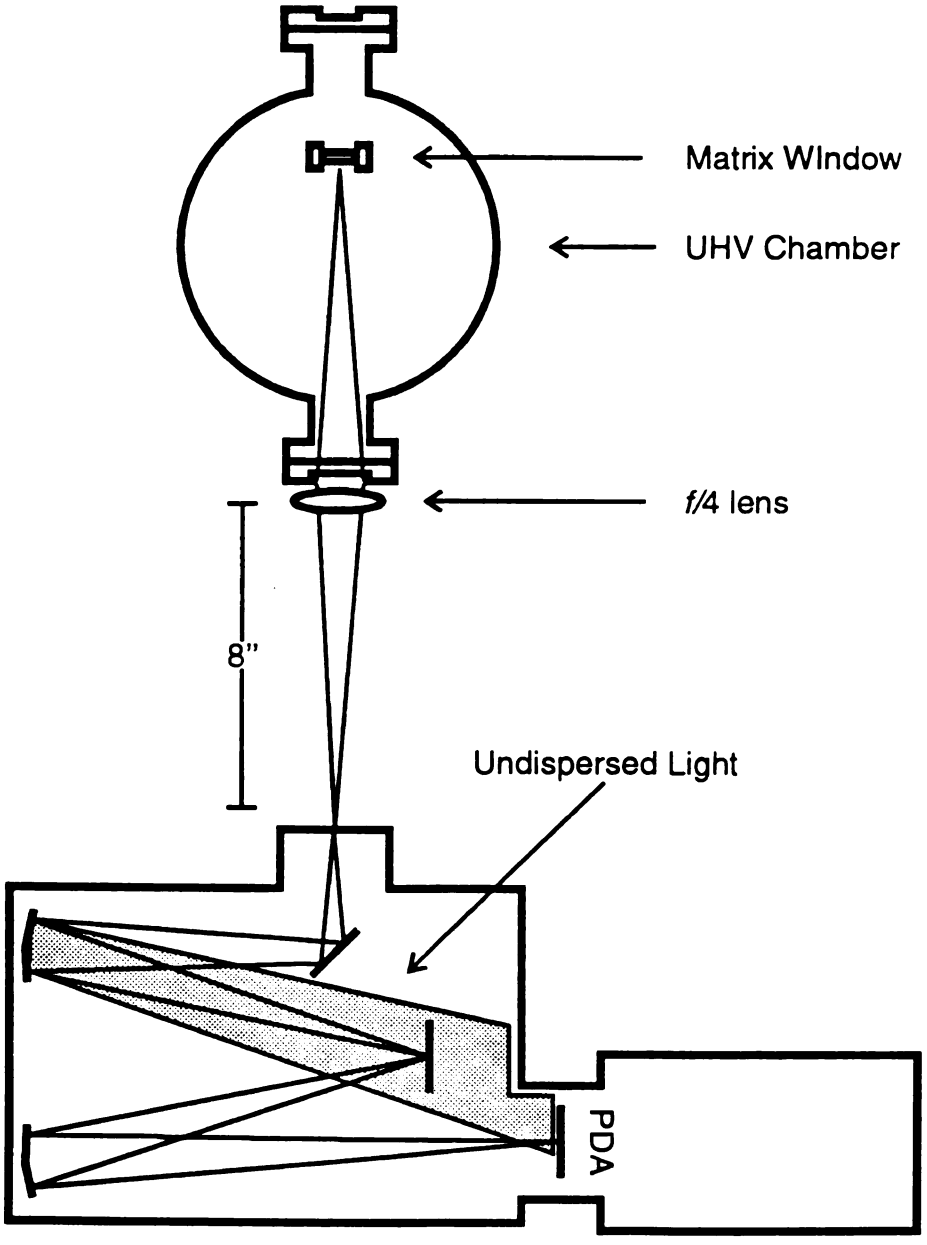

Figure 2.15: Schematic diagram of original instrumentation used to collect dispersed emission from a warming matrix. The effect of undispersed light is shown.

focused into the monochromator using two lenses (*f*/7, *f*/8) instead of just one. This configuration is shown in figure 2.16. It was successful in eliminating the undispersed emission and also resulted in enhanced collection efficiency.

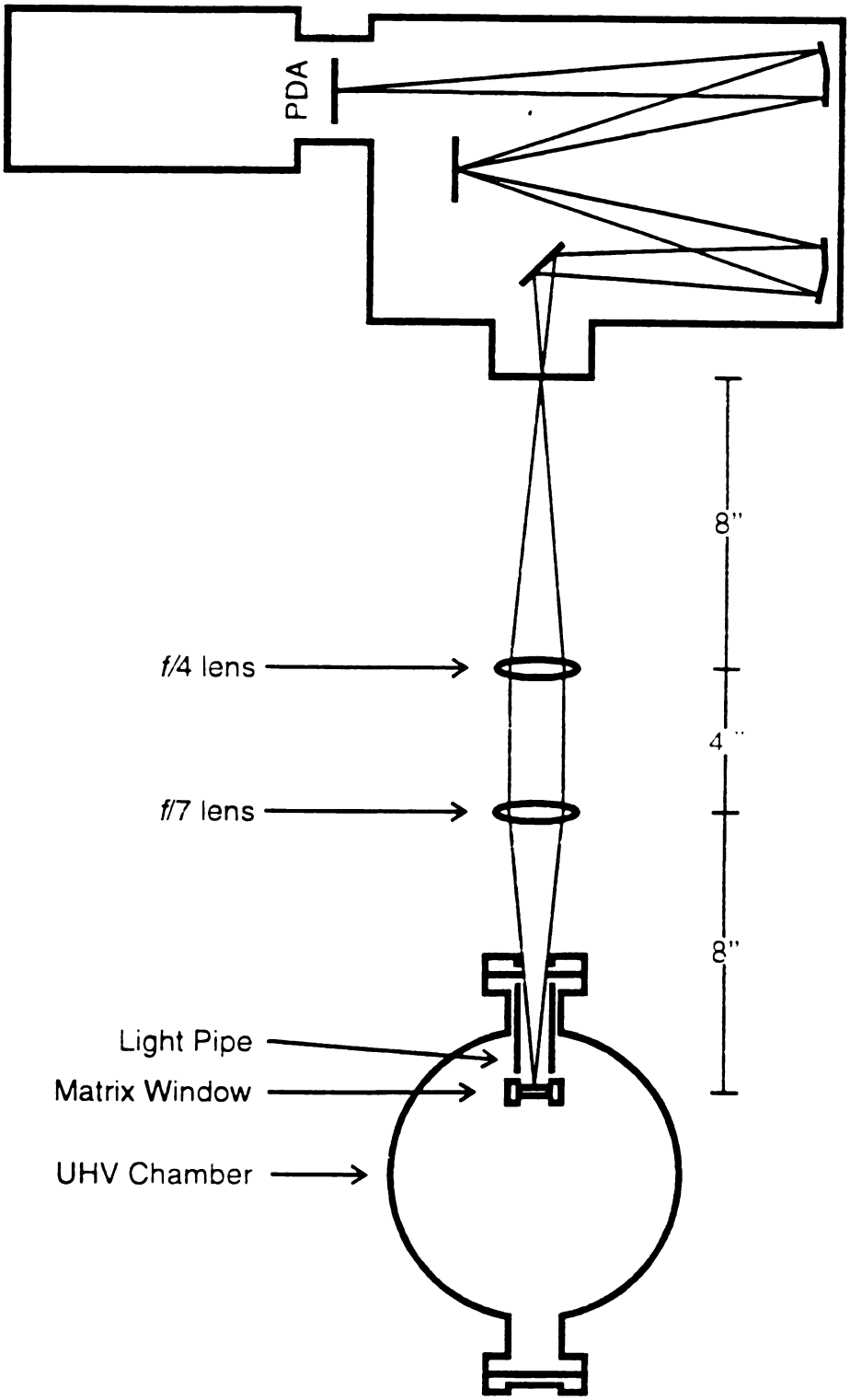

Figure 2.16 Schematic diagram of instrumentation used to collect dispersed emission from a warming matrix

List of References

(1) Sabo, M. S.; Allison, J.; Gilbert, J. R.; Leroi, G. E. *Appl. Spec.* **1991,** *45,* 535.

(2) Sabo, M. S. Ph.D. Dissertation, Michigan State University, 1991.

(3) Gilbert, J. R. Ph.D. Dissertation, Michigan State University, 1990.

(4) Halasinski, T. M. Ph.D. Dissertation, Michigan State University, 1996.

(5) Heliplex® system manual, APD cryogenics.

(6) Knight, L. B. Jr. Personal communication, 1992.

Chapter 3

Preliminary Experiments: The Infrared Detection of Mass-Selected, Matrix-Isolated CF_3^+

I. Background

The ultimate goal of this project is to couple mass-selective ion sources that produce sufficient numbers of both positively and negatively charged species with the appropriate matrix-isolation hardware to allow the determination of ionic structures by vibrational spectroscopy. We initially believed that mass-selected cation and anion sources would both be necessary to maintain charge neutrality in the rare-gas matrix. Without the presence of counter charges, the matrix will charge to an electrostatic potential equal to the kinetic energy of the incoming mass-selected ions. Once this potential is reached, the incoming ions will be deflected away from the matrix, resulting in termination of the deposition process. Under our experimental conditions, this is predicted to occur in ~ 3 ms,[1] and corresponds to a deposition of ~ 0.5 femtomoles of ions, roughly seven orders of magnitude below the detection limits of FTIR absorption spectroscopy.

Although the need for dual ion sources seems essential, previous applications of mass-selected deposition by the groups of both Maier[2] and Leroi[3] were successful using only mass-selected cations. Although these studies used the more sensitive spectroscopic probes of electronic absorption and laser-induced fluorescence, respectively, they too should have failed without the presence of counter charges for the reasons outlined above. The success of these experiments suggested that anions were indeed being generated by

some mechanism in these experiments. These results prompted us to begin preliminary experiments using only mass-selected cations upon completion of the modified Finnigan positive ion source.

II. Experimental

A. Choice of Test Cation

The first task in these preliminary studies was to choose a cation to be used to investigate the performance of the new ion source and matrix isolation system. The trifluoromethyl cation (CF_3^+) was selected as our test ion, for a variety of reasons. Spectroscopically, many aspects of CF_3^+ made it a very appealing choice. Its infrared active transitions in rare gas matrices were already known, facilitating definitive spectral identification of the species.[4,5] These transitions, typical of vibrations involving carbon-fluorine bonds, are also quite intense, thus improving the sensitivity of the experiment. The expected frequency of the antisymmetric stretch (ν_3) CF_3^+, ~ 1670 cm^{-1}, was above the 900 cm^{-1} cutoff imposed by the CaF_2 windows on the UHV chamber, and also lies near the maximum sensitivity of the MCTA detector. CF_3^+ also has a relatively low (for cations) electron affinity (9.2 eV)[6], allowing observation in both argon and neon matrices without significant spectral perturbation due to charge transfer.

Along with favorable spectroscopic properties, CF_3^+ also had several attractive mass spectrometric properties. Relatively high currents of this cation can be generated by electron impact of several gaseous precursors, such as CF_3Br, CF_3Cl, CF_4 and CF_3H. CF_3^+ (m/z 69), is the most abundant ion in the 70 eV EI mass spectra of all four precursors. The large mass separation of the halogenated fragment ions allows the beam intensity to be increased by decreasing the resolution of the quadrupole, without

introducing ionic species other than CF_3^+ into the experiment. The only exception was possible "interference" of CF_2H^+ in an investigation of CF_2^+ when CF_3H was used as the precursor. The decision to use CF_3^+ was cinched when we discovered that we already had a large tank of CF_3Cl in our laboratory.

B. Instrumental Parameters

Beams of CF_3^+ ions were generated by electron impact of several precursors using the modified Finnigan 3200 quadrupole mass spectrometer that is described in detail elsewhere.[1] Typical CF_3^+ currents, measured at the sample window with a Faraday plate in the experiments reported, ranged from $1.5\text{-}2.5 \times 10^{-8}$ amperes. This rate corresponds to an ion flux of 0.6-0.9 nanomoles per hour. The beam of mass-selected ions was co-deposited with excess neon or argon onto the sample window (CsI or sapphire) held at ~ 5 K. High-purity neon (AGA) and argon (Matheson), both 99.9995%, were used as the matrix gases. The flow rates of the matrix gas through the sprayer located in front of the window was ~ 0.5 mmole/h in all experiments. All halocarbon gases (CF_3Cl, CF_3Br, CF_4, CF_3H) were used without further purification. For the experiments described in this chapter, IR radiation was transmitted through the UHV chamber using CaF_2 windows. FTIR data were recorded by averaging either 256 or 1024 spectra between 4800 and 900 cm^{-1}, taken at 1-cm^{-1} resolution. The data were background corrected by ratioing with a spectrum collected prior to matrix deposition.

The movable Faraday plate used to measure the mass-selected ion current at the sample window was also used to collect and measure the current of both positively and negatively charged species as they were released from the matrix upon warming. The matrix was warmed by using the foil resistance heater supplied with the cryostat, and

controlled by a Lake Shore 330 temperature controller. The heater was set at the HIGH power level and a setpoint of 40 K. The current from the Faraday plate was measured and converted to a voltage signal using a Keithley 480 picoammeter, digitized with a Keithley DAS-8 data acquisition board controlled with Keithley Easyest LX 1.0 software. Unless otherwise noted, data were collected in the strip chart mode at 50 Hz.

III. Results and Discussion

A. FTIR Results

Co-deposition of 15-25 nA beams of CF_3^+ from CF_3Cl, CF_3Br, CF_4 or CF_3H and neon for up to 25 hours onto the cryogenic substrate resulted in the appearance of two new infrared absorptions, at 1670 and 1651 cm^{-1}. Only these bands, shown following generation of CF_3^+ from CF_3Cl in Figure 3.1, among absorptions due to matrix-isolated H_2O, CO_2 and precursor molecules, have intensities that correlate with the integrated ion current. As shown in Figure 3.2, the most prominent of these background absorptions are those of the precursor, CF_3Cl, and of CO_2. CO_2 which is always present as a background gas. After 11 hours of deposition, the absorbances of the most intense of these transitions, ν_1 of CF_3Cl at 1104 cm^{-1},[7] and ν_3 of CO_2 [8] were ~ 0.20. We assign the 1670- and 1651-cm^{-1} peaks to the antisymmetric stretch (ν_3) of mass-selected, matrix-isolated CF_3^+ trapped in different matrix environments. Although 19 cm^{-1} is unusually large for a site splitting, this assignment has been supported by other researchers.[9]

The positions of the 1670- and 1651-cm^{-1} bands are consistent with previous[5] and later[9] assignments of ν_3 of CF_3^+ matrix-isolated in neon. In the neon matrix work by Jacox and co-workers,[9] split absorptions at 1670, 1664 and 1651 cm^{-1} were assigned to ν_3 of CF_3^+. While we did not generally observe the feature at 1664 cm^{-1}, our work and that of

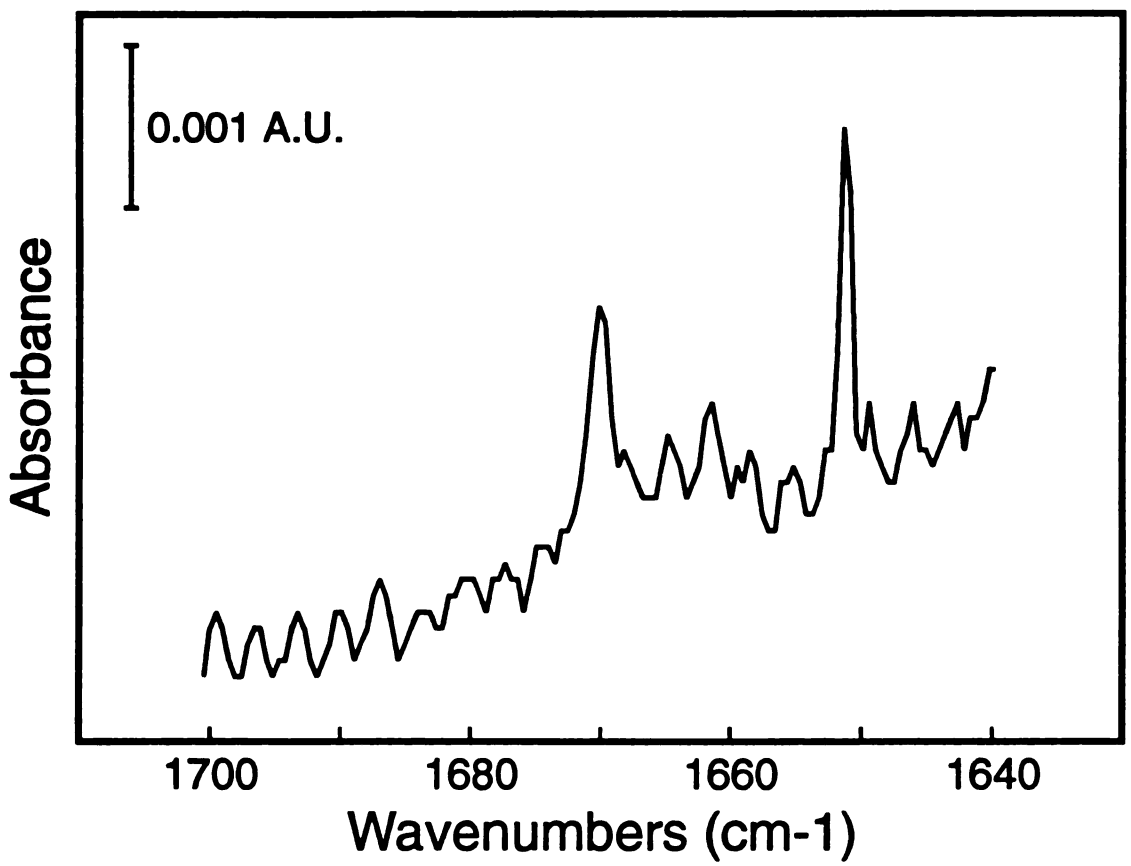

Figure 3.1: Antisymmetric stretch (ν_3) of mass-selected, matrix-isolated CF_3^+ in neon.

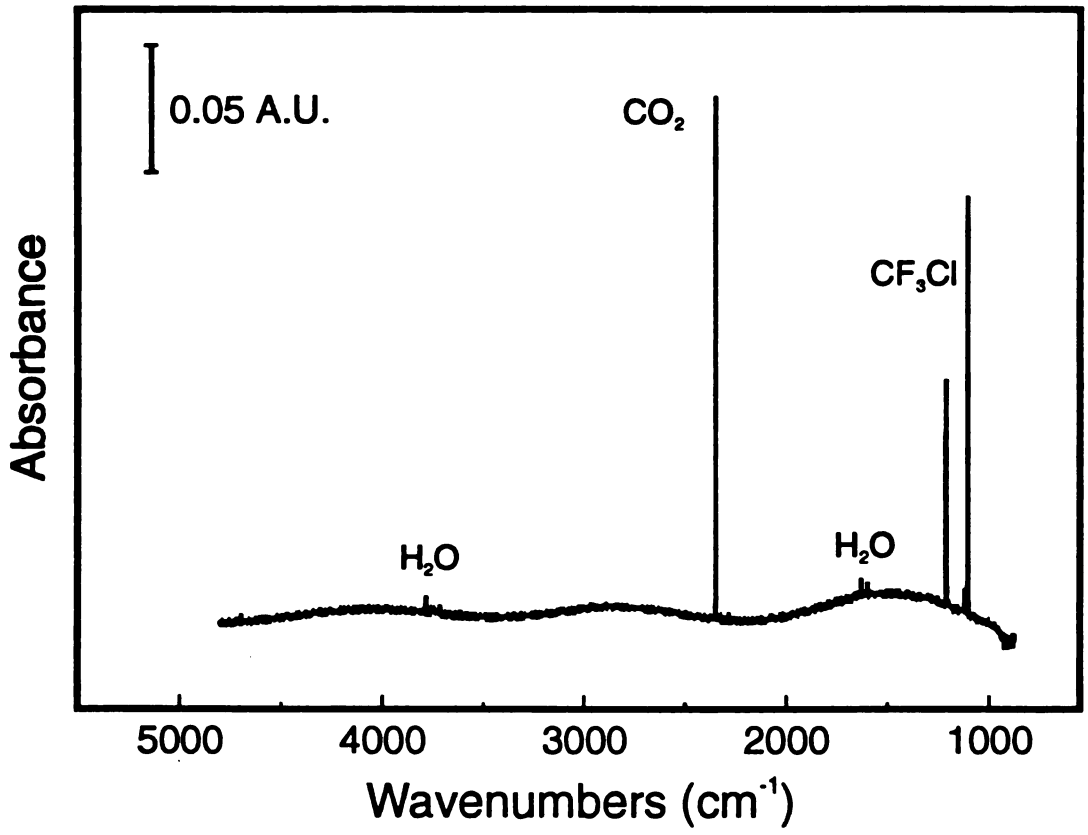

Figure 3.2: FTIR absorption spectrum in the 4800–900-cm^{-1} region of a pure neon matrix after 11 h of deposition of CF_3^+ generated from CF_3Cl.

Jacox indicated that the relative intensities of these absorptions are somewhat sensitive to the composition of the matrix.[10] The antisymmetric stretch of CF_3^+ also has been reported in the range 1663-1667 cm^{-1} in argon matrices.[4,11,12] When we deposited mass-selected CF_3^+ generated from CF_3Cl in an argon matrix at 5 K, an absorption at 1667 cm^{-1} with an apparent shoulder at 1665 cm^{-1} was observed; see Figure 3.3.

Although the frequencies of the new absorptions that we observed are consistent with those of CF_3^+, there was still the possibility that these absorptions were due to an exotic neutral species created during operation of the ion source. Control experiments demonstrate that the 1670- and 1651-cm^{-1} absorptions are not due to neutral species generated during the ionization process, and are indeed due to mass-selected, matrix-isolated CF_3^+. The results of these experiments are summarized in Figure 3.4. Trace a shows the IR absorption between 1700 and 1640 cm^{-1} of a neon matrix after 11 h of deposition of CF_3^+ (m/z 69, 20 nA) generated from CF_3Cl. When the mass spectrometer was set to select m/z 120, but all other experimental parameters were unchanged, no ions were transmitted for deposition in the matrix, yet the flux of neutrals from the ion source remained. During such experiments, the peaks at 1670 and 1651 cm^{-1} did not appear (Figure 3.4, trace b), but the rest of the spectrum was unchanged. To determine if these features were due not to mass-selected CF_3^+, but to CF_3^+ formed upon collisions of the ions with solid surfaces, gas phase species, and/or the growing matrix, mass-selected CF_2H^+ (m/z 51) [along with a small amount of CF_2^+ (m/z 50)], generated from CF_3H, was deposited into the neon matrix. As illustrated in trace c of Figure 3.4, the new peaks were again absent. It should be noted that bands attributable to CF_2H^+ or CF_2^+ were not observed, but based on previous assignments[11] the CF_2H^+ absorptions would have been

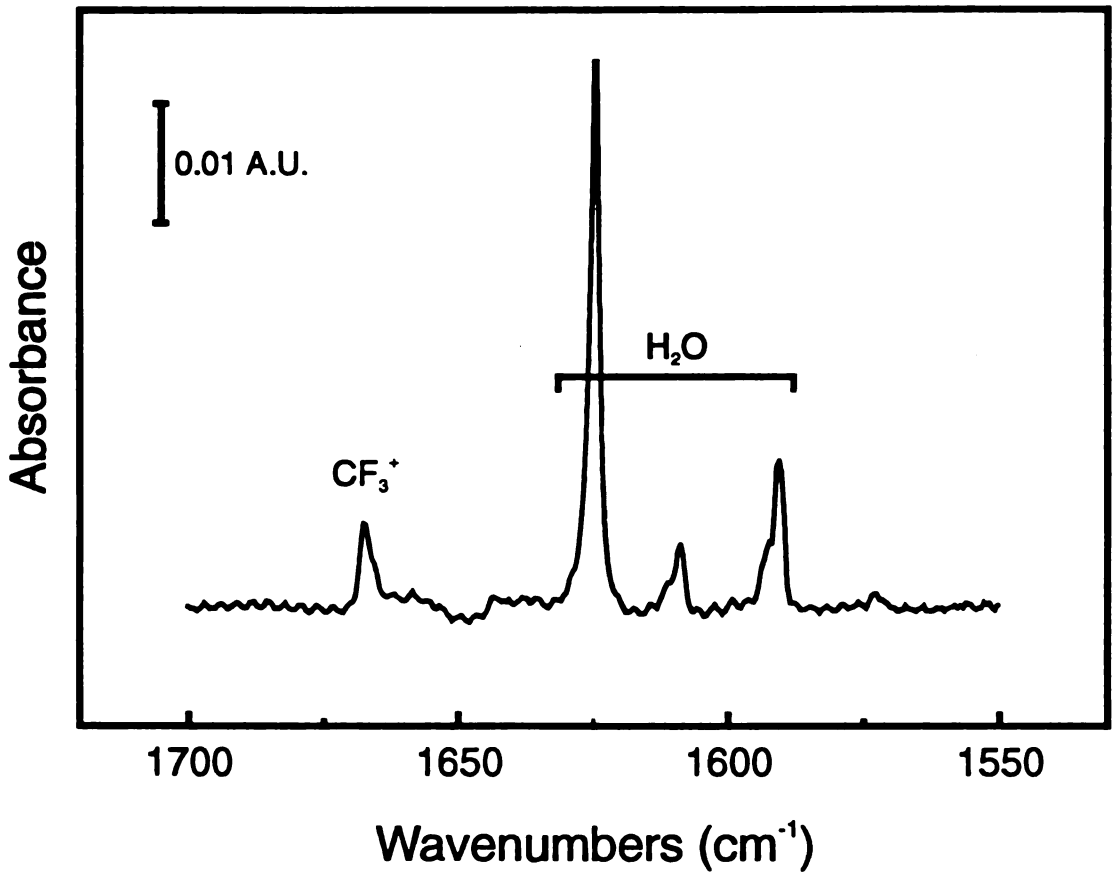

Figure 3.3: FTIR absorption spectrum in the 1700–900-cm^{-1} range of a pure argon matrix after deposition of CF_3^+ from CF_3Cl.

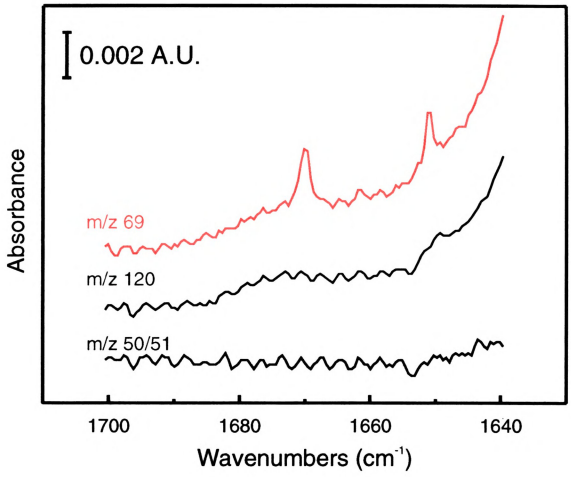

Figure 3.4: Infrared absorption spectra in the 1700 - 1640 cm^{-1} region of neon matrices after 11 hours of deposition of: a) m/z 69 (CF_3^+, 20 nA) generated from electron impact of CF_3Cl; b) m/z 120 (no ion current) while subjecting CF_3Cl to electron impact; and c) m/z 50/51 (CF_2^+/CF_2H^+, 15 nA) generated from electron impact of CF_3H.

obscured by background water absorptions, and the amount of CF_2^+ deposited was too small to observe in this experiment.

If the CF_3^+ ions are partially neutralized during deposition, spectral features due to $CF_3^\bullet$ should be observed. An extremely weak absorption was observed in neon matrices at 1254 cm^{-1}, which agrees with previous assignments[5] for $CF_3^\bullet$ in neon. The low intensity of this feature (absorbance = 0.0007), indicates that only barely detectable quantities of $CF_3^\bullet$ are present in the matrix. Features due to other neutralization/fragmentation products, such as CF_2 [13] and CF [13] are not observed.

B. Indirect Detection of Counterions

In the absence of counter charges, one cannot accumulate a sufficient number of positively-charged species in a matrix to obtain a measurable infrared absorption spectrum. When pure neon was used a the matrix material, no absorptions were observed that could be assigned to an anionic species. In some experiments CCl_4 was added to the matrix gas (1:500) to attempt to increase cation yield, and to investigate the possibility that electrons were the counter charges. CCl_4 acts as an electron scavenger by the following reaction:

$$CCl_4 + e^- \rightarrow CCl_3^\bullet + Cl^-$$

If electrons were present and migrating through the matrix, the reaction with CCl_4 will immobilize them, and hopefully reduce the number of ions lost to neutralization. Unfortunately, the products of this reaction are not directly observable by our instrumentation at that time. Electrons, and the chloride ion, of course, have no IR spectrum and the highest energy IR-active vibration of $CCl_3^\bullet$, at 898 cm^{-1}, lies just below the low energy cutoff of the CaF_2 windows of the UHV chamber. The 1670- and 1651-cm^{-1} peaks appeared both with, and in the absence of, CCl_4 in roughly equal intensity.

This result was consistent with our spectroscopic findings that neutralization was not occurring on a large scale. It also indicated the counter charge in these experiments was probably not a free electron.

When argon was employed as the host, we also observed new FTIR bands at 938 and 933 cm^{-1}, shown in Figure 3.5, when CF_3^+ was deposited. These bands correspond closely to those previously (and tentatively) assigned to CF_3Cl^- in argon by Prochaska and Andrews.[4] Presumably this species is formed by electron attachment to CF_3Cl, which is present in the matrix in abundance. The origin of the electrons, however, is not clear. They may be extracted from the grounded window holder, or they could be ejected from the various grounded components of the cryostat upon impact of the ion beam and subsequently deposited into the matrix.[14] Since corresponding peaks are not readily observed in our experiments with neon matrices, this may indicate that the mechanism of counter-ion formation is matrix dependent.

By an as yet unknown mechanism, electrical neutrality was being maintained. Some negatively-charged species are in fact present and were indirectly detected in the matrix, although their identity was not certain. When the Faraday plate, installed to monitor the impinging ion flux, was placed directly in front of the cryostat window as neon matrices containing mass-selected cations were warmed to about 20 K, current was measured. As shown in Figure 3.6, very small (picoamp) transient signals due to both positive and negative species entrained in the vaporizing matrix were measured when the neon matrix was warmed. For the control experiments, where the peaks attributable to CF_3^+ were absent, no such transient ion signals were observed. These results indicate that negatively-charged species are being produced and matrix isolated as a result of the

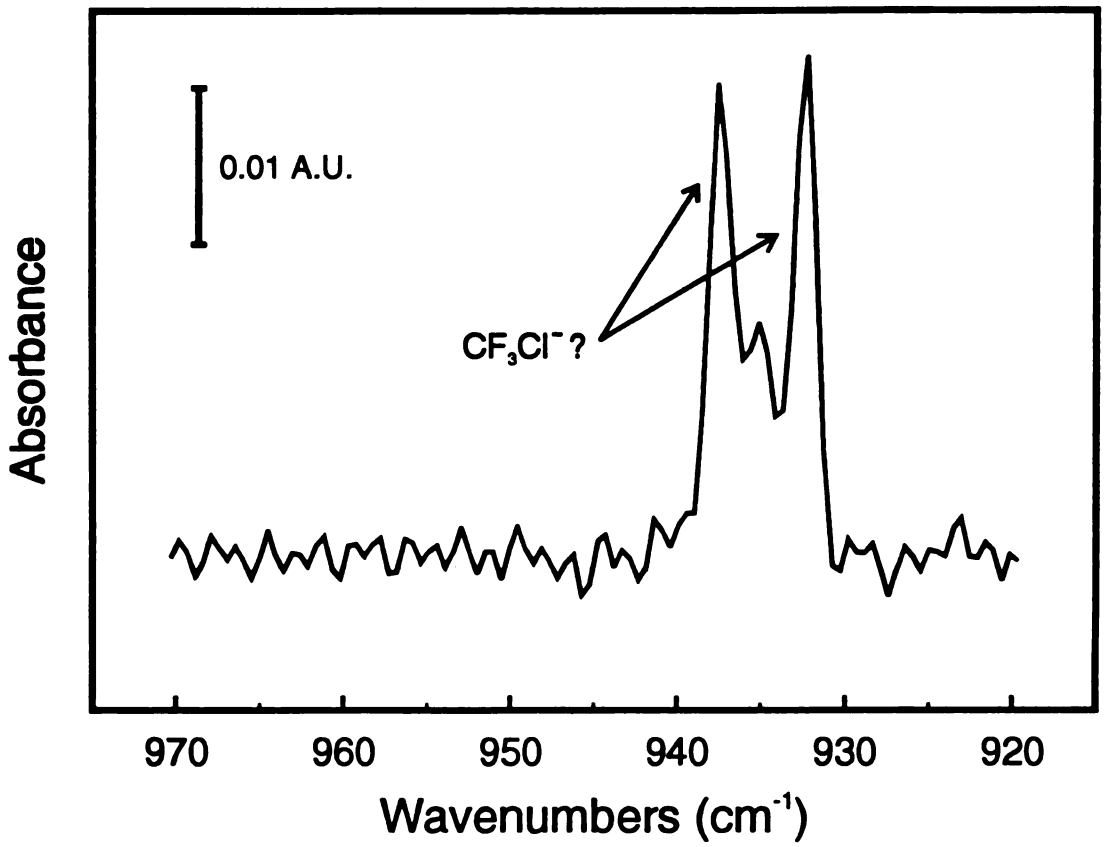

Figure 3.5: FTIR absorption spectrum in the 970–920-cm^{-1} range of a pure argon matrix after deposition of CF_3^+ generated from CF_3Cl.

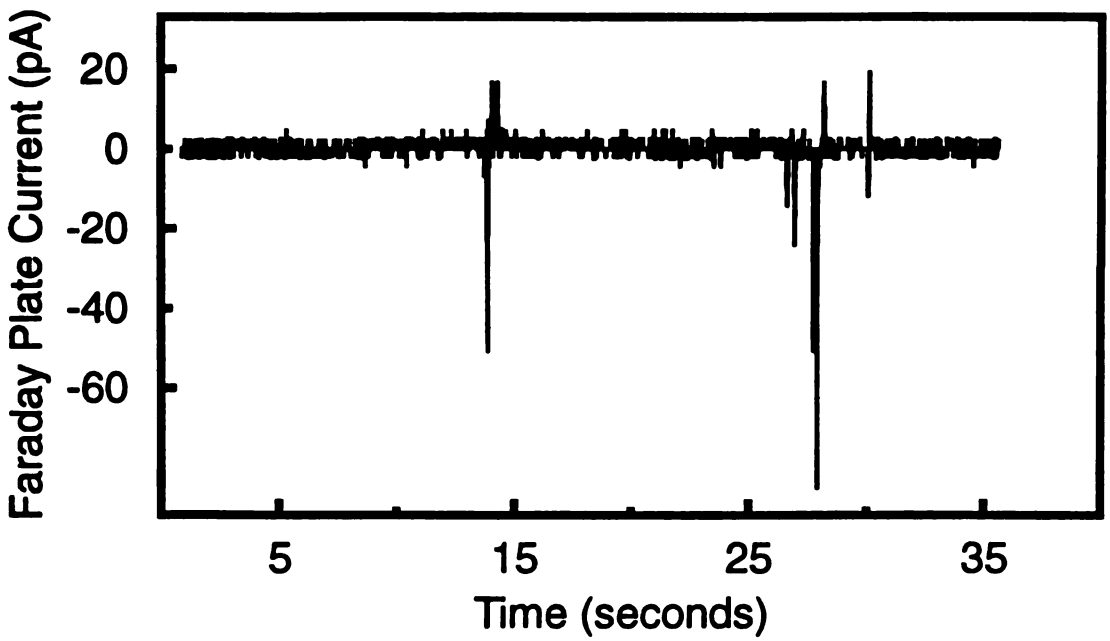

Figure 3.6: Transient current observed at the Faraday plate located ~1 cm from the substrate during warming of a neon matrix after a 25 hour deposition of 20 nA of CF_3^+ generated from electron impact of CF_3Cl. The initial temperature of the matrix was ~4.5 K The final matrix temperature temperature of ~20 K is reached within 10 seconds.

deposition of positive ions. This experiment also provides some insight into the composition of the matrix. If the matrix were to have a homogeneous distribution of positive and negative charge carriers, they would either recombine and be neutralized, or their signals would cancel. The presence of transient currents of both sign may indicate that the counter-ions are being formed in discrete time periods, rather than continuously, suggesting some sort of layering in the matrix. When an argon matrix containing CF_3^+ was subjected to two hours of 40 nA, 10 eV electron bombardment (the CF_3^+ absorption was not reduced after this electron bombardment), the transient signal shown in Figure 3.7 was measured as the substrate was warmed. In this case, desorbed negative charge carriers clearly dominate. This experiment suggests that the matrix can tolerate some charge imbalance. Perhaps during positive ion deposition, counter-ions are formed only after the potential in the matrix is sufficiently high to activate the counter ion generation process.

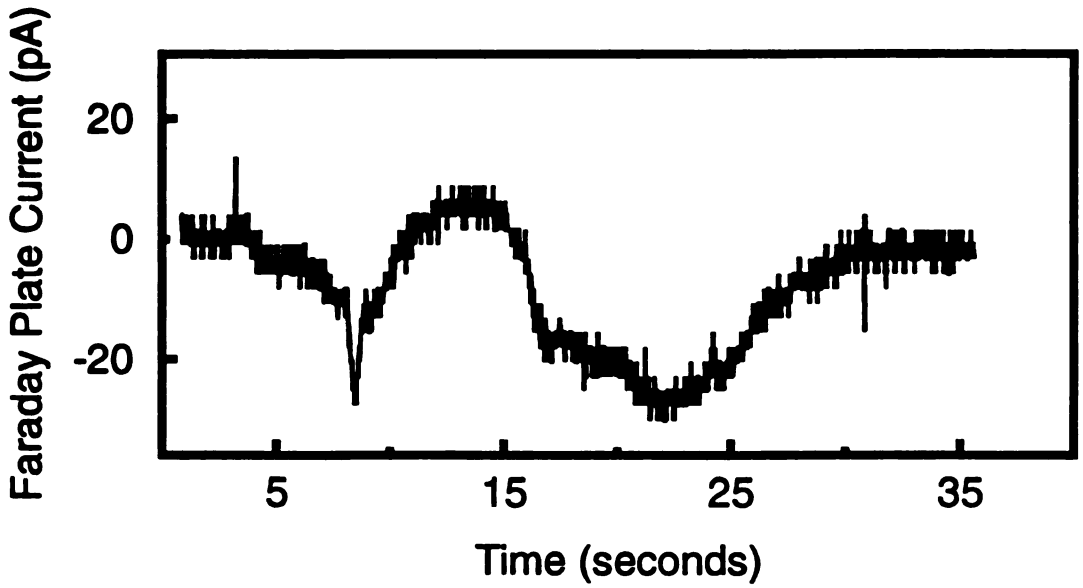

Figure 3.7: Transient current observed at the Faraday plate located ~1 cm from the substrate during warming of a argon matrix after a 25 hour deposition of 20 nA of CF_3^+ generated from electron impact of CF_3Cl, followed by 2 hour bombardment by 40 nA of 10 eV electrons The final temperature of the matrix was ~40 K.

List of References

(1) Halasinski, T. M. Ph.D. Dissertation, Michigan State University, 1996.

(2) Forney, D.; Jakobi, M.; Maier, J. P., *J. Chem. Phys.* **1989**, *90*, 600.

(3) Sabo, M. S.; Allison, J.; Gilbert, J. R.; Leroi, G. E., *Appl. Spectrosc.* **1991**, *45*, 535.

(4) Prochaska, F. T.; Andrews, L. *J. Am. Chem. Soc.* **1978**, *100*, 2102.

(5) *Chemistry and Physics of Matrix-Isolated Species*; Andrews, L., Moskovits, M., Eds.; Elsevier Science Publishing: Amsterdam, 1989.

(6) Lossing, F.P., *Bull. Soc. Chim. Belges*, **1972**, *81*, 125.

(7) Bürger, H.; Burczyk, K.; Bielefeldt, D.; Willner, H.; Ruoff, A.; Molt, K., *Spectrochim. Acta*, **1979**, *35A*, 875.

(8) Jacox, M. E.; Thompson, W. E. *J. Chem. Phys.* **1990**, *93*, 7609.

(9) Forney, D.; Jacox, M. E.; Irikura, K. K. *J. Chem. Phys.* **1994**, *100*, 8290.

(10) Jacox, M. E., National Institute of Standards and Technology, personal communication, 1994.

(11) Kelsall, B. J.; Andrews, L., *J. Phys. Chem.* **1981**, *85*, 2938.

(12) Jacox, M. E. *Chem. Phys.* **1968**, *83*, **171.**

(13) Milligan, D. E.; Jacox, M. E., *J. Chem. Phys.* **1968**, *48*, 2265.

(14) Hagstrum, H. D.; Becker, G. E., *Phys. Rev.* **1967**, *159*, 572.

Chapter 4:

The Formation of Counterions

I. Background

For the past two decades, matrix isolation has been utilized for the spectroscopic analysis of ions. A variety of cations, from simple diatomics including NO^+ [1] to polyatomic species such as the molecular ion of pentacene[2] ($C_{22}H_{14}^{\bullet+}$) have been characterized by this method. In all of these studies one has to assume that overall charge neutrality of the matrix is maintained in some way. Consider as an example the generation of $C_6F_6^{\bullet+}$ cations in a neon matrix by photoionization of matrix-isolated C_6F_6.[3] Presumably, when $C_6F_6^{\bullet+}$ is made some counterion is generated as well. In this case, like many others, the counterion may be an atomic species such as F^-, formed by electron capture of the precursor in the matrix, which is not detectable by ESR or vibrational spectroscopy. Spectroscopic peaks have been assigned to negatively charged species,[4] although correlations between anion and cation abundances usually cannot be made. In such experiments, in which the matrix is maintained at temperatures below 10 K, one may expect a variety of species to be present in the matrix that could capture electrons or in some way form stable anions, such as H_2O forming OH^-.

A few laboratories have reported success in the spectroscopic analysis of cations that have been created in conventional mass spectrometric ion sources, and mass-selected before their deposition into a growing inert gas matrix.[5,6,7] The most common mass spectrometer utilized for this purpose has been the quadrupole mass filter. If one must also deposit counterions into the matrix, then these experiments will become very

challenging. Even though mass spectrometry is a relatively mature field, the generation of large quantities of negative ions is still a "black art". The experiments described in Chapter 3 of this dissertation showed that depositing a beam of CF_3^+ ions into a growing Ne matrix over a period of hours resulted in the accumulation of sufficient numbers of cations for detection using FTIR spectroscopy without the concurrent deposition of negatively charged species. Clearly, this experiment should not have worked; in the absence of counter charges, the accumulated positive charge on the sample window would become limiting for continued deposition on the millisecond timescale. Although spectroscopic evidence of counterions was lacking in those experiments, we developed a technique whereby both positively and negatively charged species present in the matrix could be, and were, indirectly detected on a Faraday plate, held at an electric potential of 0 V, as the matrix was warmed.[5]

How are counterions generated in matrices upon cation deposition? Are there some unique features of the experimental setups, that have yielded results to date, that are critical to success? Clearly, a more complete understanding of counter ion generation is needed. This chapter describes the direct observation of counterions in matrices formed during the codeposition of mass-selected cations and neon. We have discovered that the addition of carbon dioxide to the neon matrix gas during deposition of a mass-selected ion beam results in detectable quantities of $CO_2^{\cdot-}$. Use of CO_2 as a matrix dopant also enhances positive ion accumulation efficiencies. The yield of stabilized cations increases by roughly a factor of five when CO_2 is present. Experiments utilizing matrices doped with CO_2 and the measurement of the current due to negatively-charged species have been

used to determine the mechanism that may provide the counter-charged species when mass-selected cation beams are deposited in low temperature matrices.

We have considered three possible mechanisms, illustrated in Figures 4.1–4.3. Mechanism 1 (Figure 4.1) is a condensed phase mechanism, in which accumulating positive charge in the matrix creates a field which is sufficient to extract electrons from the grounded metal window holder (with which the matrix is in contact). Thus, the primary negative charge is an electron, which migrates through the matrix and is captured by some molecular species capable of forming a stable anion. Mechanism 2 (Figure 4.2) is a gas phase mechanism. The incoming ions have sufficient kinetic energies to ionize gas phase species (exemplified by CO_2 in Figure 4.2) in front of the growing matrix, forming positive and negative charge carriers. The negative charge carriers, which may be electrons or negative ions depending on the molecules that are present in this region, are attracted toward the positive potential of the matrix. The nascent cation is repelled by the same field. Mechanism 3 (Figure 4.3) is a surface bombardment mechanism. Similar to Mechanism 2, incoming ions collisionally generate gas-phase electrons or negative ions which are subsequently attracted to the matrix. However, in this case the collisions are with cold metal surfaces and the molecules adsorbed on them (again exemplified by CO_2 in Figure 4.3).

II. Experimental

High purity neon (AGA), 99.9995%, was used as the matrix gas. Carbon dioxide, 99.8+%, was obtained from Aldrich Chemical Co. Reagent grade carbon disulfide was obtained from Fisher Scientific Co and used as received. The matrix gas, pre-mixed with

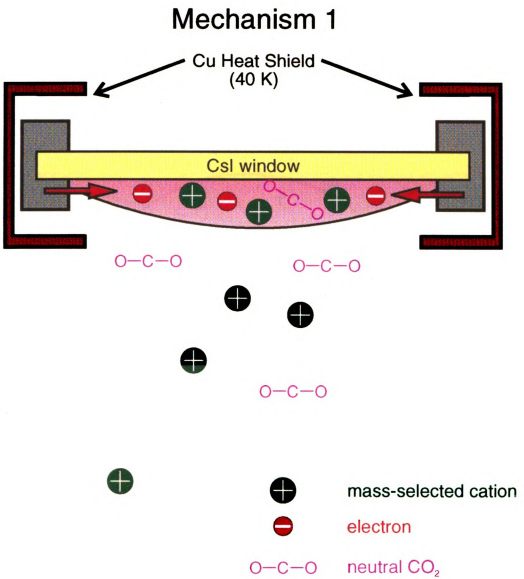

Figure 4.1: Illustration of proposed condensed phase mechanism of counterion generation in mass-selection, matrix-isolation experiments.

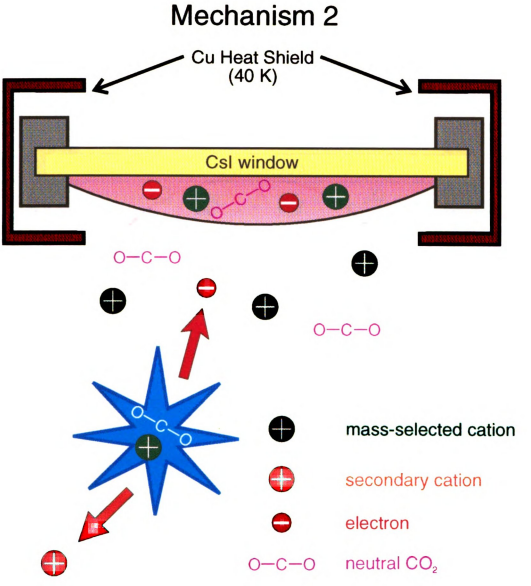

Figure 4.2: Illustration of proposed gas phase mechanism of counterion formation in mass-selected, matrix-isolated cation experiments.

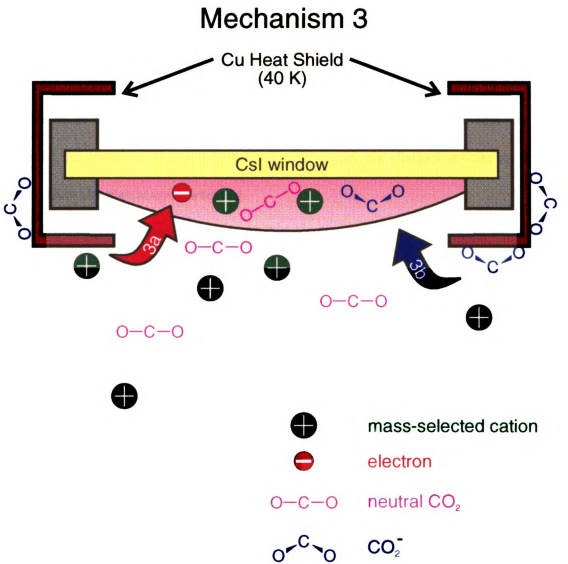

Figure 4.3: Illustration of proposed surface bombardment mechanisms of counter ion formation in mass-selected, matrix-isolated cation experiments.

measured amounts of CO_2 in some experiments, was deposited onto the sample window at a rate of ~0.5 mmole/hr. The energies of the mass-selected cation beams were in the range of 100–130 eV. In some of the experiments described in this chapter, a 70% transmission copper grid was fit onto the face of the CsI sample window as shown in Figure 2.8. Isolation of the grid and window holder makes it possible to float these components at various potentials, both during the ion accumulation process and while measuring the transient current of positively and negatively charged species as they are released from the matrix upon warming.

Potentials on components used as current detectors were established by placing a battery in-line between the metal component and a picoammeter. Electrostatic field simulations were performed with SIMION PC/PS2 Version 5.00.[8]

III. Results and Discussion

A. Spectroscopic Detection of Counterions

After successfully observing the infrared detection of mass-selected, matrix-isolated CF_3^+ ions generated from a variety of precursors,[5] we next selected for study the radical cation $CO_2^{\bullet+}$, again using neon as a matrix. These experiments were successful, with accumulated $CO_2^{\bullet+}$ detected at 1422 cm^{-1}, which had been previously assigned to ν_3 for the cation by Jacox and Thompson.[9] As shown in Figure 4.4, in these experiments we also observed spectral features at 1658 and 1665 cm^{-1}, assignable[9] to $CO_2^{\bullet-}$ (ν_3) and $(CO_2)_2^{\bullet-}$. This negative ion absorption had also been observed in other cation deposition experiments where CO_2 was not intentionally introduced into the experiment, but was present as a major component of the background gas, in part emanating at low levels from ceramic elements of the vacuum system. CO_2 is present in greater abundance in the

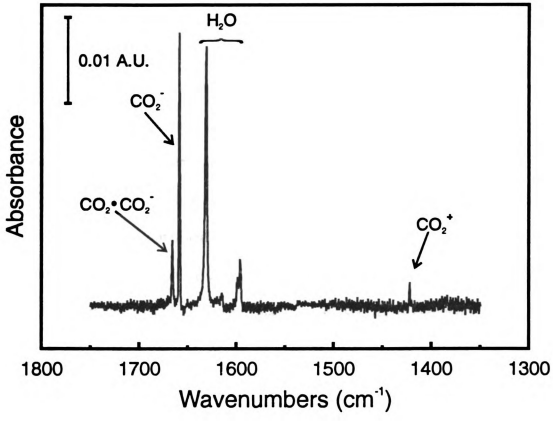

Figure 4.4: Infrared absorption spectrum of a neon matrix in the 1750–1350 cm^{-1} region following a 20 h deposition of 40 nA of $CO_2^{+\bullet}$.

vacuum chamber during $CO_2^{\bullet+}$ depositions owing to the incomplete pumping of the neutral precursor from the ion source housing.

The $CO_2^{\bullet-}$ anions observed could have a direct lineage to the incoming cations. That is, through a charge inversion process, some fraction of the incoming $CO_2^{\bullet+}$ could be converted into $CO_2^{\bullet-}$. To investigate this, we chose to repeat the experiment with CF_3^+. Figure 4.5 shows the spectrum observed when CF_3^+ is mass-selected and deposited, using a Ne:CO_2 matrix gas mixture of approximately 1000:1. Signals representing $CO_2^{\bullet-}$ are still present, showing that a process is occurring which results in their formation, but they are not formed directly from the incoming cations.

The presence of anions in the matrix is crucial to isolate sufficient quantities of cations for detection by vibrational spectroscopy. The use of CO_2-doped neon matrices and the subsequent formation of $CO_2^{\bullet-}$ provided two advantages. First, as previously noted, cation trapping is more efficient, allowing for shorter experiments. Second, it provides a direct spectroscopic probe of the counter charge identity and relative abundance, since we believe that, at the CO_2 levels used, a substantial fraction of the anionic species present in the matrix is $CO_2^{\bullet-}$ or $(CO_2)_2^{\bullet-}$. The growth curves for the cation and anion signals show a clear correlation between the relative amounts of these species.

The observation of $CO_2^{\bullet-}$ does not in itself provide information as to the mechanism of anion formation during cation deposition. However, the determination and elimination of mechanisms is made easier with the capability for spectroscopic detection of the anions present. We use the spectroscopically observable absorption due to $CO_2^{\bullet-}$ as a

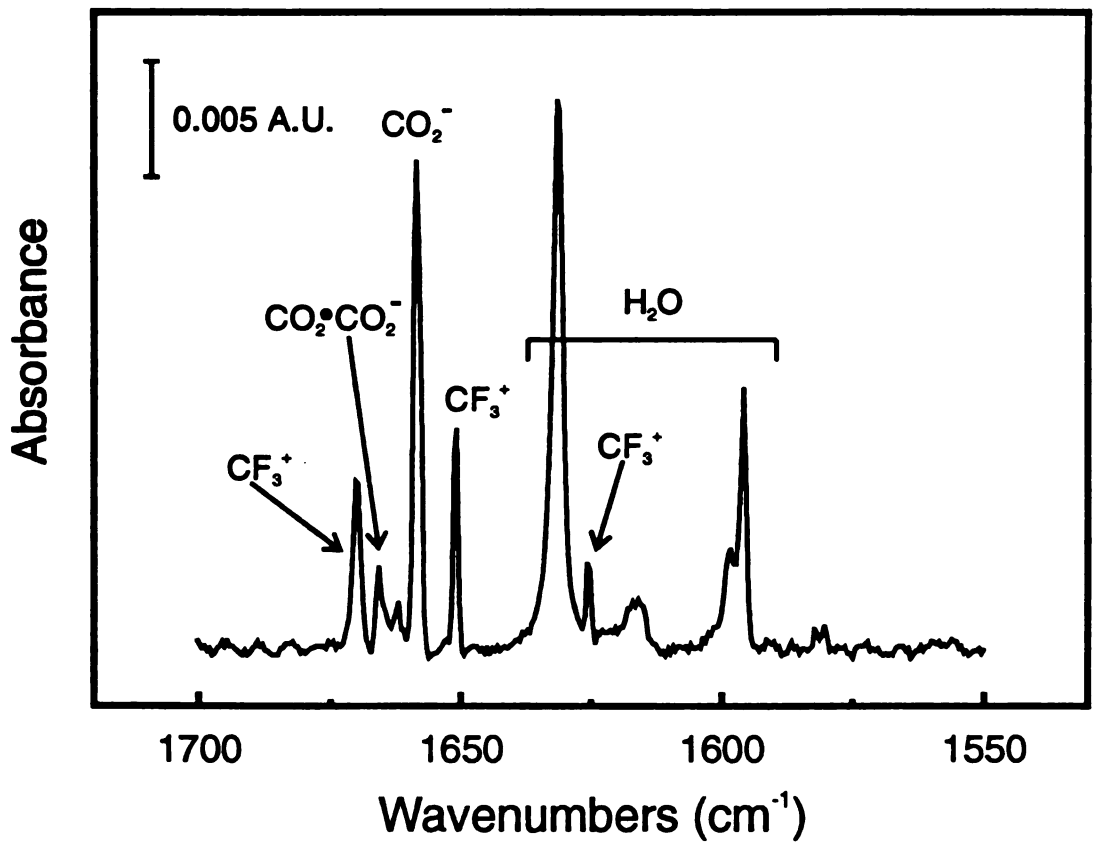

Figure 4.5: Infrared absorption spectrum of a 1000:1 Ne:CO_2 matrix in the 1750–1350 cm^{-1} region following a 13 h deposition of 20 nA of CF_3^+ formed by electron impact of CF_3Cl.

direct spectroscopic probe in our study of anion formation during mass-selected, matrix-isolated cation experiments.

B. Indirect Detection of Counterions

Isolation of the window holder also permits its use for measurement of transient currents from the matrix upon warming, similar to use of the Faraday plate which was employed in the past for these experiments. New modifications to this experiment also include the ability to float the window holder and Faraday plate at various potentials, in order to increase ion collection efficiency and to obtain separate signals for anions and cations by creating fields that will separate charges. Unexpected results are sometimes obtained when ions are collected as the matrix is warmed. This is particularly true when the Faraday plate is biased, and the window holder is held at ground. An example, obtained when the Faraday plate was biased at -70 V with respect to the grounded window holder, is shown in Figure 4.6. Although one would expect only positive ions to be collected, both positive and negative charges clearly strike the Faraday plate.

Several points are relevant in considering such results. As the matrix warms, the dynamics for released, charged species are complex. Warming may occur first at the matrix/window interface. It is unclear how inhomogeneous heating, with a neon matrix that rapidly vaporizes, influences the emanating ions. There are a variety of forces that act on ions which determine their trajectories as the matrix vaporizes. The first is applied fields, which we create to separate ions of opposite charge. However, ion/ion interactions likely create stronger and more complex fields. The many collisions of the ions with the desorbing neon must also be considered. Further, the distribution of anions and cations within the matrix and across the cold window need not be homogeneous. Thus, it is not

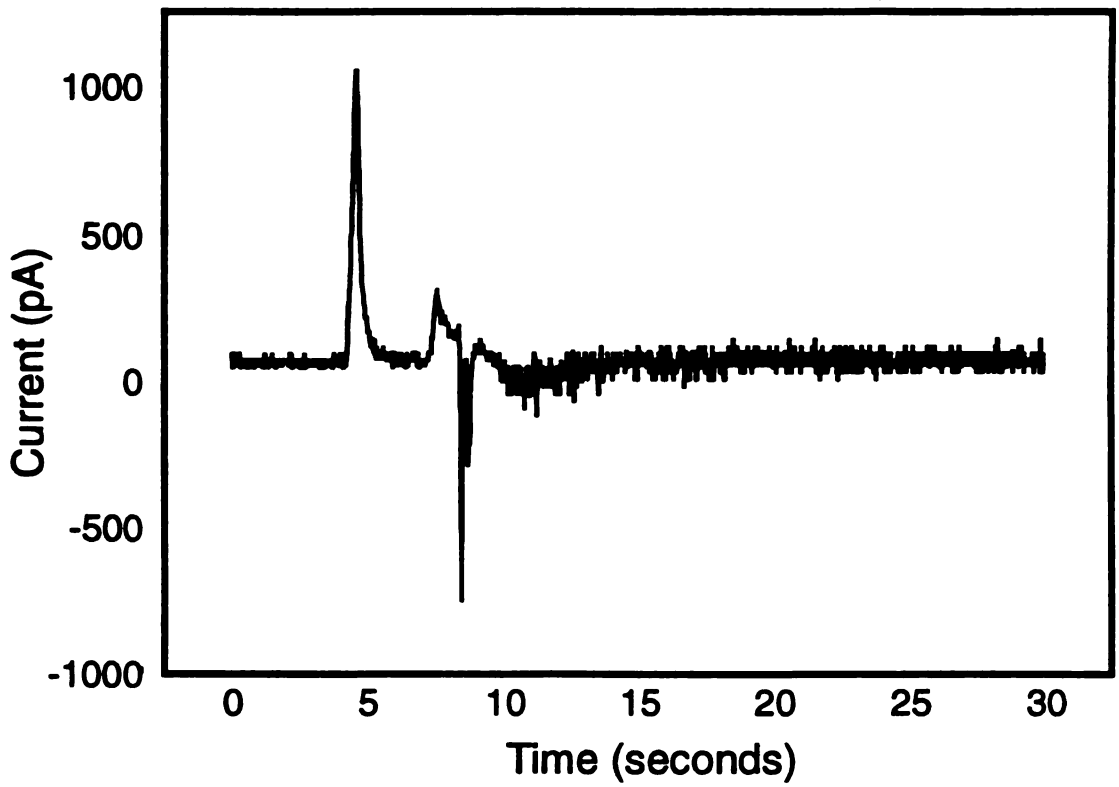

Figure 4.6: Currents observed on the Faraday plate from a warming neon matrix after a 27 h deposition of 40 nA of $CO_2^{+\bullet}$. The cryostat heater is turned on a t = 0 s. At t = 30 s, the temperature was ~40 K. The potential on the Faraday plate during the collection of the signal was -70 V with the window holder grounded.

surprising that, even when a field is established to collect cations on the Faraday plate, some anions reach the collector as well. Also, while an experiment with the window holder at ground and the Faraday plate at -70 V may be assumed to create conditions to collect only cations at the Faraday plate, all points across the salt window are not at a potential of 0 V. This situation is illustrated in Figure 4.7a, which shows a SIMION plot of the potential gradient formed between the elements that create it, the Faraday plate and the other metallic surfaces. The window location is indicated by the dotted line in the figure. The full -70 V is not realized by ions originating at the window, and the field is clearly not linear between the salt window and the collector. The complex potential surface on which desorbed ions move is not that which we hoped to form.

To create a more ideal electrostatic situation for detection and possibly sorting of desorbed ions, we placed a metallic grid across the face of the CsI window. A SIMION plot of the potential gradient formed, with the grounded grid present and with -70 V applied to the Faraday plate, is shown in Figure 4.7b. The potential surface is now considerably more linear between the sample window/grid and the Faraday plate. Figure 4.8 shows the currents observed on both surfaces with the Faraday plate held at a potential of +70 V as a matrix is warmed. In this plot it is clear that negative signals dominate at the Faraday plate and positive signals at the grid collector on the sample window, suggesting that desorbed ion motion is influenced primarily by the applied field in this case.

The results of all configurations of these experiments show that extensive cation/anion recombination takes place, and that the signals measured are only a very small fraction of the total charge present in the matrix before warming. A deposition of 20 nA

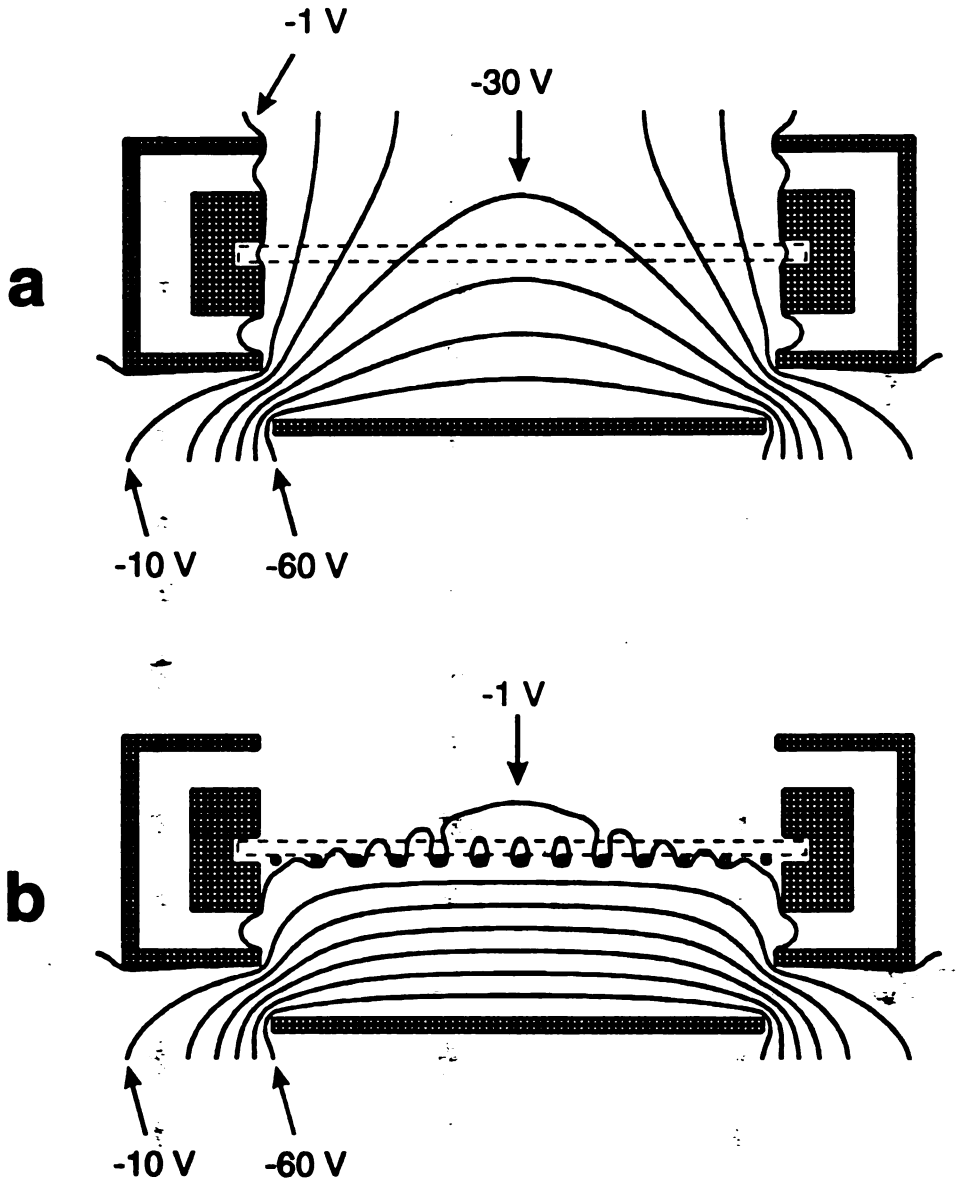

Figure 4.7: SIMION plots showing the potential surface formed between the Faraday plate and the CsI window. Equipotential lines, separated in value by 10 V, are shown. The CsI window is represented by a dashed line in both plots. The grounded copper grid has been added to part b. The Faraday plate has a potential of -70 V, and all other surfaces are at a potential of 0 V in both plots.

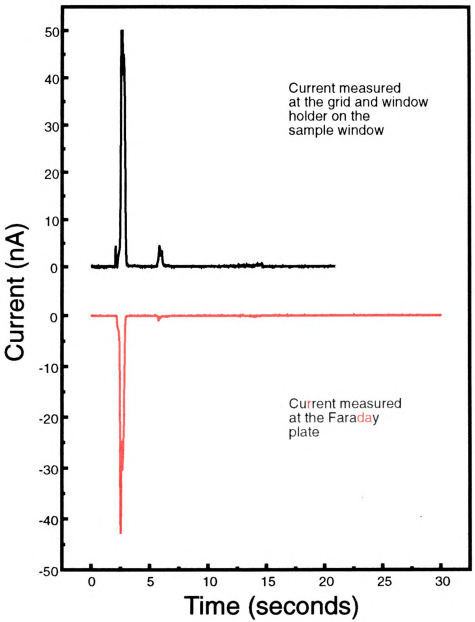

Figure 4.8 Currents observed from a 1700:1 Ne:CO_2 matrix after a 20 h deposition of 30 nA of $C_7H_7^+$ generated by electron impact ionization of toluene. Heating conditions are the same as Figure 4.6. The potential of the Faraday plate during collection of the signals was +70 V with all other elements held at 0 V.

of cations for 5 h corresponds to 2×10^{15} ions in the matrix (assuming all ions are isolated). A 50 nA ion signal for 1 s, similar to those shown in Figure 4.8, corresponds to 2.5×10^{13} ions. Clearly, most matrix-isolated ions are neutralized or impinge on surfaces other than those used here as collectors upon warming. Also, because the magnitudes of the signals vary between experiments, quantitative information cannot be extracted from them. However, such measurements provide a means for quickly detecting the presence of cationic and anionic species, of particular importance in experiments where this cannot be done spectroscopically. The technique is useful in optimizing the experimental system, since emitted ion currents can be obtained after < 2 hours of ion deposition, whereas longer times are required when spectroscopic detection is the only tool available for determining matrix composition.

C. Evaluation of Counterion Generation Mechanisms

In Mechanism 1, we considered the possibility that accumulating cations in the matrix would create a collective electric field that would assist in the extraction of electrons from the grounded nickel-plated copper window holder into the matrix with which it is in intimate contact. To investigate this mechanism, we electrically isolated the window holder, thus terminating the connection to its source of electrons (ground). If only cations are accumulated in a growing matrix, and the impinging ions have kinetic energies of 100 eV, the potential of the matrix cannot exceed 100 V. This will be established within the first second of deposition. If this potential is sufficient to extract electrons (or anionic impurities) from the grounded window holder, then isolating the window holder from ground should prohibit the continuous deposition of cations over periods of several hours. Experiments performed with the isolated window holder, with

all other parameters the same, resulted in no change in the infrared absorption spectrum. Both cationic and anionic species were observed with absorption intensities equivalent to the earlier experiments in which the window holder was not isolated. Mechanism 1 can therefore be eliminated.

Unfortunately, it is not experimentally straightforward to distinguish between Mechanisms 2 and 3. To determine if Mechanism 3 is operative, one may consider ways to deposit ions without having some fraction of them bombard metal surfaces. However, the mass-selected ion beam cannot presently be focused sufficiently well to impinge only on the growing neon matrix and not the surrounding metallic surfaces. Isolation of the metallic surfaces from ground may be useful; however, this changes the electric potentials involved in the experiment due to static charging by the unfocused ion beam. Removal of the radiation shield, another possible approach, would compromise the thermal aspects of the experiment.

Insights regarding Mechanisms 2 and 3 were first obtained during attempts to observe IR transitions of mass-selected, matrix-isolated $C_6F_6^{\bullet+}$. Several new absorptions, shown in Figure 9, were observed. These transitions, unfortunately, could be assigned to CF, CF_2, and CF_3, presumably formed from the fragmentation of $C_6F_6^{\bullet+}$. To attempt to reduce this fragmentation, the energy of the ion beam was reduced to 50 eV by using the electrically isolated metallic grid on the CsI window, as described above, and applying to it a positive potential of +80 V during the course of the matrix deposition. All surrounding surfaces were at ground potential. The bottom trace of Figure 9 shows that this approach was successful in reducing the fragmentation of the incoming cations. Other results of this experiments were unexpected. Along with a decrease in fragmentation products, a large

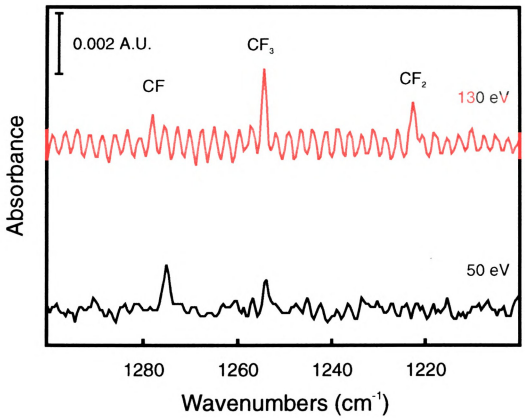

Figure 4.9: Infrared absorption spectrum of a 1500:1 Ne:CO_2 matrix in the 1300–1200 cm^{-1} region following a 22 h deposition 35 nA of 130 eV $C_6F_6^+$ ions (top trace) and similar amounts of 50 eV $C_6F_6^+$ ions (bottom trace). In both cases, the $C_6F_6^+$ ions were generated from electron impact of C_6F_6.

absorption due to $CO_2^{\bullet+}$ at 1422 cm^{-1} was observed. This absorption, shown in Figure 10, is larger than the signal observed when $CO_2^{\bullet+}$ is intentionally deposited into the matrix. We attribute the appearance of $CO_2^{\bullet+}$ to ionization of neutral CO_2 molecules in the matrix by electrons that have been formed by cation bombardment of surfaces and are accelerated towards the matrix by the potential applied to the grid. If Mechanism 2 is operative, electrons would most probably be formed immediately in front of the growing matrix where the density of gas phase particles is greatest. An electron formed in this area would likely not be accelerated to a kinetic energy required to ionize other neutral species in the matrix so efficiently. Only in Mechanism 3 would the electrons experience the full 80 V acceleration, allowing them to ionize neutral species in the growing matrix. Regarding Mechanism 3, large (~30%) secondary electron emission from metal meshes bombarded with anions has been recently reported.[10] Such processes are of concern to mass spectrometrists who work with negative ions, since ion/surface interactions can yield electrons which are detected along with incoming anions, making signals artificially large. Schlag and co-workers[10] attribute the electron origin mainly to the adsorbed residual gases, which is consistent with the temperature dependence they observed. It seems likely that a similar mechanism for electron emission occurs to some extent in our experiments.

Other evaluations of Mechanism 2 suggest that it is not the process by which positive ions are created and deposited into the matrix. As stated in Chapter 3, experiments performed with mass-selected ion beams of $CF_2^{\bullet+}$ fail to produce absorptions due to isolated CF_3^+ ions in the matrix. Only when ion beams of CF_3^+ are mass-selected and matrix-isolated are absorptions due to CF_3^+ observed. This is reasonable; even if 100 eV $CF_2^{\bullet+}$ ions collided with neutral, gas phase precursor CF_3Cl molecules to form CF_3^+

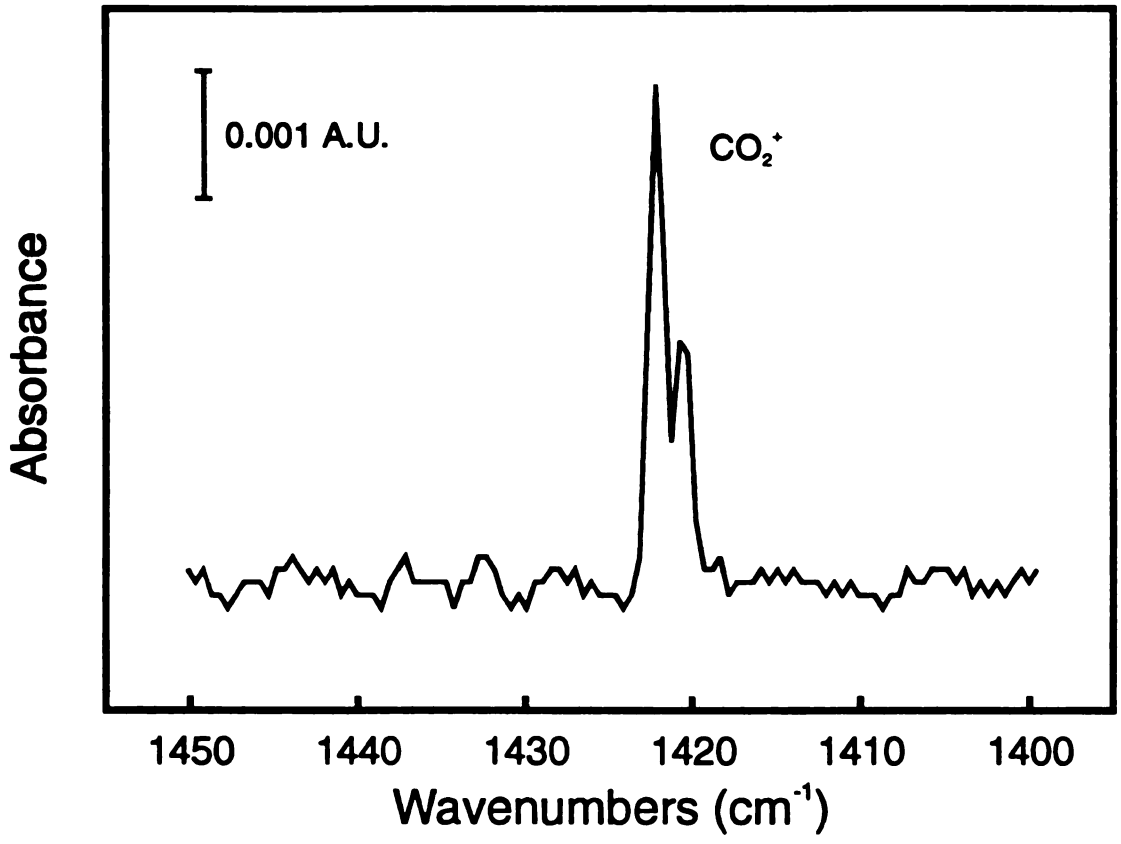

Figure 4.10: Infrared absorption spectrum of a 1500:1 Ne:CO_2 matrix in the 1450–1400 cm^{-1} region showing $CO_2^{+\bullet}$ formed when a copper grid was used to decelerate incoming $C_6F_6^{+\bullet}$ cations. Depositions conditions are identical to those represented by the bottom trace of Figure 4.9.

and Cl^-, the $CF_2^{\bullet+}$ in the matrix would not create a field that would attract gaseous, low energy CF_3^+ ions toward the window. Only the ions in the mass-selected ion beam have sufficient energy to overcome the slight positive potential of the matrix and become isolated. Therefore, when the window grid is positively biased and we detect $CO_2^{\bullet+}$, this cation is not being deposited into the matrix, but is formed in the matrix upon electron bombardment.

D. Direct Observation of Anion Generation

To further investigate whether Mechanism 2 or 3 is the cause of negatively charged species being deposited into the matrix, the CsI window was replaced with a copper plate to measure current that may impinge on the location of the salt window in these experiments. This copper plate can be grounded or biased while being used as a Faraday plate. Several experimental configurations were investigated, and four are shown as Configurations 1–4 in Figures 4.11–4.14, respectively. In each case, the experimental configuration is shown on the left, the results of the experiments are shown in the middle, and our interpretation of the results is shown on the right. For each pair of data traces, the top trace shows current measured at the copper plate that was substituted for the CsI window, and the bottom trace is current measured at the retracted Faraday plate, which lies approximately 1 inch to the right of the copper plate, outside of the radiation shield. Each pair of traces was obtained simultaneously. A manual gate valve was opened/closed to start/stop the incoming $CS_2^{\bullet+}$ ion beam. The ion beam was presented for two one-minute periods (approximately 30–90 seconds and 150–210 seconds into the measurement) during the displayed time period. Matrix gas (Ne:CO_2 1000:1) was present in all experiments.

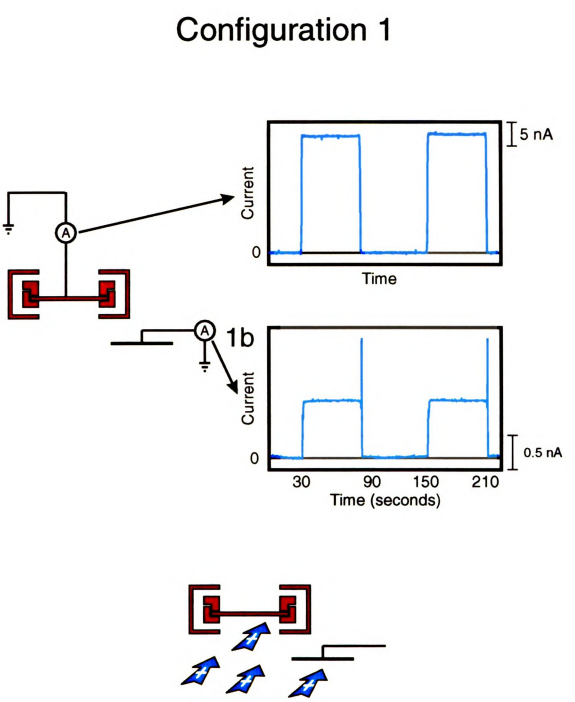

Figure 4.11: Direct measurement of anion generation, Configuration 1. The experimental setup is indicated on the left, data in the center, and the interpretation on the bottom.

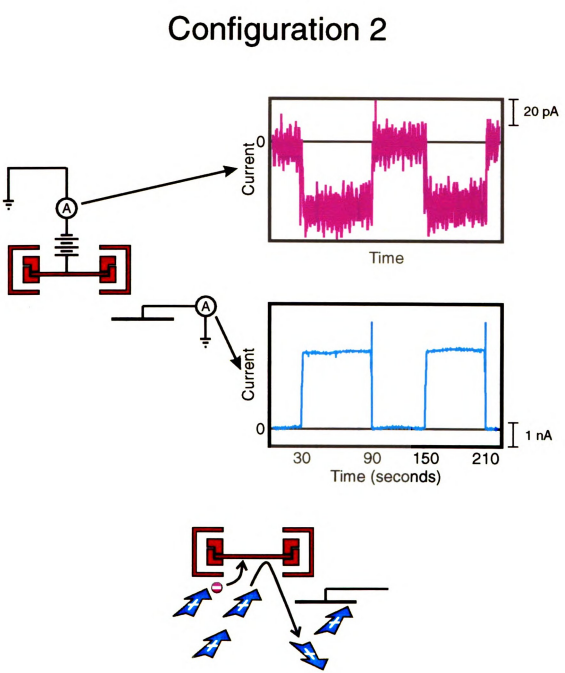

Figure 4.12: Direct measurement of anion generation, Configuration 2. The experimental setup is indicated on the left, data in the center, and the interpretation on the bottom.

Configuration 3

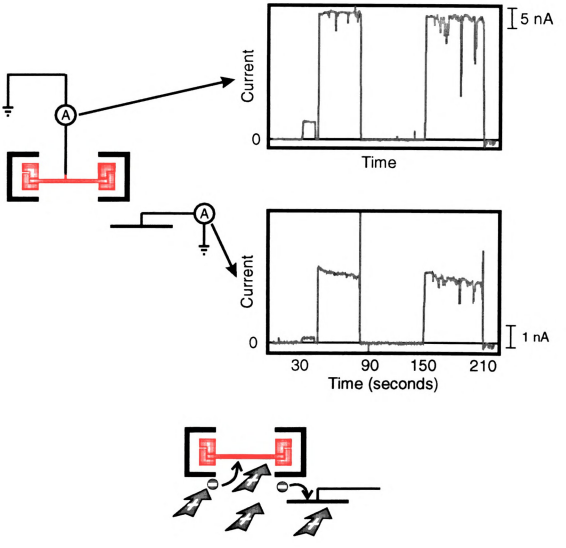

Figure 4.13: Direct measurement of anion generation, Configuration 3. The experimental setup is indicated on the left, data in the center, and the interpretation on the bottom.

Configuration 4

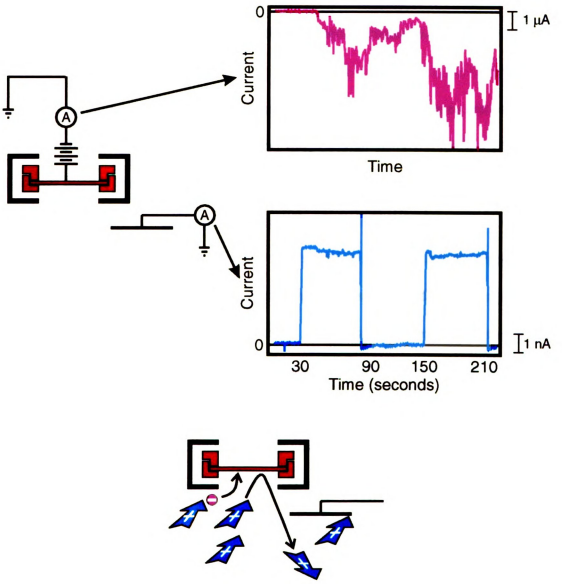

Figure 4.14 Direct measurement of anion generation, Configuration 4. The experimental setup is indicated on the left, data in the center, and the interpretation on the bottom.

When all surfaces are at room temperature, Configuration 1 (Figure 4.11), the incoming cation beam has a current of approximately 30 nA, as shown in trace 4.11a. The retracted Faraday plate, which sits to the side of the radiation shield, collects approximately 1 nA of cation current (trace 4.11b), demonstrating that not all of the incoming ions strike the surface on which the spectroscopically-observable matrix is formed.

Are negative charges being formed in this experiment, when gases are present and all surfaces are at room temperature? To test this, Configuration 2 (Figure 4.12) is used. The copper plate is biased at a positive potential of 250 V. This design is preferable for detecting any negative current formed for the following reason. In Configuration 1, trace 4.11a could represent the sum of positive and negative ions striking the copper plate. With a +250 V bias on the copper plate, incoming cations are repelled and only negative charges are collected. Trace 4.12a shows that a small negative current is formed when a positive ion beam is admitted into the experimental chamber. We believe that the signal shown in this trace represents negative charges which are formed by ion bombardment of nearby metal surfaces, on which molecules are adsorbed. These negative charge carriers are attracted to the positively-biased copper plate. Note that the fraction of incoming positive ions collected by the Faraday plate in Configuration 2 is slightly larger than in Configuration 1 due to the positive potential applied to the copper plate in the latter case.

If Mechanism 3 is operative, then cooling the radiation shield should have a dramatic effect on such measurements. This situation is created using Configuration 3.(Figure 4.13) The cryostat radiation shield can be cooled to a temperature of ~40 K, and, via a heater on the window holder block, the copper plate can be maintained at

approximately 225 K. Under such conditions, with Ne and CO_2 present, CO_2 should accumulate on the radiation shield, leading to the formation of a larger negative current upon cation bombardment. When the radiation shield is cooled, and the copper plate held at ground, the data shown in traces 4.13a and 4.13b are collected. As in Configuration 1, incoming cations are detected. The negative deflections which are superimposed on the cation signal in traces 4.13a and 4.13b are due to negatively-charged species striking the copper plate and the Faraday plate. Several aspects of the data warrant comment. First, we have evaluated many experiments that employ Configuration 3 and the negative deflections detected at the copper plate, such as those clearly seen in the 150–210 second time window of trace 4.13a, correlate with identical features in the current detected at the Faraday plate, trace 4.13b. This suggests that ion bombardment of the cold surface results in ejection of negative charges into the gas phase. They then impinge on a variety of grounded surfaces, and thus show a specific time correlation. Second, it is unexpected that the negative charge generation is not continuous. This remains the most surprising aspect of this data set. Finally, the negative current deviations are relatively small compared to the cation signal. If this is the case, then the process of ion bombardment of cold surfaces on which CO_2 is condensed is not yielding an anionic current sufficient to balance the charge of the incoming cationic current. However, in Configuration 3 the copper plate is held at a potential of 0 V; during the experiment it is likely that the matrix holds a net positive charge.

To optimize our ability to measure negative charges from the cation bombardment of the cold radiation shield, Configuration 4 is used. With a positive potential on the copper plate, as in Configuration 2, incoming cations are repelled from this plate and a

field is created which will collect most of the negative charges that are formed. As expected, the grounded Faraday plate shows a simple cation signal in trace 4.14b. However, the temporal and signal intensity aspects of the data shown in 4.14a are surprising. Negative charge generation under these conditions is very different from that detected in Configuration 2. Negative charge is not detected promptly upon cation bombardment, and does not cease promptly when the incoming ion beam is blocked by the gate valve. Also, negative charge currents larger than expected are collected. At present this is not fully understood. The total cationic current striking the entire radiation shield is at most 200 nA; the observations require that more than one negative charge carrier is generated per incoming cation. This would suggest a surprisingly efficient utility of the cation kinetic energy. Unfortunately, we are working in an energy regime in which few relevant ion/surface interaction experiments have been performed. Considering that anions impinge on the biased surface at energies of ~250 eV in this configuration, it is possible that part of the total negative current measured in 4.14a includes anions losing two electrons each at the surface and leaving as cationic species.[11] That is, the current sensed may not be a simple measure of the primary negative charges formed. The difference between the data in traces 4.12a and 4.14a may also suggest that part of the current detected in 4.14a is field assisted, due to the positive potential on the copper plate.

However, the important observation from Configuration 4 is that the number of negative charges that can be produced per second, induced by cation bombardment, is enhanced when the radiation shield is cooled. Since we know that a portion of the ion beam strikes this copper surface, and that CO_2 condenses on the surface, we present this as strong support for Mechanism 3. It should be noted that results similar to these are

obtained when the CsI window is present and the window holder is used to measure ionic currents, and that the results are independent of the identity of the mass-selected cation. It was also observed that the absorptions due to $CO_2^{\bullet-}$ are much less intense over the course of a positive ion deposition when argon is used as the matrix gas in place of neon. Presumably, argon competitively adsorbs onto the cold metal surfaces, reducing the probability for negative ion formation from adsorbed CO_2. While the behavior of CO_2 is the focal point here since it is added to the matrix gas, other molecules such as water can likely play the same role when there is no matrix additive introduced to assist in counter ion formation.

Explicitly, we suggest that both electrons and anions leave the cold radiation shield upon energetic ion bombardment. Experimental results presented above in the discussion of Figure 4.10, where a biased grid was placed on the window, suggested that electrons are released, consistent with the report of Schlag et al.[10] It was also observed that the absorbance due to the $(CO_2)\cdot(CO_2^{\bullet-})$ anion is present whenever $CO_2^{\bullet-}$ is spectroscopically observed. Despite widely varying Ne:CO_2 ratios in the matrix, the ratio of peak intensities of the absorbances due to the two species is maintained in the 5:1 to 8:1 (monomer:dimer) range. This suggests that cation bombardment of the cold, CO_2-covered metal surfaces produces electrons, $CO_2^{\bullet-}$ and $(CO_2)\cdot(CO_2^{\bullet-})$ in relatively constant ratios, presumably because the concentration of CO_2 on the surface is more constant than either in the gas phase or the matrix, for the variety of experiments we have performed.

E. Discussion

The literature on the structure and physical characteristics of $CO_2^{\bullet-}$ and $(CO_2)_2^{\bullet-}$, as well as information available from the surface science literature concerning the structure of

CO_2 on metal surfaces, yields an important context for the proposed mechanism. There are several reports confirming the creation of negatively charged species upon bombardment of metallic surfaces with positively charged ions,[11,12] including the formation of $CO_2^{\bullet-}$.[13] The temperature of the metallic surfaces surrounding the matrix window must play an important role in Mechanism 3. The radiation shield itself is maintained at approximately 40 K, cold enough to freeze the relatively high concentration of CO_2 from the nearby matrix gas sprayer, but not cold enough to freeze the neon matrix gas. CO_2 is therefore selectively collected onto the metal surface. A portion of the diverging positive ion beam hits the copper radiation shield continuously during our experiments. It seems likely that the bombardment of these surfaces with positive ions may sputter off negatively charged $CO_2^{\bullet-}$ ions and electrons. For some $CO_2^{\bullet-}$ ions, the time of flight to the matrix may exceed the lifetime of the ion (20–90 microseconds),[14,15] and they may dissociate into neutral CO_2 and electrons. However, electrostatic field simulations using SIMION show that negative species formed near the edge of the hole in the radiation shield reach the positively-charged matrix in times shorter than the reported lifetime.

The fact that $CO_2^{\bullet-}$ is observed in our experiment may be a key to the mechanism of its formation. While the $CO_2^{\bullet-}$ anion was first detected in matrices by ESR in 1961 following gamma ray irradiation of an alkali halide matrix of sodium formate,[16] the nature of its stability has been the subject of considerable discussion. It has been suggested that isolated $CO_2^{\bullet-}$ should not exist, unless stabilized by complexation in a matrix with a cation[17] such as Na^+. Several reports have concluded that CO_2 adsorbed on a copper surface is a bent and negatively charged entity.[18] The electron affinity of CO_2 has been measured to be approximately -0.6 eV.[15] This does not indicate that the anion is

inherently unstable, but reflects the relative stability between the neutral, linear molecule and the bent anion.[19] $CO_2^{\bullet-}$ ions can be generated in negative ion mass spectrometry from gas phase organic molecules that contain a "bent CO_2 unit".[14,20] Comparisons of $CO_2^{\bullet-}$ with the stable, isoelectronic species $NO_2^{\bullet}$ have been made as well.[21] Thus, while the electron affinity of the linear neutral molecule is negative, direct $CO_2^{\bullet-}$ generation from surface-adsorbed CO_2, where the molecule is bent and can readily accept an electron, or electron capture of CO_2 molecules in very low temperature inert gas matrices are certainly plausible processes to yield this anion in a neon matrix.

The CO_2 dimer electron affinity has been estimated to be +0.8 eV by collisional electron transfer between a crossed molecular beam of CO_2 clusters and a seeded supersonic beam of alkali-metal atoms.[22] Although ab initio calculations for the electron affinity for the dimer show that it may still be slightly negative (-0.31 eV),[23] it is apparent that solvation of a single CO_2 molecule by other molecules, such as CO_2, increases its electron affinity. The metallic surfaces in our experiments may not only assist in forming bent CO_2, which has a positive electron affinity, but their cold temperature may also help to form clusters of the CO_2 molecules, further facilitating the formation of anions.

In our laboratory, $CO_2^{\bullet-}$ has been detected in matrix isolation experiments involving a variety of mass-selected cations. These ions include both even electron cations (CH_3^+, CF_3^+, $C_7H_7^+$, $C_2H_2O^+$) and radical cations ($CO_2^{\bullet+}$ $CS_2^{\bullet+}$, $C_6F_6^{\bullet+}$).

IV. Conclusions

A working model, which incorporates the mechanism suggested and other aspects of the experiment that we now realize are important, is presented in Figure 4.15. Successive points in time are shown, representing one extreme view of the system. At

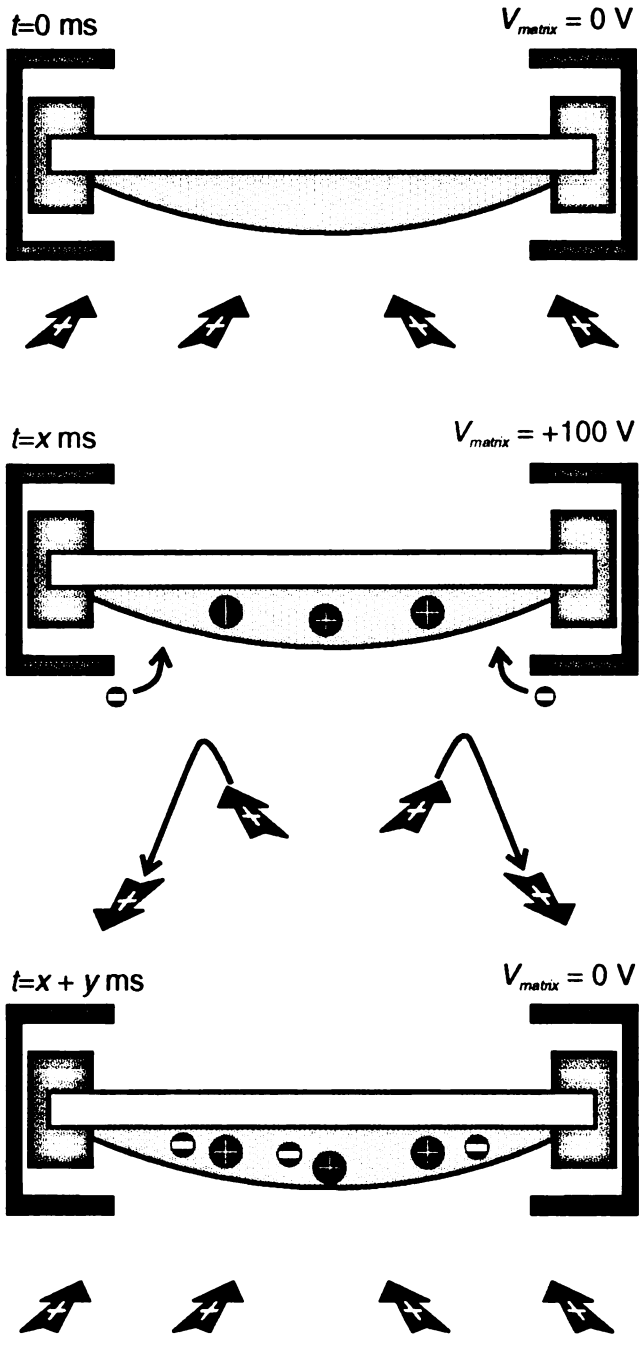

Figure 4.15: Illustration of the proposed processes occurring during deposition of a 100 eV positive ion beam and neon on the CsI sample window and the metallic radiation shield.

$t = 0$, incoming cations are collected in the growing inert gas matrix. If the ions have kinetic energies of 100 eV, the matrix can sustain a net positive charge of +100 V. At this point, $t = x$ ms, subsequent incoming cations are repelled from the matrix and no further accumulation can occur. The positively-charged matrix then attracts negative charges emanating from condensed molecules on cold surfaces. The matrix continues to attract the negative charges until the net matrix potential is 0 V ($t = x + y$ ms). Additional incoming cations can then be deposited and the process can continue.

This is clearly an extreme model, which would lead to a layered matrix. More realistically, some mean potential of the matrix must be established, which lies between 0 and +100 V. The matrix, then, always has a net positive potential, attracting negative charges. However, its potential is never sufficiently high to repel incoming cations, since anion generation and accumulation is also occurring at a high rate. The cations, thus, serve a variety of purposes. Not only are they the analytes in these spectroscopic experiments, but they create a positively charged matrix, and this is required for the accumulation of negative charges that are formed on nearby surfaces.

In some experiments, the quantity of available cations may exceed the number of available anions, and the mean matrix potential will be high. In other experiments, where generation of negative charges occurs with high rates, the mean matrix potential may be close to 0 V. The mean matrix potential must have an important influence on the results of experiments involving matrix isolation of ions. How can a beam of 100 eV CF_3^+ cations lead to their spectral detection, when only 3–4 eV are required to break a bond? We propose that the mean matrix potential serves to decelerate the incoming ions, creating a field which slows them down so that the full initial kinetic energy is not relevant to the

deposition process. The deposition kinetic energy is determined by the difference between the accelerating voltage in the ion source and the mean matrix potential, $K.E._{(deposition)} = e(V_{accel} - V_{matrix,\,mean})$. This may explain why some cations are more difficult to detect than others in such experiments. An ionic species such as $C_6F_6^{\bullet+}$ which we can generate and deposit, but have not yet detected using vibrational spectroscopy, may create a situation in which the mean matrix potential is close to 0 V; thus the incoming ions maintain high kinetic energies when they encounter the surface, resulting in collision-induced dissociation and charge transfer processes. In contrast, the experiments involving CF_3^+ may lead to sufficiently high mean matrix potentials that the incoming cations undergo relatively "soft landings". Clearly the mean matrix potential, while difficult to directly measure, is an important experimental consideration in the success of such experiments.

List of References

(1) Jacox, M. E.; Thompson,W. E. *J. Chem. Phys.* **1990**, *93*, 7609.

(2) (a) Szczepanski, J.; Wehlburg, C.; Vala, M. *Chem. Phys. Lett*, **1995**, *232*, 221. (b) Hudgins, D. M.; Allamandola, L. J. *J. Phys. Chem.* **1995**, *99*, 8978.

(3) Bondybey, V. E.; Miller, T. A. *J. Chem. Phys.* **1980**, *73*, 3053.

(4) Prochaska, F. T.; Andrews, L. *J. Am. Chem. Soc.* **1978**, *100*, 2102.

(5) Halasinski, T. M.; Godbout, J. T.; Allison, J.; Leroi, G. E. *J. Phys. Chem.* **1994**, *98*, 3930.

(6) Maier, J. P. *Mass Spectrom. Rev.* **1992**, *11*, 119.

(7) Knight, L. B., Jr. in: *Chemistry and Physics of Matrix-Isolated Species*; Andrews, L., Moskovits, M., Eds.; Elsevier Science Publishing: Amsterdam, **1989**.

(8) Dahl, D. A.; Delmore, J. E. SIMION PC/PS2 Version 5.00, Idaho National Engineering Laboratory, **1991**.

(9) Jacox, M. E.; Thompson, W. E. *J. Chem. Phys.* **1989**, *91*, 1410.

(10) Fraunberg, W.-D. v.; Drechsler, G.; Bäßmann, C.; Boesl, U.; Schlag, E. W. *Int. J. Mass Spectrom. Ion Processes* **1994**, *133*, 211.

(11) Bier, M. E.; Vincenti, M.; Cooks, R. G. *Rapid Commun. Mass Spectrom.* **1987**, *1*, 92.

(12) Middleton, R.; Klein, J.; Fink, D. *Nucl. Instr. and Meth.* **1989**, *B43*, 231.

(13) (a) Arnot, F. L.; Beckett, C. *Proc. Roy. Soc. (London)*, **1938**, *A168*, 103. (b) Schubert, S.; Imke, U.; Heiland, W.; Snowden, K. J.; Reijnen, P. H.; Kleyn, A. W. *Surface Sci.* **1988**, *205*, L793.

(14) Cooper, C. D.; Compton, R. N. *Chem. Phys. Lett.* **1972**, *14*, 29.

(15) Compton, R. N.; Reinhardt, P. W.; Cooper, C. D. J. *Chem. Phys.* **1975**, *63*, 3821.

(16) Ovenall, D. W.; Whiffen, D. H. *Mol. Phys.* **1961**, *4*, 135.

(17) Koppe, R.; Kasai, P. H. *J. Phys. Chem.* **1994**, *98*, 11331.

(18) (a) Linder, H.; Rupprecht, D.; Hammer, L.; Müller, K.; *J. Electron Spectrosc. Relat. Phenom.* **1987**, *44*, 141. (b) Copperwaite, R. G.; Davies, P. R.; Morris, M. A.; Roberts, M. W.; Ryder, R. A. *Catal. Lett.* **1988**, *1*, 11. (c) Carley, A. F.; Roberts, M. W.; Strutt, A. J. *Catal. Lett.* **1994**, *29*, 169.

(19) (a) Cadez, I.; Tronc, M.; Hall, R. I. *J. Phys. B: Atom. Molec. Phys.* **1974**, *7*, L132. (b) Krauss, M.; Neumann, D. *Chem. Phys. Lett.* **1972**, *14*, 26.

(20) Ropp, G. A.; Melton, C. E. *J. Am. Chem. Soc.* **1958**, *80*, 3509.

(21) Carmichael, I.; Bentley, J. *J. Phys. Chem.* **1985**, *89*, 2951.

(22) (a) Bowen, K. H.; Liesegang, G. W.; Sanders, R. A.; Herschbach, D. R. *J. Phys. Chem.* **1983**, *87*, 557. (b) Quitevis, E. L.; Herschbach, D. R. *J. Phys. Chem.* **1989**, *93*, 1136.

(23) Fleischman, S. H.; Jordan, K. D. *J. Phys. Chem.* 1987, **91**, 1300.

Chapter 5

Visible Emission From Warming Neon Matrices

or

It Seemed Like a Good Idea at First

I. Background

In some FTIR experiments, we did not observe absorptions assignable to the mass-selected cation being deposited, even though the total integrated ion current deposited was comparable to those of experiments in which IR transitions were observed. There are three general, likely explanations for these negative results:

- the ions are being neutralized in the matrix
- the mass-selected ions undergo fragmentation upon collision with the matrix
- the ions are intact in the matrix, but a relatively low molar absorptivity makes them unobservable by our spectrometer.

The results of the experiments in which mass-selected, matrix-isolated cations were observed by FTIR spectroscopy indicate that neutralization in the matrix does not occur to an appreciable extent. It seems probable that the mass-selected cations would fragment as a result of a 130-eV collision with the matrix substrate. The actual collision energy, however, may be much less since it depends on the potential of the matrix window as well as the kinetic energy of the ion beam. This potential could presumably have any value between 0 and 130 V. Unfortunately, this effective potential cannot be measured, and it may be different for different chemical systems. Fragmentation of the incoming

cations could be troublesome for three reasons. First, the mass-selectivity would be violated. Then, the fragments themselves may have a low molar absorptivity, making their detection difficult. Moreover, even if it is observable, the IR spectra of the fragments may not be well known, making their identification difficult. If the lack of observation of the cation is due simply to inadequate instrumental sensitivity, then instrumental modifications can be made to improve the overall sensitivity of the experiment. Unfortunately, differentiation between fragmentation and insufficient sensitivity requires that the sensitivity improvements be made.

Electronic spectroscopy (absorption and emission) has been used to identify mass-selected, matrix-isolated cations.[1,2] Electronic absorption will not provide ground-state structural information directly, and emission measurements may not be fully diagnostic. Nonetheless, these techniques do have the advantage of being 10–1000 times more sensitive than FTIR. If the emission spectra of the mass-selected cation, and its neutralization product and its possible fragments are known, emission spectroscopy might help to determine if the mass-selected cations are not observed because of fragmentation, or simply because of inadequate sensitivity.

Unfortunately, the adaptation of a traditional luminescence spectrometer to the UHV chamber was not feasible. The was due mainly to the inability to accommodate a light source and detector without major modifications to the chamber. We were, however, able to perform some preliminary emission experiments using what is presumably charge-recombination energy from the matrix-isolated cations and anions as an excitation source. While the emitting species observed in such experiments are not the ions originally trapped in the matrix, it was hoped that by using systems we believe we

understand, we could establish a relationship between the ions in the matrix and the resulting emission. If a relationship could be established, emission spectroscopy could be used as a sensitive, albeit indirect method to identify species present in the matrix that are not observable by FTIR spectroscopy.

The observation of emission from a warming rare-gas matrix has been suggested as an informal test for the presence of ions in the matrix.[3] The emission, however, could emanate from a variety of sources. The emission could occur as the result of the recombination of oppositely charged species. In the gas phase, the recombination creates one or more highly excited neutral species, as demonstrated below:

$$CO_2^{\bullet+} + CO_2^{\bullet-} \rightarrow CO_2^{\bullet} + CO_2^{\bullet}$$

The neutral species may then relax to their ground states by the emission of light. In this example, both products are shown in an excited electronic state, but in many cases only one of the products may be formed in an excited electronic state. Rather than simple electron transfer, the cation and anion may also undergo some chemistry, for example:

$$\begin{aligned} CO_2^{\bullet+} + CO_2^{\bullet-} &\rightarrow CO + O_2 + CO \\ &\rightarrow CO_3 + CO \end{aligned}$$

The energy deposited into the neutral species is the difference between the electron affinity of the cation and of the anion. Since the cations we have studied to date have electron affinities of 8.9 eV or greater, the charge recombination process can deposit a significant amount energy into the products. Because the amount of energy involved is more than enough to break a chemical bond, the recombination products often release internal energy by breaking one or more bonds. This is frequently observed,[4] for example, in the recombination of a polyatomic cation with an electron, such as:

$$OCS^{+} + e^{-} \rightarrow CO^{\bullet} + S^{\bullet}$$

Again all, or some, of the neutral products may be formed in an excited electronic state. Other possible sources of emission are excited neutral species formed from the recombination of neutral radical species that may be present in the matrix, such as:

$$CH_3^{\bullet} + CH_3^{\bullet} \rightarrow C_2H_6^{\bullet}$$

Excited species may also be formed from radical-molecule or ion-molecule reactions between the wide variety of species present in the matrix. The species available for such reactions include the ubiquitous CO_2 and H_2O, as well as the ion precursor and possibly some of its neutral fragments.

Certain aspects our system merit elaboration. One concern is the identity of the negative charge carrier. The matrix hosts used in these experiments were a mixture of Ne and CO_2. In these matrices, we believe that a large number of the negative charge carriers are present are in the form of $CO_2^{\bullet-}$ or one of its aggregates.[5] The electron affinity of CO_2^{-} is negative, yet the anion has a relatively long lifetime.[6] It is not clear if this species will remain intact once the matrix is no longer rigid. It is possible that above the annealing temperature, the predominant negative charge carrier could be an electron rather than $CO_2^{\bullet-}$. Electrons are considered to be relatively mobile in rare-gas matrices.[7] If they are the dominant negative charge carrier, then the conditions under which recombination occurs are not clear. If electrons are free to migrate before the matrix surrounding them is completely vaporized and larger species are still trapped, then the recombination will occur under condensed-phase conditions. While fragmentation may be expected in gas phase neutralization, it should be less likely under inert, condensed-phase conditions. If the ions recombine in the matrix, the matrix cage effect will suppress fragmentation, and

the excess energy will be effectively dissipated by numerous collisions with the host atoms and molecules. If the recombination occurs in the gas phase, then fragmentation is expected to occur readily.

II. Experimental

The apparatus used to observe the emission from warming matrices is described in Chapter 2. High purity neon (AGA), 99.9995% premixed with CO_2 (Aldrich, 99.8+%) in an ~1000:1 ratio was used as the matrix gas. The matrix deposition rate was ~0.5 mmol/h. Compounds used as precursors for the mass selected cations [Ar (AGA), CF_3Cl (Matheson), OCS (Matheson), CS_2 (Fisher) and CH_3Br (Aldrich)] were all used as received. The energy of the mass-selected cation beams was 130 eV. Deposition times depended on the intensity of the emission from the different ionic species and varied from 5 to 25 hours. The matrix was warmed by turning off the cryostat after stopping the deposition. The time-dependence of the window temperature is shown in Figure 5.1. The apparatus used to collect the emission from warming matrices is described in detail in Chapter 2, Section VII. All optical measurements were made with the lab as darkened as possible. During the collection of the total emission, the PMT was generally operated at a potential of 800–1000 V. Data were collected at 10 Hz for 300 seconds. In the dispersed emission experiments, the monochromator was used with slit widths from 1.5 to 3.0 mm, depending on the emission intensity of the particular system. The 300 groove/mm grating used in this study had a relative linear dispersion (RLD) of 14.8 nm/mm. This resulted in a slit-width limited spectral resolution[8] of 22 and 44 nm (FWHM), respectively. Spectra were collected by integrating over 5 s intervals, for a total of 300 s.

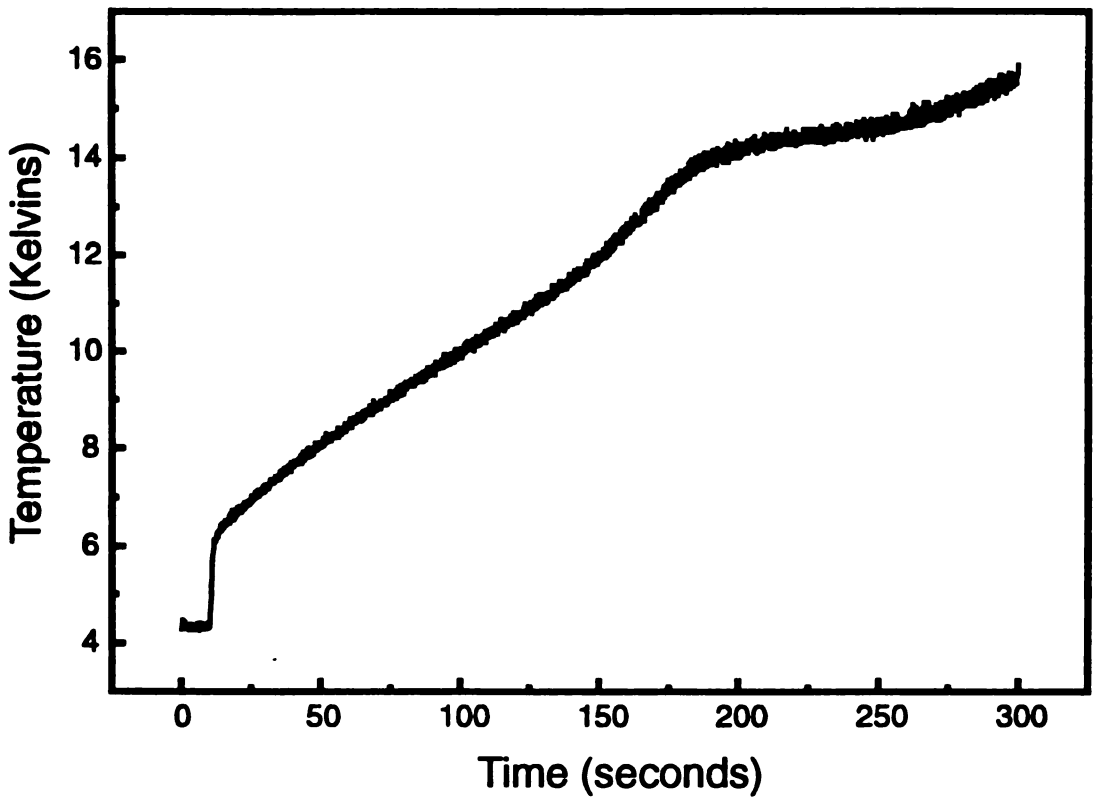

Figure 5.1: The temperature of the cryostat window holder as a function of time as the cryostat is turned off. The cryostat was turned off approximately 10 s after data collection was started. This temperature profile was obtained concurrently with the emission data shown in Figure 5.3

III Results and Discussion

A. Total Emission Studies

The first attempt to observe emission from a warming ion-containing matrix was carried out by simply visualizing the matrix as the cryostat was turned off. After a 24 h deposition of CH_3^+, generated from CH_3Br, the matrix exhibited a blue-white emission as it warmed. This emission was plainly visible 1 m away from the outside of the UHV chamber, and lasted for several minutes.

Figure 5.2 shows the undispersed emission from a 1000:1 Ne:CO_2 matrix containing CF_3^+ generated from CF_3Cl. The emission from a 1000:1 Ne:CO_2 matrix containing $CS_2^{\bullet+}$ generated from CS_2 is shown Figure 5.3. This matrix had been subjected to several short annealing cycles before being warmed beyond 14 K.

These annealings are believed to be responsible for the qualitative differences between the two spectra. While most of the matrix gas and mass-selected ions deposited are frozen onto the cryostat window, some may end up on metallic window holder. Due to its higher thermal conductivity, the window holder heats faster than the CsI window. The first sharp signal in Figure 5.2 is attributed to the ions isolated on the window holder, while the second broad signal is due to the ions on the CsI window. In the $CS_2^{\bullet+}$ experiment, the ions isolated on the surface of the window holder were most likely lost during the repeated annealing cycles. The difference between the times of the two emission maxima is most likely a result of timing inconsistencies in the experiment and the $CS_2^{\bullet+}$ deposition being longer, resulting in a larger matrix that takes longer to warm.

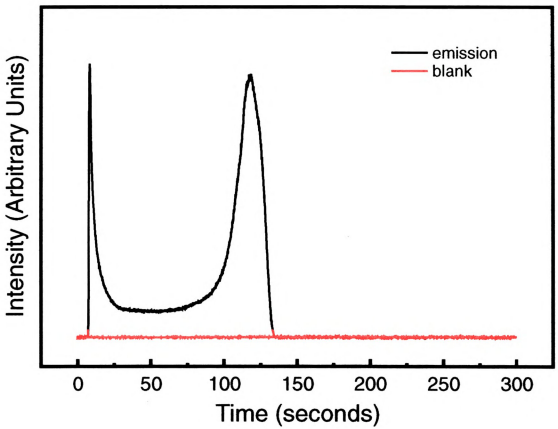

Figure 5.2: Total emission observed during warming of a 1000:1 Ne:CO_2 matrix after the deposition of CF_3^+ generated from CF_3Cl.

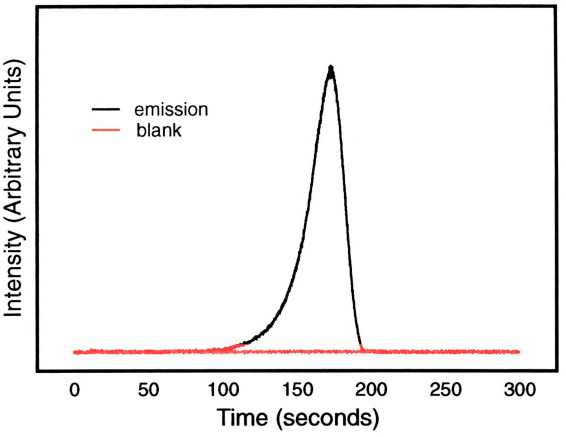

Figure 5.3: Total emission observed during warming of a 1000:1 Ne:CO_2 matrix after the deposition of $CS_2^{+\bullet}$ generated from CS_2. This matrix was subject to several short annealing cycles before being warmed irreversibly.

B. Dispersed Emission Studies

While the total emission experiments helped quantify and provide some temporal information about the emission from the warming ion-containing matrices, they could provide no insight as to the identity of the emissive species. It was hoped that the species responsible for the luminescence could be identified by dispersing the emission. Owing to experimental limitations, however, interpretations of the results of these measurements are highly speculative. First, the low resolution of the spectra make vibrational or rotational analysis impossible. The limited spectral range of the photodiode array (350–800 nm) also limits the amount of information that can be obtained. The question of the conditions under which recombination occurs further complicates assignment of the emission.

1. $Ar^{\bullet+}$

The warming of a 1000:1 Ne:CO_2 matrix after depositing $Ar^{\bullet+}$ generated from Ar resulted in the emission shown in Figure 5.4. The temporal profile of the emission is shown in Figure 5.5. The intensity of the spectra varied with time, but the same bands, centered roughly at 589, 550, 532, and 494 nm were observed, indicating that the same species is responsible for the emission throughout the warming period.

$Ar^{\bullet+}$ was chosen to simplify analysis of the experiment, since at least the complication of fragmentation is obviously not possible in this case. Using $Ar^{\bullet+}$, however, does add some complications. Its relatively high electron affinity (15.75 eV) [9] will allow charge exchange chemistry with CO_2 and H_2O which is not possible with the other ions studied. This chemistry could lead to the formation of CO_2^+ and H_2O^+. The emission should presumably emanate from an excited Ar atom, CO_2 or H_2O. The emission observed can be assigned to transitions originating from the $3p^5 8p$ *(J=1)* and $3p^5 5d$ *(J=2)*

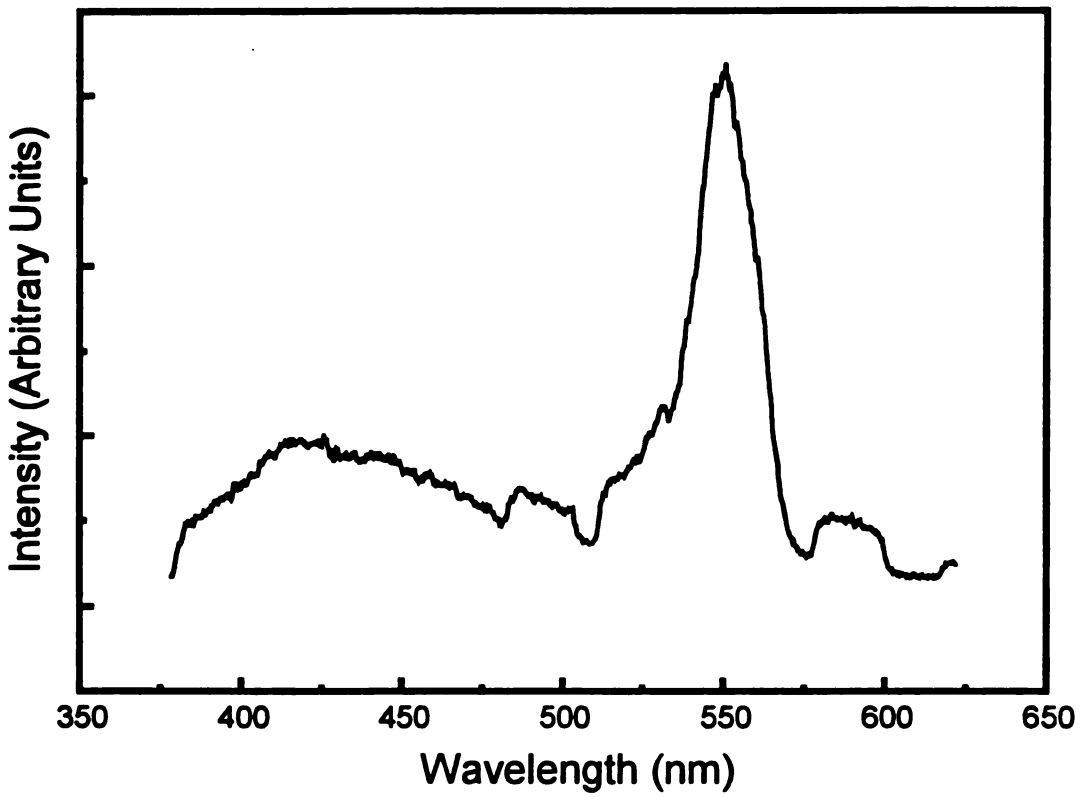

Figure 5.4: Dispersed emission observed during warming of a 1000:1 Ne:CO_2 matrix after the deposition of Ar^{**} generated from Ar. This single spectrum is representative of the emission observed throughout the ntire warming.

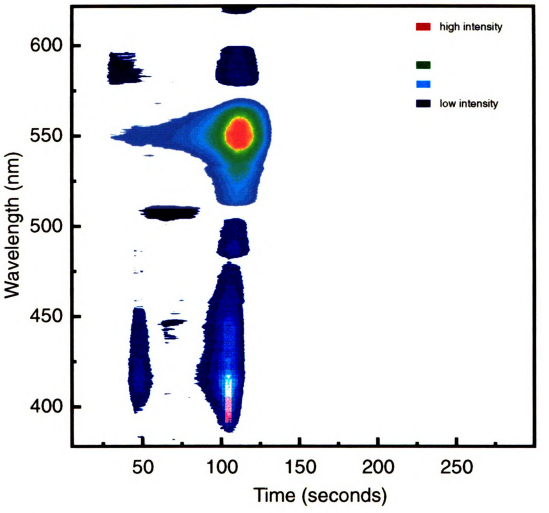

Figure 5.5: Contour plot showing temporal profile of the dispersed emission observed during the warming of a 1000:1 Ne:CO_2 matrix after the deposition of Ar^{**} generated from Ar.

electronic configurations of Ar.[9] Although the spectral bands are quite broad for atomic transitions, their width (~20 nm FWHM) is what is expected from the 1.5 mm slit width used in this experiment. Both of the upper electronic configurations have the same core configuration ($3p^5$) as Ar^{*+} and ΔJ for each transition is ± 1, following the general rules for atomic transitions.[10] These assignments are demonstrated graphically in Figure 5.6.

2. CF_3^+

When a 1000:1 Ne:CO_2 matrix containing CF_3^+ generated from CF_3Cl was warmed, emission from approximately 400 to 700 nm was observed. Figures 5.7 and 5.8 show the temporal evolution of the emission over two partially overlapping wavelength ranges. Figure 5.9 shows individual spectra from each wavelength range in greater detail. The temporal profile of this emission is similar to the total emission results shown in Figure 5.2. The spectra collected vary only in intensity, indicating that the same species is responsible for the emission throughout the warming process.

The assignment of this emission (and of all the polyatomic ions) unfortunately is not as straightforward as that for the visible luminescence observed in the Ar^{*+} experiment. The emission observed during the recombination of CF_3^+ is consistent with previous assignments for both $CF_3^{\bullet}$ [11,12,13,14] and CF_2.[15] Washida et al.[11,12,13,14] observed emission in the 400–700-nm range during vacuum UV photolysis of several trifluoromethyl compounds. A sample of the emission collected during these studies is reproduced in Figure 5.10. It should be noted the authors reported that the position and width of this band were dependent of several experimental conditions such as the photolysis wavelength, pressure, and the presence of a buffer gas. Based on experimental results[11,12,13] and theoretical calculations,[14] they assigned this emission as originating from

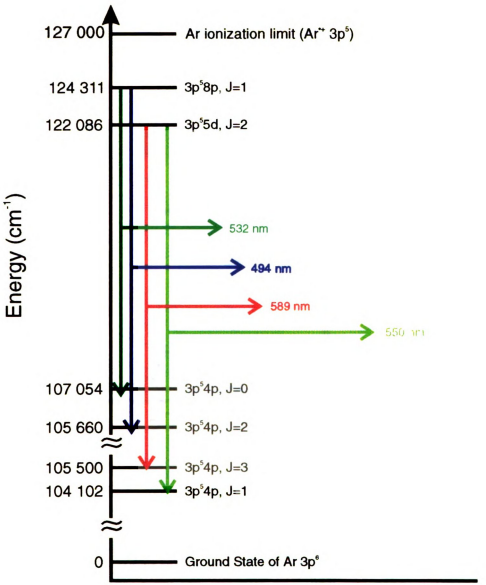

Figure 5.6: Tentative assignments of Argon emission.

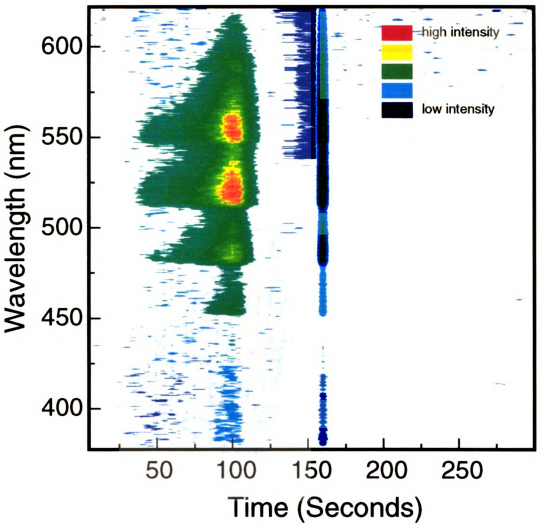

Figure 5.7: Contour plot showing temporal profile of the dispersed emission in the 350-650 nm range observed during the warming of a 1000:1 Ne:CO_2 matrix after the deposition of $CF_3^{\bullet}$ generated from CF_3Cl.

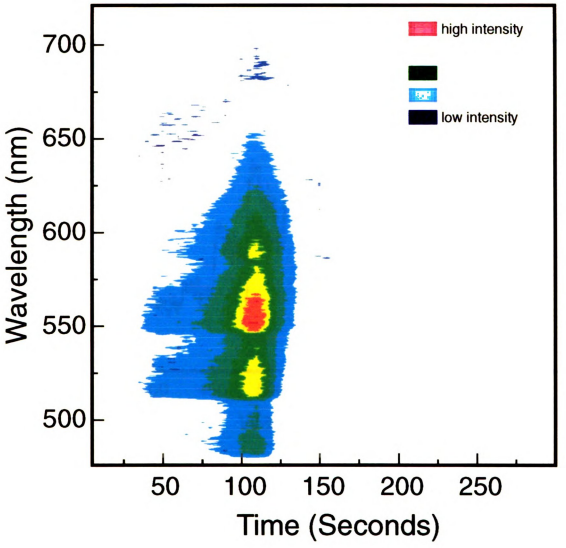

Figure 5.8: Contour plot showing temporal profile of the dispersed emission in the 450-750 nm range observed during the warming of a 1000:1 Ne:CO_2 matrix after the deposition of CF_3^+ generated from CF_3Cl.

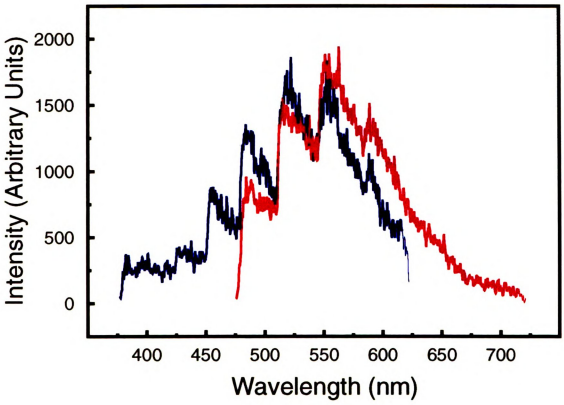

Figure 5.9: Dispersed emission observed from a warming 1000:1 Ne:CO_2 matrix after deposition of CF_3^+ generated from CF_3Cl. Spectra shown are representative of the emission observed during the entire 5 minute warmup. The blue trace was taken from the data set shown in Figure 5.7 and scaled 2x. The red trace was taken from the data set shown in Figure 5.8 and not scaled

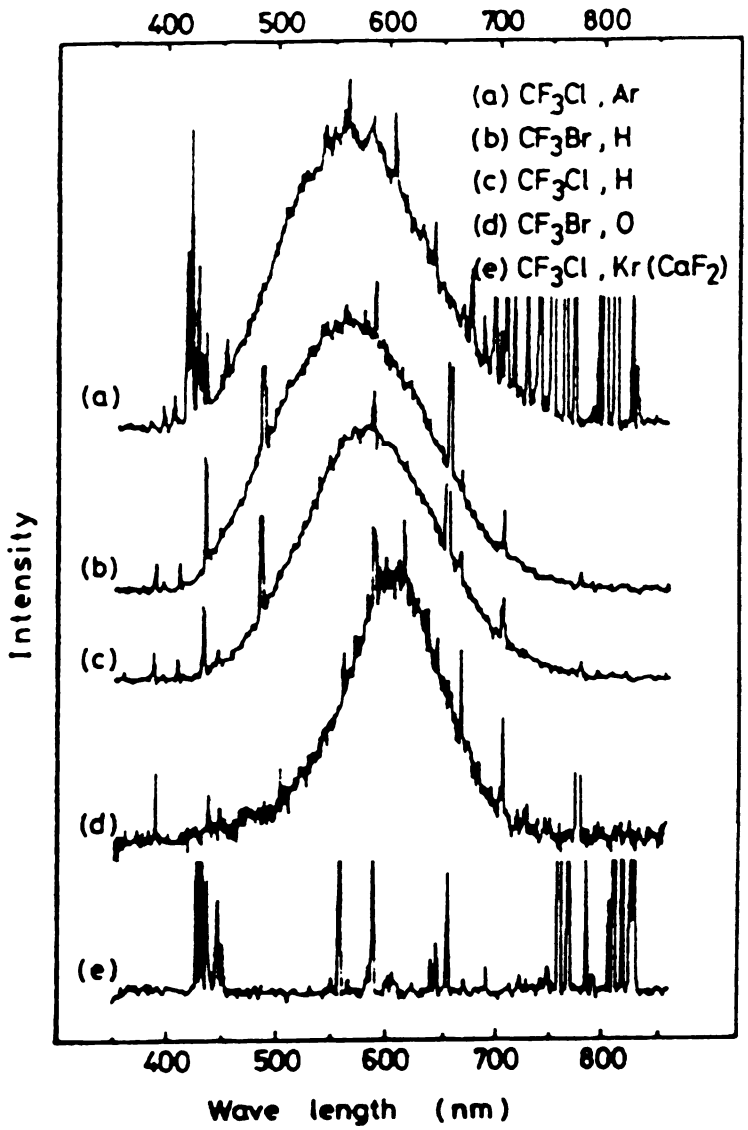

Figure 5.10: Visible $CF_3^{\cdot}$ emission reported by Washida et. al. Spectrum repoduced from reference 13. Bottom trace (e) is the discharge lamp reference.

one of two $CF_3^{\bullet}$ Rydberg states approximately 8 eV above the ground state (E' and A_2'') and ending in another Rydberg state (A_1') approximately 6 eV above the ground state.

When CF_3^+ is neutralized to form $CF_3^{\bullet}$, the radical is formed with as much as 8.9 eV of excess energy. Given the typical C-F bond strength of 5.5 eV,[16] it could be possible to form a CF_2 fragment with as much as 3.4 eV (27 424 cm^{-1}) of excess energy. This is sufficient to access a low lying triplet state ($\tilde{a}^3B_1$, 19 824 cm^{-1}) of CF_2.[15] The phosphorescence from this state to the ground state ($\tilde{X}^1A_1$) has also been reported[15] in the 450–700-nm range. The emission spectrum observed by Koda is reproduced in Figure 5.11. Unfortunately, a definitive assignment of the matrix emission cannot be made with the data currently available. $CF_3^{\bullet}$ and $CF_2^{\bullet}$ could be differentiated by their UV emission spectra, where these two compounds have distinctly different emission bands.

3. $CS_2^{\bullet+}$

The warming of a 1000:1 Ne:CO_2 matrix after deposition of $CS_2^{\bullet+}$ generated from CS_2 resulted in a relatively complex emission band from 400–700 nm. A typical temporal profile of the emission is shown in Figure 5.12, and an individual spectrum is shown in greater detail in Figure 5.13. This emission, however, was not very reproducible. The energies of the admittedly ill-defined features were somewhat consistent, but their relative intensities were not. FTIR experiments with $CS_2^{\bullet+}$ generated from CS_2 indicated that after several hours of deposition the cold copper surfaces seemed to become "fouled" and exhibit severely decreased anion production. This could possibly be the result of a C_xS_y polymer forming on the copper surface. These emission experiments may be even more

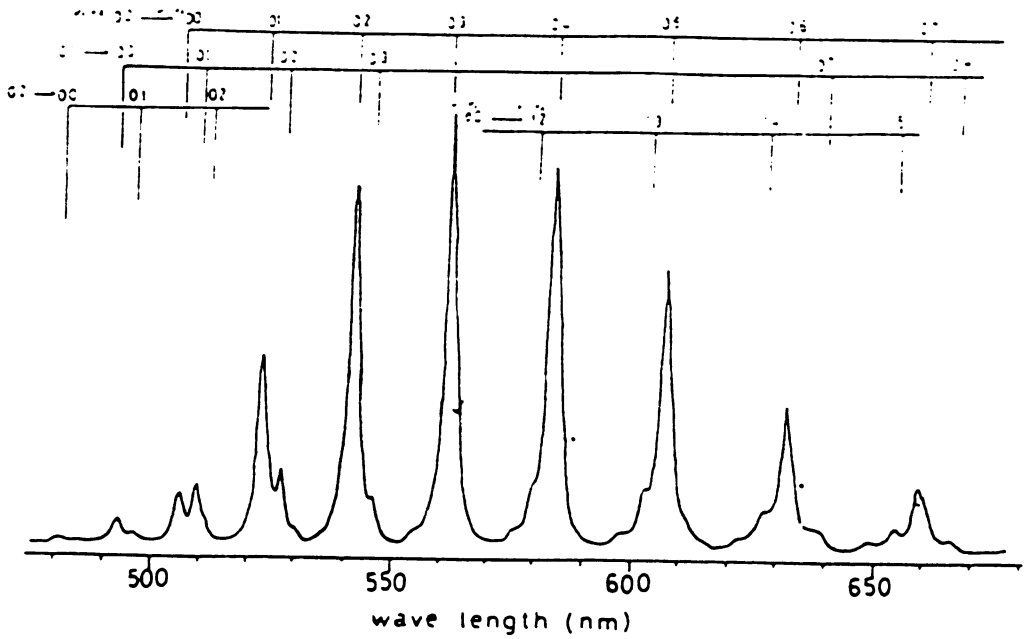

Figure 5.11: Visible CF_2 emission reported by Koda. Spectrum repoduced from reference 15.

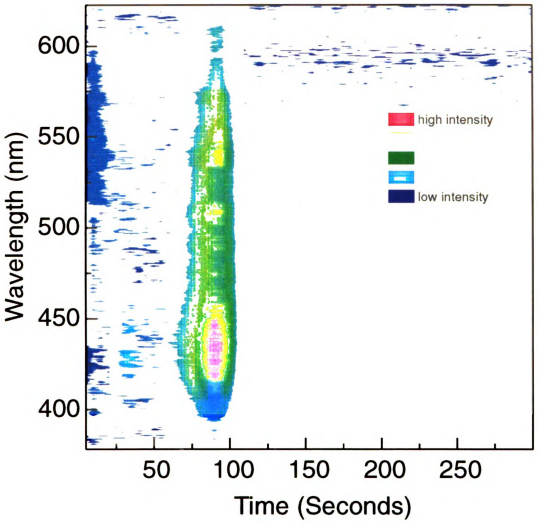

Figure 5.12 Contour plot showing temporal profile of the dispersed emission observed during the warming of a 1000:1 Ne:CO_2 matrix after the deposition of CS_2^{+} generated from CS_2.

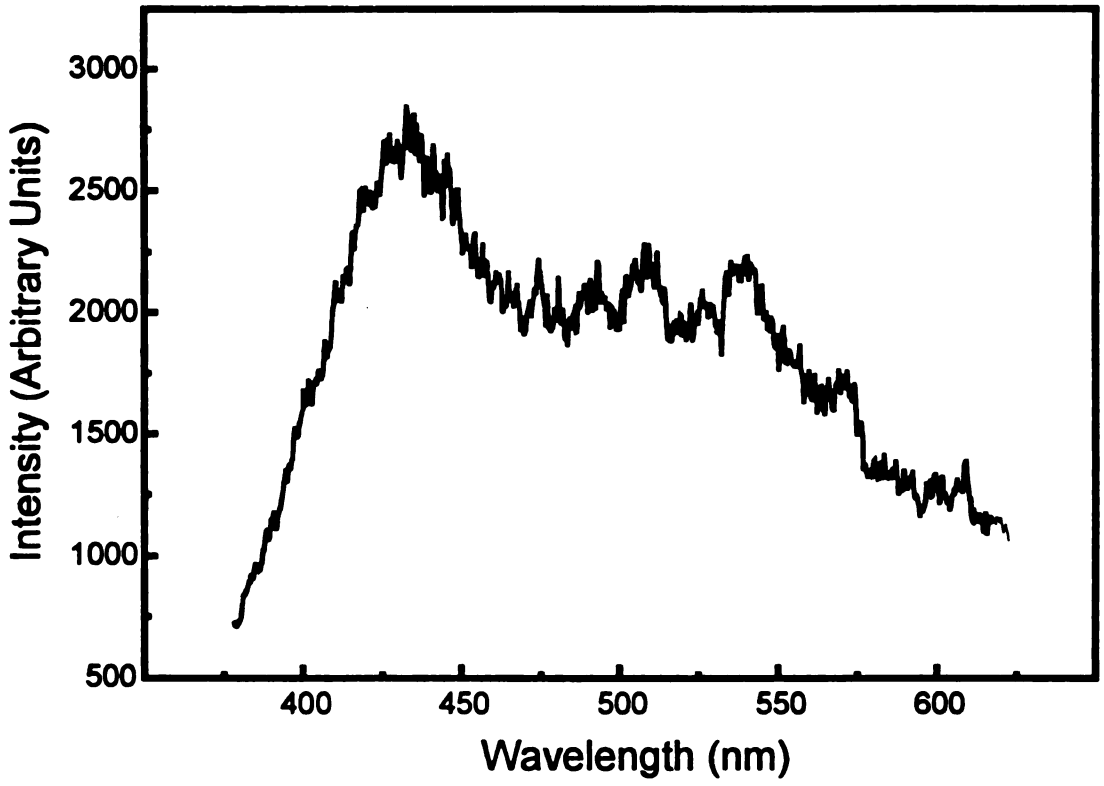

Figure 5.13: Dispersed emission observed during warming of a 1000:1 Ne:CO_2 matrix after the deposition of $CS_2^{+\bullet}$ generated from CS_2. This single spectrum is representative of the emission observed throughout the entire warming.

sensitive to the experimental parameters, and perhaps they should be repeated under more reproducible conditions.

The $CS_2^{\bullet+}$ emission experiments can be interpreted in similar fashion to the CF_3^+ results. When $CS_2^{\bullet+}$ is neutralized, the CS_2 neutral is formed with as much as 10.1 eV of excess energy.[17] This is more than sufficient to break one of the C-S bonds, which only requires 4.5 eV.[17] The resulting CS fragment could then be formed with as much as 5.6 eV (45 170 cm^{-1}) of excess energy. The emission observed correlates roughly with that previously assigned to transitions within a triplet manifold of CS,[18] reproduced in Figure 5.14. The lowest of these states lies approximately 27 700 cm^{-1} above the ground state of CS. The emission observed would therefore have to originate from energy levels from 43 100 to 50 400 cm^{-1} above the ground state. While these could be assigned to vibrationally excited CS in either the $\tilde{d}^3\Delta$ or the $\tilde{e}^3\Sigma^-$ state,[19] population of the upper levels would require more energy than can be attained from neutralization alone. The extra energy needed, however, is not very large (5200 cm^{-1}, 0.64 eV) and could possibly be supplied by the energy of the collision between the ions if they experience some acceleration towards each other or from some electric field before recombining.

Another possibility is that the emitting species is S_2, formed from the reaction:

$$CS_2^{\bullet+} + \text{negative charge carrier}^{\cdot} \rightarrow C + S_2$$

This reaction is exothermic by approximately 9.9 eV.[20] This, however, is more than twice the bond dissociation energy of S_2, 4.4 eV.[21] If the internal energy of the S_2 molecule is quenched rapidly enough by the matrix, emission from it could be observed. The lowest energy symmetry-allowed transition of S_2 is the $\tilde{B}^3\Sigma_u^- \rightarrow \tilde{X}^3\Sigma_g^-$ transition.[21] The energy

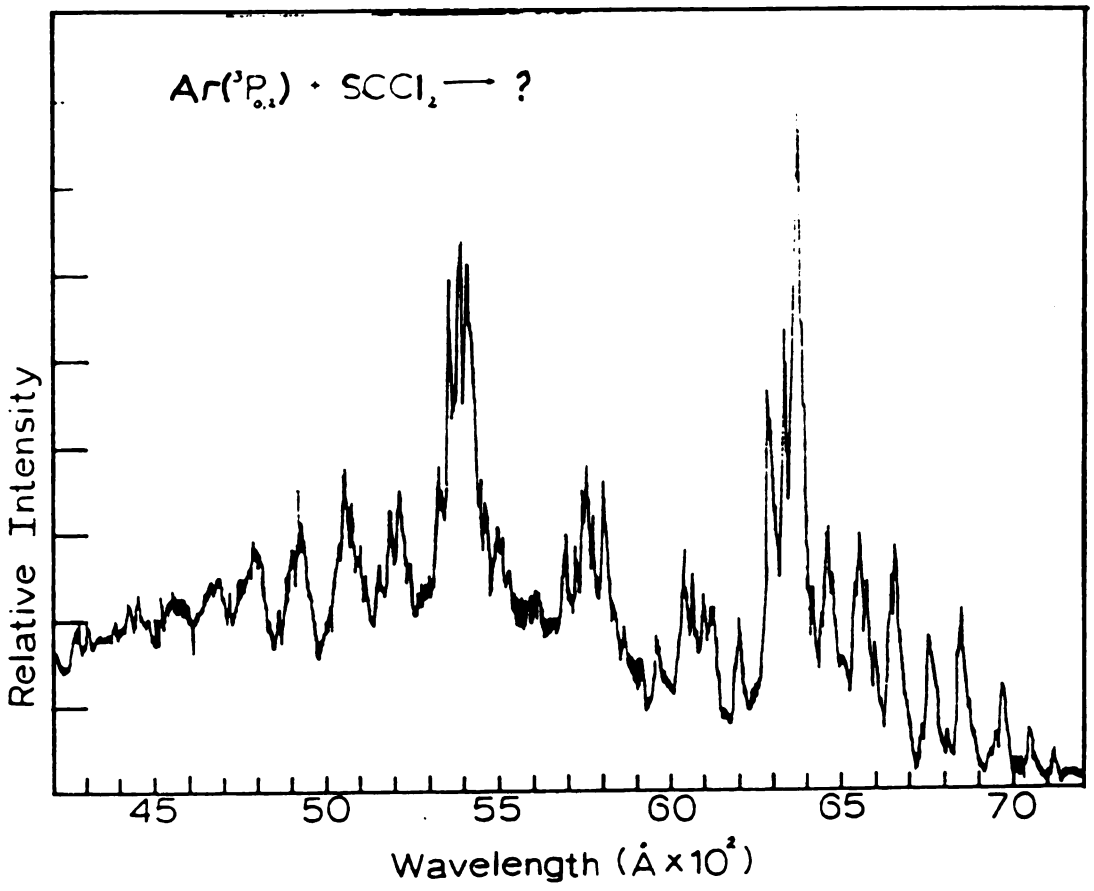

Figure 5.14: Visible CS emission reported by Coxon and co-workers. Spectrum reproduced from reference 18.

difference between these two states, however, is 31 835 cm^{-1},[21] which is too large for the emission observed.

This observed emission could also be assigned to transitions of CS_2. The energy of the observed emission corresponds reasonably with the energy difference between the $\tilde{A}^1B_2$ (45 950 cm^{-1}) and $\tilde{a}^3A_2$ (26 187 cm^{-1}) levels.[17] If these Rydberg states are responsible for the emission, then the relaxation of the neutral, excited CS_2^* by collisions with the matrix would need to be very efficient to prevent fragmentation.

4. OCS^{*+}

The warming of a 1000:1 Ne:CO_2 matrix after deposition of OCS^{*+} generated from OCS resulted in very intense emission in the 400–600-nm range. The emission intensity varies with time as the matrix is warmed as shown in Figure 5.15. The same spectrum is observed throughout the warming, varying only in intensity. A single spectrum, showing the spectral distribution in greater detail, is reproduced in Figure 5.16.

The emission from the OCS^{*+} experiments is equally ambiguous. The broad feature centered at ~420 nm could be assigned to the well known $\tilde{B}^1\Sigma \rightarrow \tilde{A}^1\Pi$ transition of CO. The spectrum observed from a gas phase CO sample is reproduced in Figure 5.17.[22] This CO emission has been previously observed in OCS passed through a RF discharge.[4] Bezuk et al. found that the CO fragments were not formed directly in the $\tilde{B}^1\Sigma$ state, but were excited into that state by collisions with electrons in the plasma. In our experiment, if the only energy available is the electron affinity of OCS^{*+}, then the CO fragment can be made with at most 7.5 eV (60 200 cm^{-1}), after 3.7 eV (29 844 cm^{-1}) is used to break the C-S bond. This is not sufficient energy to access even the $\tilde{A}^1\Pi$ state. The remaining energy (26 750 cm^{-1}, 3.3 eV), could, however, be supplied by the some other source, such

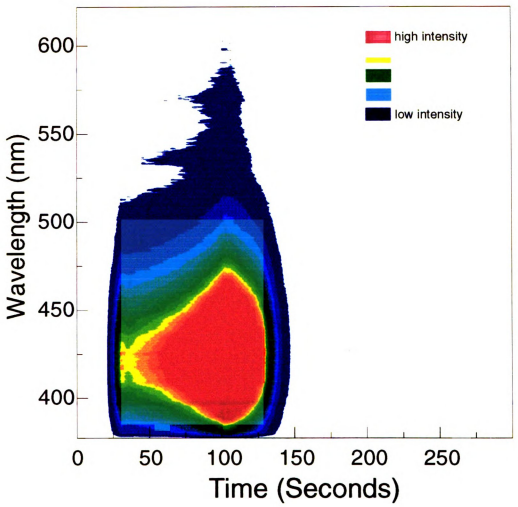

Figure 5.15 Contour plot showing the temporal profile of the dispersed emission observed during the warming of a 1000:1 Ne:CO_2 matrix after the deposition of OCS^{+} generated from OCS.

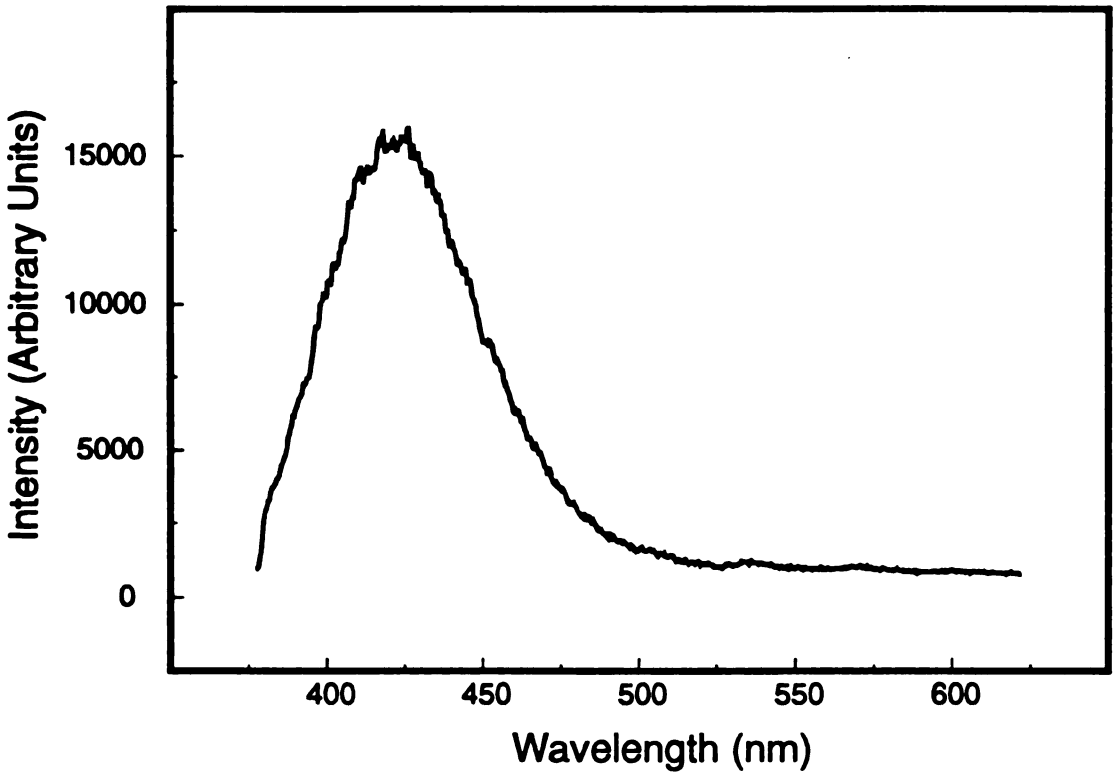

Figure 5.16: Dispersed emission observed during warming of a 1000:1 Ne:CO_2 matrix after the deposition of OCS^{+} generated from OCS. This single spectrum is representative of the emission observed throughout the entire warming.

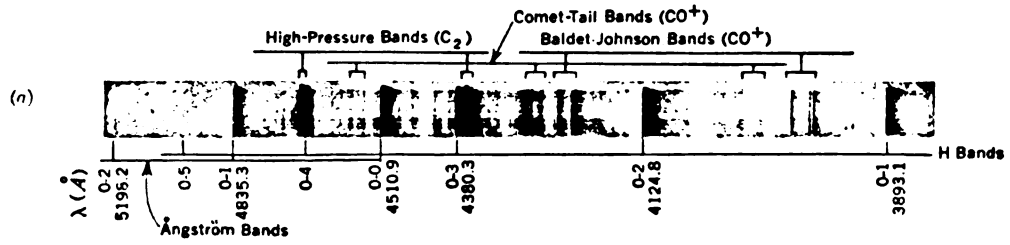

Figure 5.17: Visible CO emission shown by Herzberg. Spectrum reproduced from reference 22.

as collision with the negatively charged species (such as an electron) as in the study of Bezuk et al.[4]

If it is assumed that the excited OCS^* molecule is quenched rapidly enough to prevent dissociation , then this emission could also be attributed to a transition from the $\tilde{D}$ state to the $\tilde{A}$ state.[23] The energy of this transition (ν_{00}) is approximately 24 600 cm^{-1}, in reasonable agreement with the observed emission.

5. CH_3^+

The warming of a 1000:1 Ne:CO_2 matrix after deposition of CH_3^+ generated from CH_3Br resulted in the observation of two bands, centered at approximately 575 and 637 nm. The temporal profile is shown in Figure 5.18. The results from this ion system were unique in that the spectral distribution of the emission did change with time. Figure 5.19 shows an emission at early time, when the 637-nm feature is prominent. At later times, as shown in Figure 5.20, the 575-nm feature is dominant.

The emission from the CH_3^+ depositions was by far the most puzzling because the recorded spectra did not exhibit the simple time variance observed for the previous four ions. Spectra recorded at different times are distinctly different. The temporal evolution of the 637-nm feature is similar to that observed for the other experiments. The 575-nm feature, however, reaches maximum iintensity at a later time. If fragmentation of the C-H (4.9 eV, 39 523 cm^{-1}) bond occurs, the resulting CH_2 fragment can be formed with as much as 40 653 cm^{-1} of excess energy. This would allow the formation of methylene in the $\tilde{c}^1A_1$ state. Both bands observed could be assigned to the $\tilde{c}^1A_1 \rightarrow \tilde{b}^1B_1$ transition of CH_2,[24] with varying degrees of vibrational excitation. The bands also coincide with

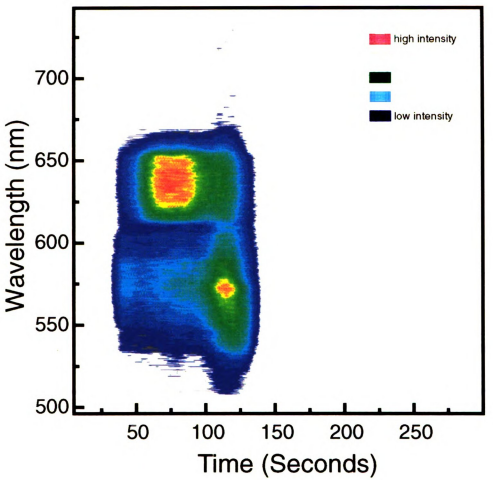

Figure 5.18 Contour plot showing temporal profile of the dispersed emission observed during the warming of a 1000:1 Ne:CO_2 matrix after the deposition of CH_3^* generated from CH_3Br.

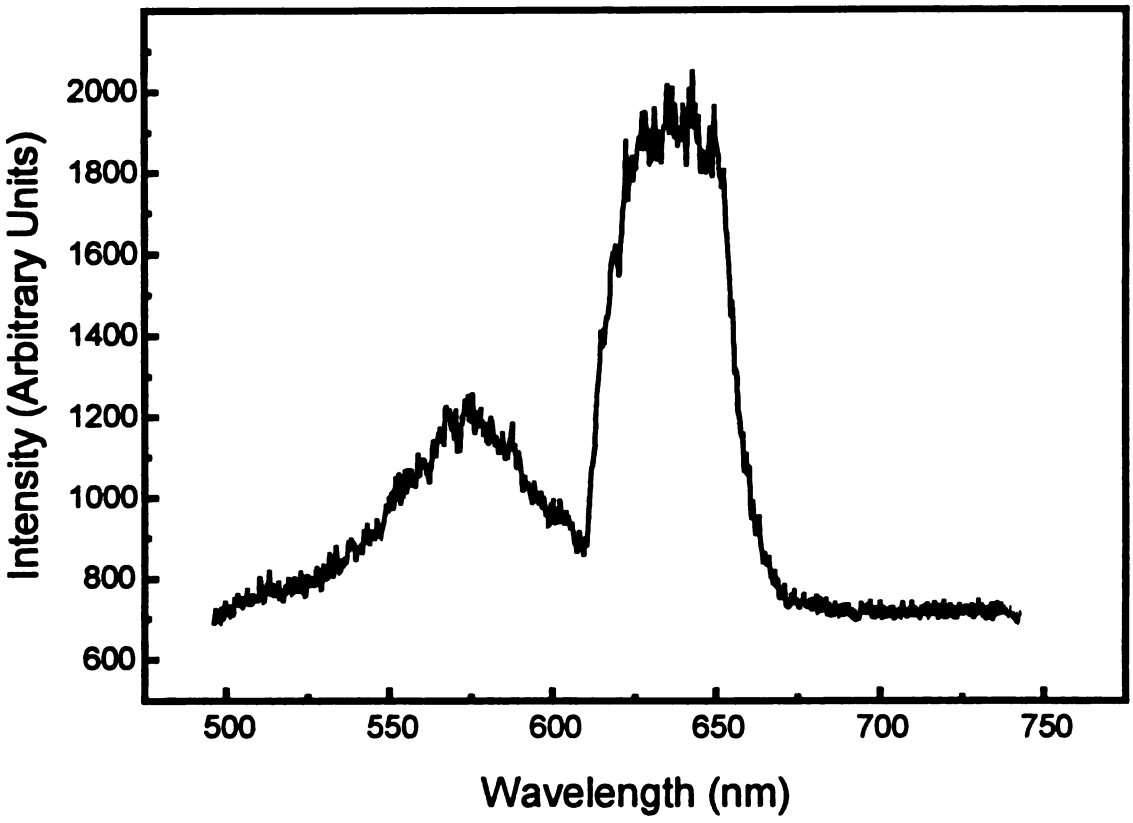

Figure 5.19: Dispersed emission observed during warming of a 1000:1 Ne:CO_2 matrix after the deposition of CH_3^+ generated from CH_3Br. This spectrum was taken approximately 60 s after the cryostat was turned off, and is representative of the early emission when the 637-nm band is dominant.

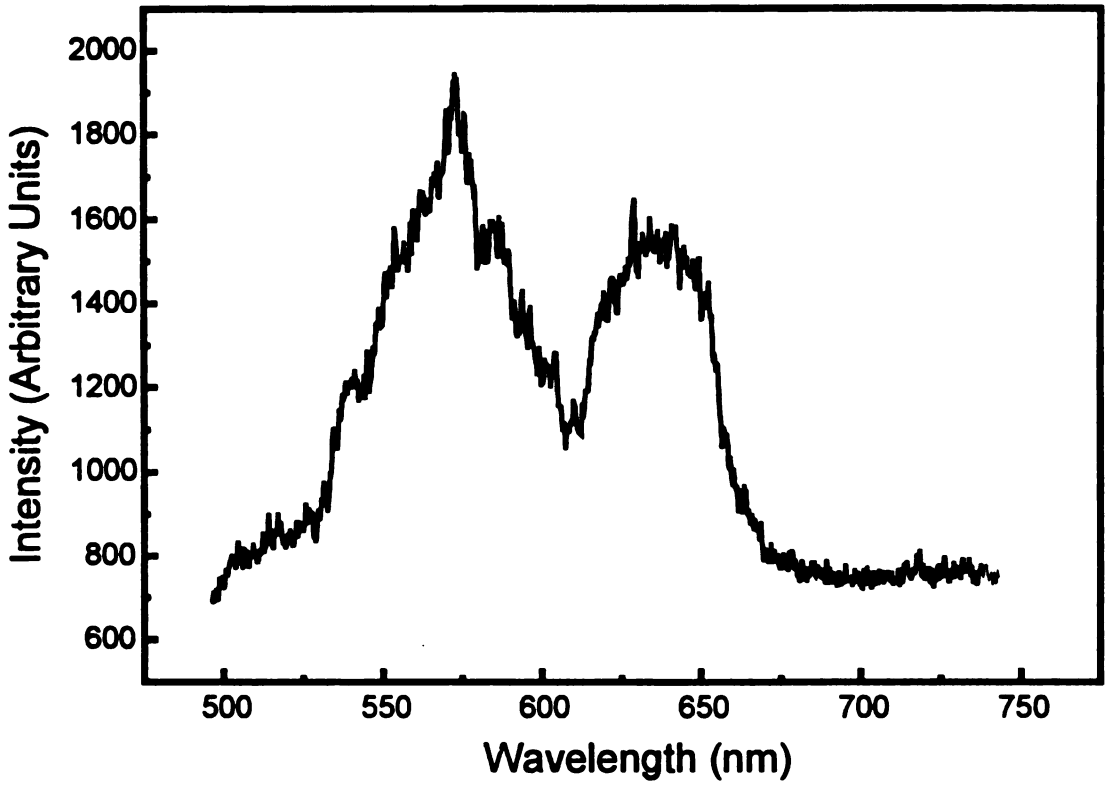

Figure 5.20: Dispersed emission observed during warming of a 1000:1 Ne:CO_2 matrix after the deposition of CH_3^+ generated from CH_3Br. This spectrum was taken approximately 100 s after the cryostat was turned off, and is representative of the late emission when the 575-nm band is dominant.

assignments made to various ro-vibrational transitions within the $\tilde{b}^1B_1 \rightarrow \tilde{a}^1A_1$ manifold,[25] although the extensive band structure observed by García-Moreno and Moore, a small portion of which is reproduced in Figure 5.21,[25] was not observed here. The different temporal profiles of the two bands suggest that they not be assigned to the same electronic manifold. If fragmentation does not occur, both transitions, assuming some vibrational excitation, could be assigned to the $\tilde{D}^2A_1'$ or $\tilde{C}^2E'' \rightarrow \tilde{B}^2A_1$ transition of CH_3.[26]

An alternate explanation is that the 637-nm emission is coming from CH, which could be produced by an H_2 elimination such as:

$$CH_3^+ + \text{negative charge carrier}^- \rightarrow CH + H_2$$

This reaction is exothermic by ~5.2 eV.[20] While this is more greater than the dissociation energy of CH (3.47 eV)[27], the molecule could be kept intact by the matrix cage. The emission observed could be assigned to the $\tilde{B}^2\Sigma^-$ or $\tilde{A}^2\Delta \rightarrow \tilde{X}^2\Pi$ transition of CH,[27,28] if the molecule is vibrationally excited. Perhaps the early emission is from CH_3, or CH recombining in the matrix while the emission at later time is due to gas-phase recombination which results in the fragmentation of $CH_3^{\bullet *}$ to $CH_2^{\bullet}$.

C. Discussion

Although definitive assignments of the emission observed from warming ion-containing matrices were not possible, a few general conclusions, can be made. First, because the emission observed in each of the five sets of experiments was different, it is clearly dependent in some way on the mass-selected cation which is deposited into the matrix. The relationship of the observed emission to the identity of the cation is not

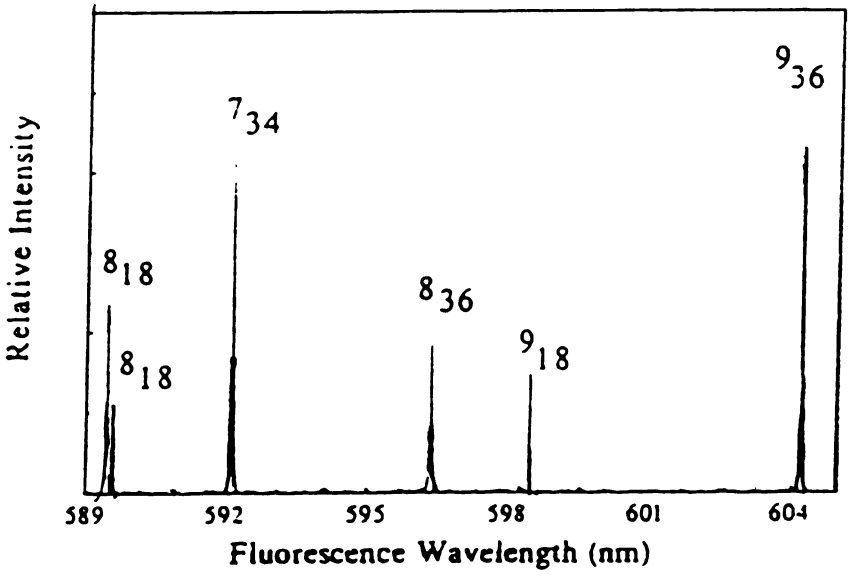

Figure 5.21: Portion of the visible CH_2 emission reported by García-Moreno and Moore. Spectrum repoduced from reference 25.

certain. Second, if the observed emission is indeed due to the neutralization of the matrix-isolated, mass-selected cations, the most probable assignments take place while the matrix is still somewhat rigid and can suppress fragmentation. Lastly, in all but one case (CH_3^+), the spectral distribution of the emission did not exhibit significant temporal change; that is, the same spectrum was always observed, only the intensity changed with time. This suggests that in most cases the same species or set of species is responsible for emission throughout the warming process.

IV. Conclusions

The results of these luminescence experiments from warming matrices that contain trapped ions show that this technique will not be generally useful as an indirect method for determining the composition of ion-containing matrices. Some of the problems are due to experimental limitations. The total emission experiments performed with the PMT detector indicate that a relatively large amount of light was being produced. In some cases, however, relatively low light levels were observed when the PDA/monochromator system was used. Much of the emission from those systems may be occurring in the UV. Since the spectral range of the PDA detector is limited to the visible wavelengths, this potential information is being lost. Use of a PMT as a UV detector is not feasible, owing to the transient nature of the emission. Due to the low light levels, relatively large slit widths must be used in the dispersed emission experiments, which severely degrades the resolution of the spectra that are obtained.

Even if improvements were made in the instrumentation, such experiments would be of only limited value as a more sensitive detection method, as proposed in the introduction of this chapter. The crucial limitation of the methodology is that the ions in

the matrix, which we seek to characterize, are not the species that produce the emission. Another fundamental question that remains pertains to the conditions under which recombination occurs. The total emission experiments performed during annealing demonstrate that emission can be observed without significant loss of the matrix or its contents as seen by FTIR.[29] This result indicates that if recombination is in fact responsible for the emission, it occurs in the matrix, presumably as diffusion of the trapped species is permitted, rather than in the vapor phase. This question might be answered by repeating the experiment for the dispersed emission with the $CO_2^{\bullet+}$ ion. If the recombination is a gas phase process, a CO fragment is expected. In that case, the emission should be similar to that observed for $OCS^{\bullet+}$.

Although the recombination/emission experiment could be improved, clearly the most effective use of electronic spectroscopy (absorption or luminescence), would involve observations on the ionic species while they are still trapped in the matrix. This would, however, require significant modifications to the instrument. These modifications are outlined in the following chapter.

List of References

(1) Forney, D.; Jakobi, M.; Maier J. P. *J. Chem. Phys.* **1989,** *90,* 600.

(2) Sabo, M. S.; Allison, J.; Gilbert, J. R.; Leroi, G. E. *Appl. Spectrosc.* **1991,** *45,* 535.

(3) Knight, L. b. J. Personal communication, 1992.

(4) Bezuk, S. J.; Miller, L. L.; Platzner, I. *J. Phys. Chem.* **1983,** *87,* 131.

(5) Godbout, J. T.; Halasinski, T. M.; Leroi, G. E.; Allison, J. *J. Phys. Chem.* **1996,** *100,* 2892.

(6) (a) Cooper, C. D.; Compton, R. N.; *Chem. Phys. Lett.* **1972,** *14,* 29.

(b) Compton, R. N.; Reinhardt, P. W.; Cooper, C. D. *J. Chem. Phys.* **1975,** *63,* 3821.

(7) Kasai, P. H. *Acc. Chem. Res.* **1971,** *4,* 329.

(8) Ingle, J. D. Jr.; Crouch, S R. *Spectrochemical Analysis;* Prentice Hall: Englewood Cliffs, New Jersey; p 71.

(9) Moore, C. E. *Atomic Energy Levels Volume I;* NBS circular 469, **1949,** pp 211-226.

(10) Kuhn, H. G. *Atomic Spectra;* Academic: New York, NY, 1969; Chapter 1.

(11) Suto, M.; Washida, N. *J. Chem. Phys.* **1983,** *78,* 1007.

(12) Suto, M.; Washida, N. *J. Chem. Phys.* **1983,** *78,* 1012.

(13) Suto, M.; Washida, N.; Akimoto, H.; Nakamura, M. *J. Chem. Phys.* **1983,** *78,* 1019.

(14) Washida, N.; Suto, M.; Shigero, N.; Nagashima, U.; Morokuma, K. *J. Chem. Phys.* **1983,** *78,* 1025.

(15) Kodo, S. *Chem. Phys. Lett.* **1978,** *55,* 353.

(16) Hildenbrand, D. L. *Chem. Phys. Lett.* **1975,** *32,* 523.

(17) Herzberg, G. *Molecular Spectra and Molecular Structure Volume III - Electronic Spectra and Electronic Structure of Polyatomic Molecules;* Krieger: Malabar, Fl, 1991; pp 600–601.

(18) Taylor, G. W.; Setser, D. W.; Coxon, J. A.; *J. Mol. Spectrosc.* **1972,** *44,* 108.

(19) Field, R. W.; Bergeman, T. H. *J. Chem. Phys.* **1970,** *54,* 2936.

(20) Thermochemical data taken from: Lias, S. G.; Bartmess, J. E.; Liebmann, J. F.; Holmes, J. L.; Levin, R. D.; Mallard, W. G. *J. Phys. Chem. Ref. Data.* **1988,** *17,* Suppl. 1.

(21) Herzberg, G. *Molecular Spectra and Molecular Structure Volume I - Spectra of Diatomic Molecules;* D. Van Nostrand: Princeton, NJ, 1950; p 566.

(22) Herzberg, G. *Molecular Spectra and Molecular Structure Volume I - Spectra of Diatomic Molecules;* D. Van Nostrand: Princeton, NJ, 1950; p 35.

(23) Herzberg, G. *Molecular Spectra and Molecular Structure Volume III - Electronic Spectra and Electronic Structure of Polyatomic Molecules;* Krieger: Malabar, Fl, 1991; pp 599–601.

(24) Herzberg, G. *Molecular Spectra and Molecular Structure Volume III - Electronic Spectra and Electronic Structure of Polyatomic Molecules;* Krieger: Malabar, Fl, 1991; pp 583–584.

(25) García-Moreno, I.; Moore, C. B. *J. Chem. Phys.* **1993,** *99,* 6429.

(26) Herzberg, G. *Molecular Spectra and Molecular Structure Volume III - Electronic Spectra and Electronic Structure of Polyatomic Molecules;* Krieger: Malabar, Fl, 1991; p 609.

(27) Herzberg, G. *Molecular Spectra and Molecular Structure Volume I -Spectra of Diatomic Molecules;* D. Van Nostrand: Princeton, NJ, 1950; p 518.

(28) Castillejo, M.; Martín, M.; de Nalda, R.; Oujja, M. *Chem. Phys. Lett.* **1995,** *237,* 368.

(29) Halasinski, T. M.; Godbout, J. T.; Allison, J.; Leroi, G. E. *J. Phys. Chem.* **1996,** accepted.

Chapter 6

Conclusions and Suggestions for Future Work

I. Conclusions

The ultimate goal of the research described in this dissertation was to obtain the vibrational spectra of mass-selected, matrix-isolated cations. This goal was reached: the FTIR spectra of several mass-selected, matrix-isolated cations such as CF_3^+,[1] $CO_2^{\bullet+}$,[2] and $CS_2^{\bullet+}$ [3] generated in an electron-impact ionization source have been observed. Another goal of this project was also to gain an understanding of the mechanism by which charge neutrality is maintained during the deposition of cations. We have addressed this issue and discovered that negatively charged particles are produced from the bombardment of cold metallic surfaces, and the molecules adsorbed on them. The addition of CO_2 to the system was found to result in the production of large quantities of $CO_2^{\bullet-}$ and $(CO_2)_2^{\bullet-}$.[2]

While this research was successful, not all issues have been resolved, and several questions remain. One interesting finding of this work was the observation of fragmentation products from some cations, such as $C_6F_6^{\bullet+}$ and $OCS^{\bullet+}$ but not from others, such as CF_3^+ and $CS_2^{\bullet+}$. The fragmentation was first thought to result from collisions of the relatively high (130 eV) kinetic energy ion beam with the growing matrix. These fragments may, however, be formed from the neutral molecules frozen onto parts of the cryostat assembly. Bombardment of the molecules on these surfaces by the mass-selected cation beam can fragment and vaporize the adsorbed molecules.

Cations with low molar absorptivities still provide a challenge. The cations observed to date have had relatively high molar absorptivities. Ions with medium or low

absorbances still cannot generally be observed in a reasonable amount of time (1 filament lifetime, 25–50 hours), owing to a combination of low beam intensity and instrumental sensitivity.

II. Instrumental Modifications

A. FTIR System Improvements

1. Gain-Ranging Amplifier System

The implementation of a gain-ranging amplifier in the FTIR detection system will reduce the background noise of the system by at least an order of magnitude, facilitating the observation of very weak absorptions. While this type of signal processing was used in the Bomem DA3 spectrometer, it is not present in the Nicolet 520P spectrometer, which replaced the Bomem. The hardware necessary to implement gain-ranging amplification was purchased with funds from a Chemistry Department Equipment Committee grant. The electronic circuitry necessary to measure the FTIR detector output and subject it to variable-gain amplification has been designed and installed. The circuit diagrams of the components are shown in Appendices X-X. The hardware is fully functional, but some LabVIEW programming is required to make the system operational. This programming involves data storage and manipulation. The raw data collected across the separate gain channels must stored as they are collected. Once the data collection is over the information from the separate gain channels must be processed and used to "splice" one final interferogram together. The interferogram will then be transformed to a absorption spectrum. This processing can be accomplished with the built-in data handling and math functions of LabVIEW. If more extensive data manipulation is required, C subroutines can be implemented into the LabVIEW VI.

B. Electronic Spectroscopy of Matrix-Isolated Species

The ability to observe the electronic as well as the FTIR spectra of the species trapped in the rare gas matrix would be very advantageous. Although electronic spectroscopy does not yield structural information as directly as vibrational spectroscopy, its higher sensitivity makes the technique useful in experiments when simple detection of ions is the goal, rather than structural analysis. The higher sensitivity of electronic spectroscopy (both absorption and emission) will facilitate the detection of species present in amounts to small too observe by FTIR. Since electronic spectroscopy is more sensitive, the electronic transitions of ions have been studied and documented much more extensively than their vibrational spectra. Simultaneously performing both experiments would provide the advantage of the ability to correlate electronic and vibrational transitions, when the latter are observed. This technique has been used very successfully by the Vala group to assign vibrational transitions of matrix-isolated ions.[4]

The implementation of an electronic absorption/emission spectrometer that can collect data concurrently with the FTIR system will require substantial modification to the existing UHV and optical systems. One way to accommodate both experiments is to modify the chamber to have two separate beam paths, as shown in Figure 6.1. The dual path system has several advantages. The primary advantage of this configuration is that different windows can be used for each beam path, so there will be no compromise in accommodating the IR and UV spectral ranges with a single window material. Fluorescence as well absorption experiments could be performed if desired. If absorption experiments are performed (IR as well as UV/VIS), they will have the benefit of an effective doubling of the sample pathlength.

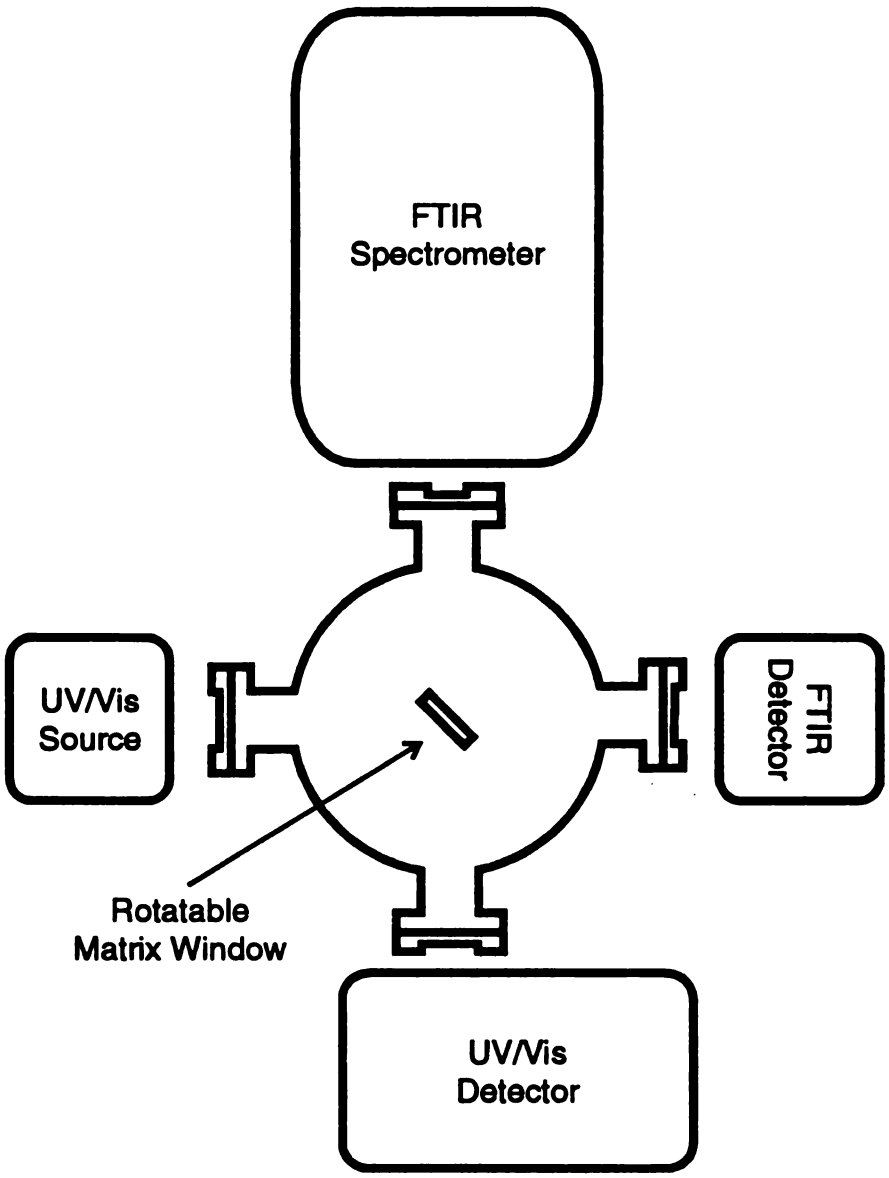

Figure 6.1: Schematic diagram of proposed modifications to accommodate both FTIR and UV/Vis absorption and luminescence measurements of matrix isolated species.

There are, however, some drawbacks to this system. Since the cryostat will need to be rotated into different positions for deposition, and FTIR and UV/Vis spectroscopy, the Conflat® flanges used in the cryostat's current vacuum housing will need to be replaced with a dual concentric o-ring system. It may also be a challenge to find a mirror material with sufficient reflectivity from the mid-IR to UV. If the proposed geometry is used, the Faraday plate's linear motion feedthrough (LMF) and electrical feedthrough will need to be moved to accommodate the new optical port. An alternative to this is to use fiber optics (if UHF-compatible are available) to simplify the UV/VIS optical path.

List of References

(1) Halasinski, T. M.; Godbout, J. T.; Allison, J.; Leroi, G. E. *J. Phys. Chem.* **1994,** *98,* 3930.

(2) Godbout, J. T.; Halasinski, T. M.; Leroi, G. E.; Allison, J. *J. Phys. Chem.* **1996,** *100,* 2892.

(3) Halasinski, T. M.; Godbout, J. T.; Allison, J.; Leroi, G. E. *J. Phys. Chem.* submitted.

(4) (a) Szczepanski, J.; Roser, D.; Personette, W.; Eyring, M.; Pellow, R.; Vala, M. *J. Phys. Chem.* **1992,** *96,* 7876. (b) Szczepanski, J.; Vala, M; Talbi, D.; Parisel, O.; Ellinger, Y. *J. Chem. Phys.* **1993,***98,* 4494. (c) Vala, M; Szczepanski, J.; Pauzat, F.; Parisel, O.; Talbi, D.; Ellinger, Y. *J. Phys. Chem.* **1994,** *98,* 9187. (d) Szczepanski, J.; Wehlburg, C.; Vala, M. *Chem. Phys. Lett.* **1995,** *232,* 221. (e) Szczepanski, J.; Drawdy, J.; Wehlburg, C.; Vala, M. *Chem. Phys. Lett.* **1995,** *245,*539.